# CLIMATE DIAGNOSTICS BULLETIN

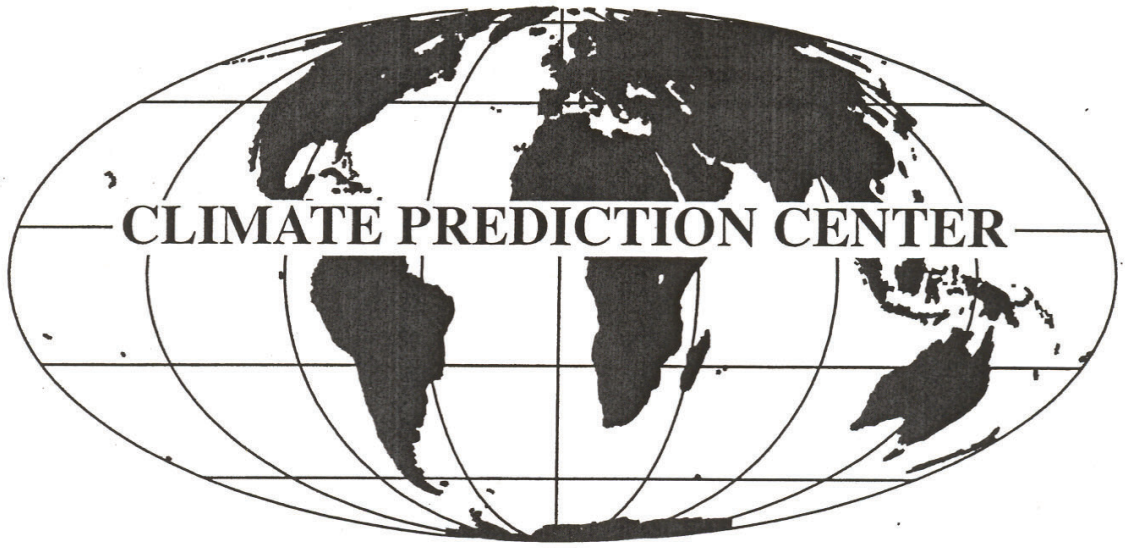


# SEPTEMBER 2019

## NEAR REAL-TIME OCEAN / ATMOSPHERE

## Monitoring, Assessments, and Prediction

**U.S. DEPARTMENT OF COMMERCE**
**National Oceanic and Atmospheric Administration**
**National Weather Service**

**National Centers for Environmental Prediction**

# CLIMATE DIAGNOSTICS BULLETIN


## CLIMATE PREDICTION CENTER
**Attn: Climate Diagnostics Bulletin**
**Room 3116, NCWCP**
**5830 University Research Court**
**College Park, MD 20740**



**Chief Editor:** Gerald D. Bell
**Editors:** Wei Shi, Michelle L'Heureux, and Michael Halpert
**Bulletin Production:** Wei Shi

**ExternalCollaborators:**
Center for Ocean-Atmospheric Prediction Studies (COAPS)
Cooperative Institute for Research in the Atmosphere (CIRA)
Earth & Space Research
International Research Institute for Climate and Society (IRI)
Joint Institute for the Study of the Atmosphere and Ocean (JISAO)
Lamont-Doherty Earth Observatory (LDEO)
NOAA-CIRES, Climate Diagnostics Center
NOAA-AOML, Atlantic Oceanographic and Meteorological Laboratory
NOAA-NESDIS-STAR, Center for Satellite Applications and Research
NOAA-NDBC, National Data Buoy Center
Scripps Institution of Oceanography

**Software:** Most of the bulletin figures generated at CPC are created using the Grid Analysis and Display System (GrADS).

**- Climate Diagnostics Bulletin available on the World Wide Web**

The CDB is available on the World Wide Web. The address of the online version of the CDB is:

**http://www.cpc.ncep.noaa.gov/products/CDB**

If you have any problems accessing the bulletin, contact Dr. Wei Shi by E-mail:

*Wei.Shi@noaa.gov*

# Table of Contents


TROPICS

Highlights . . . . . page 6

Table of Atmospheric Indices . . . . . page 7

Table of Oceanic Indices . . . . . page 8

| | FIGURE |
|---|---|
| **Time Series** | |
| Southern Oscillation Index (SOI) | T1 |
| Tahiti and Darwin SLP Anomalies | T1 |
| OLR Anomalies | T1 |
| CDAS/Reanalysis SOI & Equatorial SOI | T2 |
| 200-hPa Zonal Wind Anomalies | T3 |
| 500-hPa Temperature Anomalies | T3 |
| 30-hPa and 50-hPa Zonal Wind Anomalies | T3 |
| 850-hPa Zonal Wind Anomalies | T4 |
| Equatorial Pacific SST Anomalies | T5 |
| **Time-Longitude Sections** | |
| Mean and Anomalous Sea Level Pressure | T6 |
| Mean and Anomalous 850-hPa Zonal Wind | T7 |
| Mean and Anomalous OLR | T8 |
| Mean and Anomalous SST | T9 |
| Pentad SLP Anomalies | T10 |
| Pentad OLR Anomalies | T11 |
| Pentad 200-hPa Velocity Potential Anomalies | T12 |
| Pentad 850-hPa Zonal Wind Anomalies | T13 |
| Anomalous Equatorial Zonal Wind | T14 |
| Mean and Anomalous Depth of the 20°C Isotherm | T15 |
| **Mean & Anomaly Fields** | |
| Depth of the 20°C Isotherm | T16 |
| Subsurface Equatorial Pacific Temperatures | T17 |
| SST | T18 |
| SLP | T19 |
| 850-hPa Vector Wind | T20 |
| 200-hPa Vector Wind | T21 |
| 200-hPa Streamfunction | T22 |
| 200-hPa Divergence | T23 |
| 200-hPa Velocity Potential and Divergent Wind | T24 |
| OLR | T25 |
| SSM/I Tropical Precipitation Estimates | T26 |
| Cloud Liquid Water | T27 |
| Precipitable Water | T28 |
| Divergence & E-W Divergent Circulation | T29 - T30 |
| Pacific Zonal Wind & N-S Divergent Circulation | T31 - T32 |

Appendix 1: Outside Contributions

| | |
|---|---|
| Tropical Drifting Buoys | A1.1 |

FIGURE


Pacific Wind Stress and Anomalies A1.2
Satellite-Derived Surface Currents A1.3 - A1.4

FORECAST FORUM

Discussion . . . . . page 49

Canonical Correlation Analysis Forecasts F1 - F2
NCEP Coupled Model Forecasts F3 - F4
NCEP Markov Model Forecasts F5 - F6
LDEO Model Forecasts F7 - F8
Linear Inverse Modeling Forecasts F9 - F10
ENSO-CLIPER Model Forecast F11
Model Forecasts of Niño 3.4 F12

EXTRATROPICS

Highlights . . . . . page 64

Table of Teleconnection Indices . . . . . page 66

Global Surface Temperature E1
Temperature Anomalies (Land Only) E2
Global Precipitation E3
Regional Precipitation Estimates E4 - E5
U. S. Precipitation E6

Northern Hemisphere

Teleconnection Indices E7
Mean and Anomalous SLP E8
Mean and Anomalous 500-hPa heights E9
Mean and Anomalous 300-hPa Wind Vectors E10
500-hPa Persistence E11
Time-Longitude Sections of 500-hPa Height Anomalies E12
700-hPa Storm Track E13

Southern Hemisphere

Mean and Anomalous SLP E14
Mean and Anomalous 500-hPa heights E15
Mean and Anomalous 300-hPa Wind Vectors E16
500-hPa Persistence E17
Time-Longitude Sections of 500-hPa Height Anomalies E18

Stratosphere

Height Anomalies S1 - S2
Temperatures S3 - S4
Ozone S5 - S6
Vertical Component of EP Flux S7
Ozone Hole S8

Appendix 2: Additional Figures

Arctic Oscillation and 500-hPa Anomalies A2.1
Snow Cover A2.2

# Tropical Highlights - September 2019

During September 2019, sea surface temperatures (SSTs) were below-average in the eastern equatorial Pacific and above-average in the western equatorial Pacific (Fig. T18, Table T2). The latest monthly Niño indices were -0.8°C for the Niño 1+2 region, -0.02°C for the Niño 3.4 region and +0.6°C for the Niño 4 region (Table T2, Fig. T5). The depth of the oceanic thermocline (measured by the depth of the 20°C isotherm) was above-average in the western equatorial Pacific and below-average in the eastern equatorial Pacific (Figs. T15, T16). The corresponding sub-surface temperatures were 0-2°C above average in the western equatorial Pacific, and 1-3°C below average in the eastern equatorial Pacific (Fig. T17).

Also during September, the lower-level easterly winds were weaker-than-average (indicated by westerly anomalies) across the equatorial Pacific (Table T1, Fig. T20). The upper-level wind anomalies were easterly over much of the equatorial Pacific (Table T1, Fig. T21). Meanwhile, tropical convection was suppressed over Indonesia as well as across the tropical Pacific (Figs. T25, E3). Collectively, these oceanic and atmospheric anomalies reflected ENSO-neutral conditions.

For the latest status of the ENSO cycle see the ENSO Diagnostic Discussion at:
http://www.cpc.ncep.noaa.gov/products/analysis_monitoring/enso_advisory/index.html

| Month | SLP Anomalies | | Tahiti minus Darwin SOI | 850-hPa Zonal Wind Index | | | 200-hPa Wind Index | OLR Index |
|---|---|---|---|---|---|---|---|---|
| | Tahiti | Darwin | | 5N-5S 135E-180 | 5N-5S 175W-140W | 5N-5S 135W-120W | 5N-5S 165W-110W | 5N-5S 160E-160W |
| SEP 19 | 0.2 | 2.3 | -1.2 | -0.7 | -0.8 | -0.6 | -1.1 | 0.6 |
| AUG 19 | 0.7 | 0.9 | -0.1 | -0.3 | 0.5 | 0.1 | 0.1 | 0.1 |
| JUL 19 | 0.1 | 0.8 | -0.4 | -0.4 | -0.6 | -0.5 | -0.8 | 0.2 |
| JUN 19 | 0.0 | 0.9 | -0.5 | 0.5 | 0.4 | 0.2 | 0.5 | -0.3 |
| MAY 19 | 0.1 | 0.8 | -0.4 | -1.3 | -0.5 | -0.6 | -0.4 | -0.7 |
| APR 19 | 0.5 | 0.2 | 0.1 | 0.7 | 0.5 | 0.1 | 0.4 | -0.8 |
| MAR 19 | -0.5 | 0.1 | -0.3 | -0.2 | -0.1 | 0.4 | 0.1 | -1.2 |
| FEB 19 | -0.4 | 2.2 | -1.4 | -1.6 | -0.7 | -0.7 | -0.2 | -1.9 |
| JAN 19 | 0.1 | 0.1 | 0.0 | -1.0 | -0.4 | -0.5 | 0.6 | -0.6 |
| DEC 18 | 0.7 | -1.2 | 1.0 | 0.2 | 0.3 | -0.5 | 0.2 | -0.1 |
| NOV 18 | 0.4 | 0.5 | -0.1 | -0.2 | -0.3 | -0.7 | -0.1 | -0.3 |
| OCT 18 | 0.9 | 0.2 | 0.4 | -0.2 | -0.8 | -1.9 | -0.5 | 0.4 |
| SEP 18 | -1.6 | 0.1 | -0.9 | -1.1 | -0.7 | -0.5 | -0.5 | 0.3 |

TABLE T1 - Atmospheric index values for the most recent 12 months. Indices are standardized by the mean annual standard deviation, except for the Tahiti and Darwin SLP anomalies which are in units of hPa. Positive (negative) values of 200-hPa zonal wind index imply westerly (easterly) anomalies. Positive (negative) values of 850-hPa zonal wind indices imply easterly (westerly) anomalies. Anomalies are departures from the 1981-2010 base period means.

| Month | PACIFIC SST | | | | | | | | ATLANTIC SST | | | | GLOBAL | |
|---|---|---|---|---|---|---|---|---|---|---|---|---|---|---|
| | Niño 1+2 0-10S 90W-80W | | Niño 3 5N-5S 150W-90W | | Niño 3.4 5N-5S 170W-120W | | Niño 4 5N-5S 160E-150W | | N.ATL 5N-20N 60W-30W | | S. ATL 0-20S 30W-10E | | TROPICS 10N-10S 0-360 | |
| SEP 19 | -0.8 | 19.5 | -0.2 | 24.6 | -0.0 | 26.7 | 0.6 | 29.3 | 0.4 | 28.5 | -0.0 | 23.0 | 0.1 | 27.3 |
| AUG 19 | -0.4 | 20.2 | -0.1 | 24.9 | 0.2 | 27.0 | 0.9 | 29.5 | 0.0 | 27.8 | -0.2 | 22.9 | 0.2 | 27.4 |
| JUL 19 | -0.3 | 21.3 | 0.1 | 25.7 | 0.4 | 27.6 | 0.9 | 29.7 | 0.1 | 27.3 | 0.0 | 23.8 | 0.3 | 27.7 |
| JUN 19 | -0.3 | 22.6 | 0.4 | 26.8 | 0.6 | 28.2 | 0.8 | 29.6 | 0.1 | 26.9 | 0.1 | 25.0 | 0.3 | 28.3 |
| MAY 19 | 0.2 | 24.4 | 0.6 | 27.7 | 0.7 | 28.6 | 0.8 | 29.6 | 0.1 | 26.4 | 0.2 | 26.4 | 0.4 | 28.8 |
| APR 19 | 0.1 | 25.7 | 0.7 | 28.2 | 0.8 | 28.6 | 0.7 | 29.2 | 0.2 | 26.1 | 0.5 | 27.5 | 0.4 | 29.0 |
| MAR 19 | 0.3 | 26.9 | 0.7 | 27.9 | 1.0 | 28.2 | 0.9 | 29.1 | -0.1 | 25.6 | 0.6 | 27.7 | 0.4 | 28.6 |
| FEB 19 | 0.3 | 26.4 | 0.5 | 26.9 | 0.7 | 27.4 | 1.0 | 29.1 | 0.2 | 25.8 | 0.2 | 26.8 | 0.3 | 28.2 |
| JAN 19 | 0.5 | 25.1 | 0.5 | 26.2 | 0.5 | 27.1 | 0.7 | 29.0 | -0.3 | 25.7 | 0.2 | 25.8 | 0.3 | 27.9 |
| DEC 18 | 0.8 | 23.6 | 1.0 | 26.1 | 1.0 | 27.5 | 1.0 | 29.5 | -0.4 | 26.4 | 0.2 | 24.9 | 0.4 | 28.1 |
| NOV 18 | 0.7 | 22.8 | 1.0 | 26.0 | 1.0 | 27.6 | 1.0 | 29.6 | -0.3 | 27.4 | -0.0 | 24.0 | 0.4 | 28.1 |
| OCT 18 | 0.4 | 21.2 | 0.9 | 25.8 | 0.9 | 27.6 | 1.0 | 29.6 | -0.1 | 28.0 | 0.1 | 23.4 | 0.3 | 27.8 |
| SEP 18 | -0.1 | 20.3 | 0.3 | 25.2 | 0.3 | 27.1 | 0.5 | 29.1 | 0.1 | 28.2 | -0.1 | 22.9 | 0.2 | 27.4 |

TABLE T2. Mean and anomalous sea surface temperature (°C) for the most recent 12 months. Anomalies are departures from the 1981–2010 adjusted OI climatology (Smith and Reynolds 1998, *J. Climate*, **11**, 3320-3323).

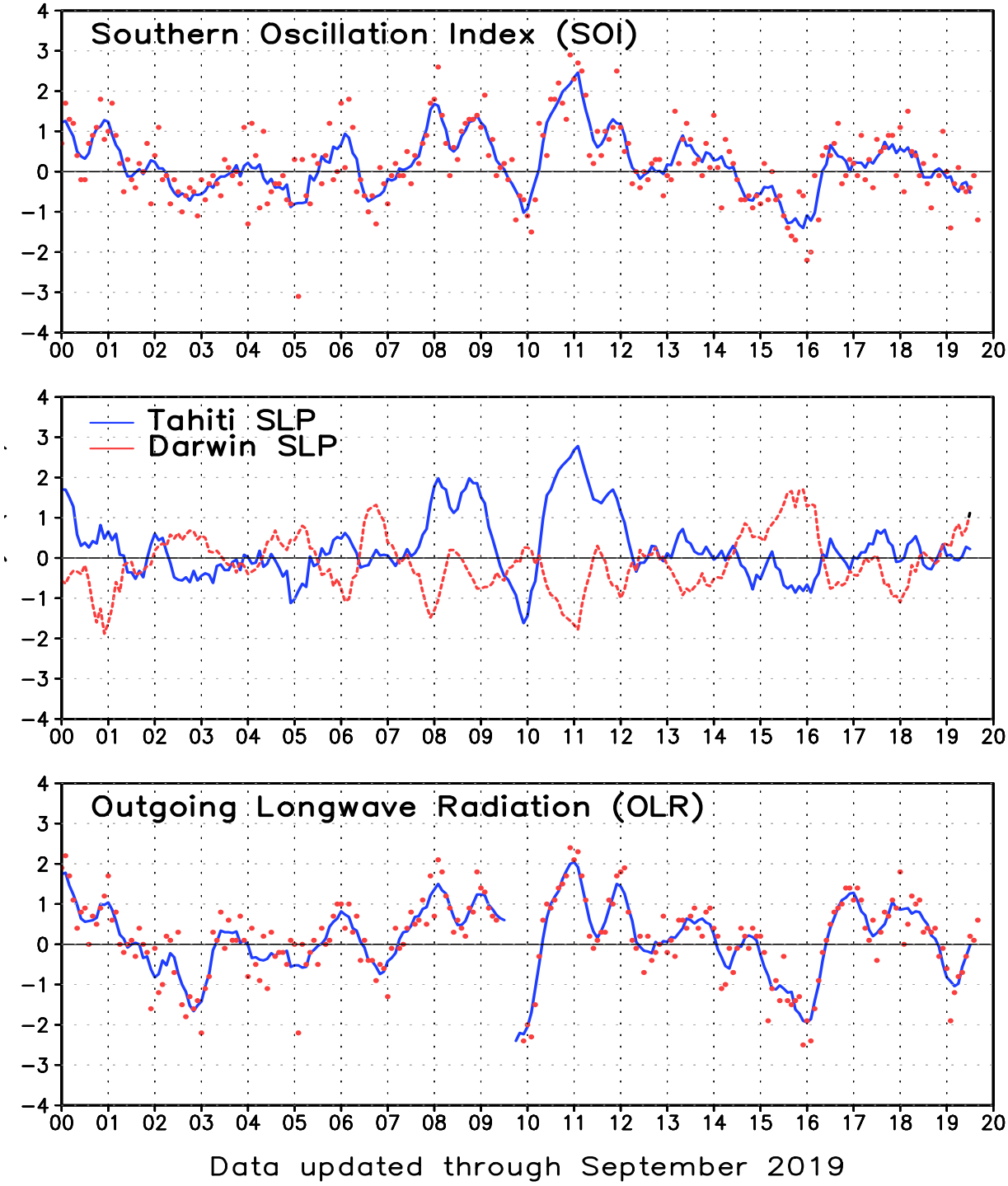


FIGURE T1. Five-month running mean of the Southern Oscillation Index (SOI) (top), sea-level pressure anomaly (hPa) at Darwin and Tahiti (middle), and outgoing longwave radiation anomaly (OLR) averaged over the area 5N-5S, 160E-160W (bottom). Anomalies in the top and middle panels are departures from the 1981-2010 base period means and are normalized by the mean annual standard deviation. Anomalies in the bottom panel are departures from the 1981-2010 base period means. Individual monthly values are indicated by "x"s in the top and bottom panels. The x-axis labels are centered on July.

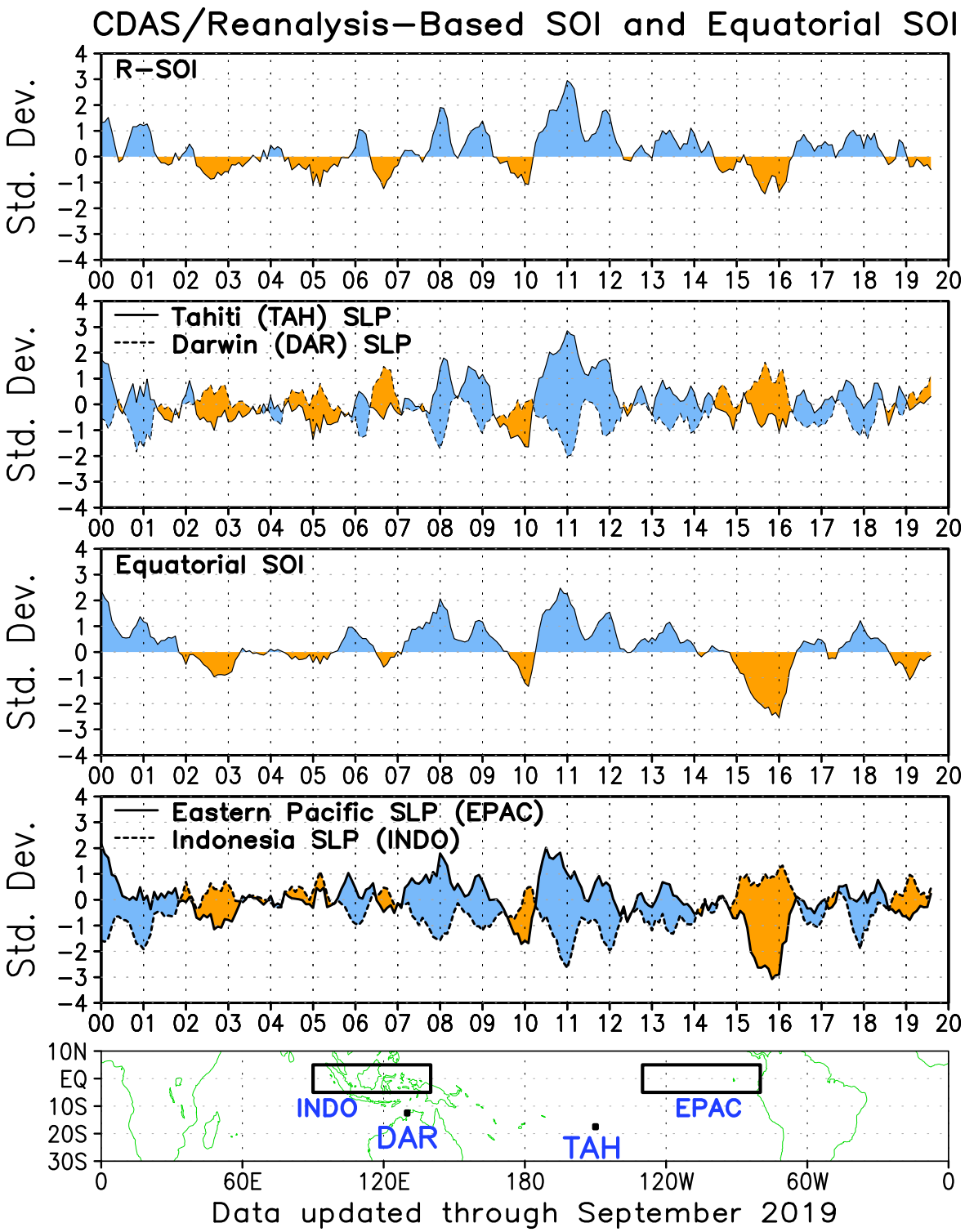


FIGURE T2. Three-month running mean of a CDAS/Reanalysis-derived (a) Southern Oscillation Index (RSOI), (b) standardized pressure anomalies near Tahiti (solid) and Darwin (dashed), (c) an equatorial SOI ([EPAC] - [INDO]), and (d) standardized equatorial pressure anomalies for (EPAC) (solid) and (INDO) (dashed). Anomalies are departures from the 1981-2010 base period means and are normalized by the mean annual standard deviation. The equatorial SOI is calculated as the normalized difference between the standardized anomalies averaged between 5°N–5°S, 80°W–130°W (EPAC) and 5°N–5°S, 90°E–140°E (INDO).

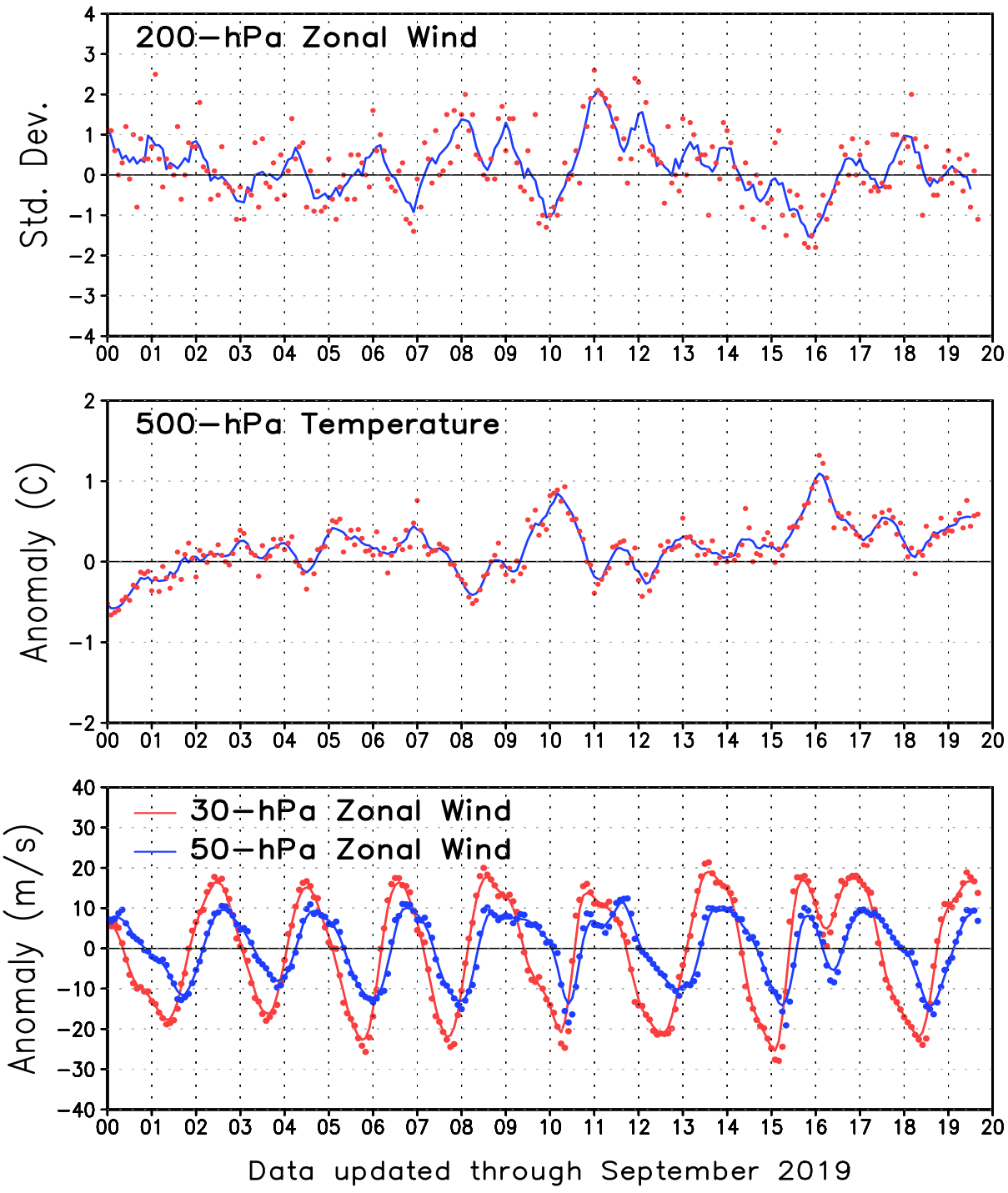


FIGURE T3. Five-month running mean (solid lines) and individual monthly mean (dots) of the 200-hPa zonal wind anomalies averaged over the area 5N-5S, 165W-110W (top), the 500-hPa virtual temperature anomalies averaged over the latitude band 20N-20S (middle), and the equatorial zonally-averaged zonal wind anomalies at 30-hPa (red) and 50-hPa (blue) (bottom). In the top panel, anomalies are normalized by the mean annual standard deviation. Anomalies are departures from the 1981-2010 base period means. The x-axis labels are centered on January.

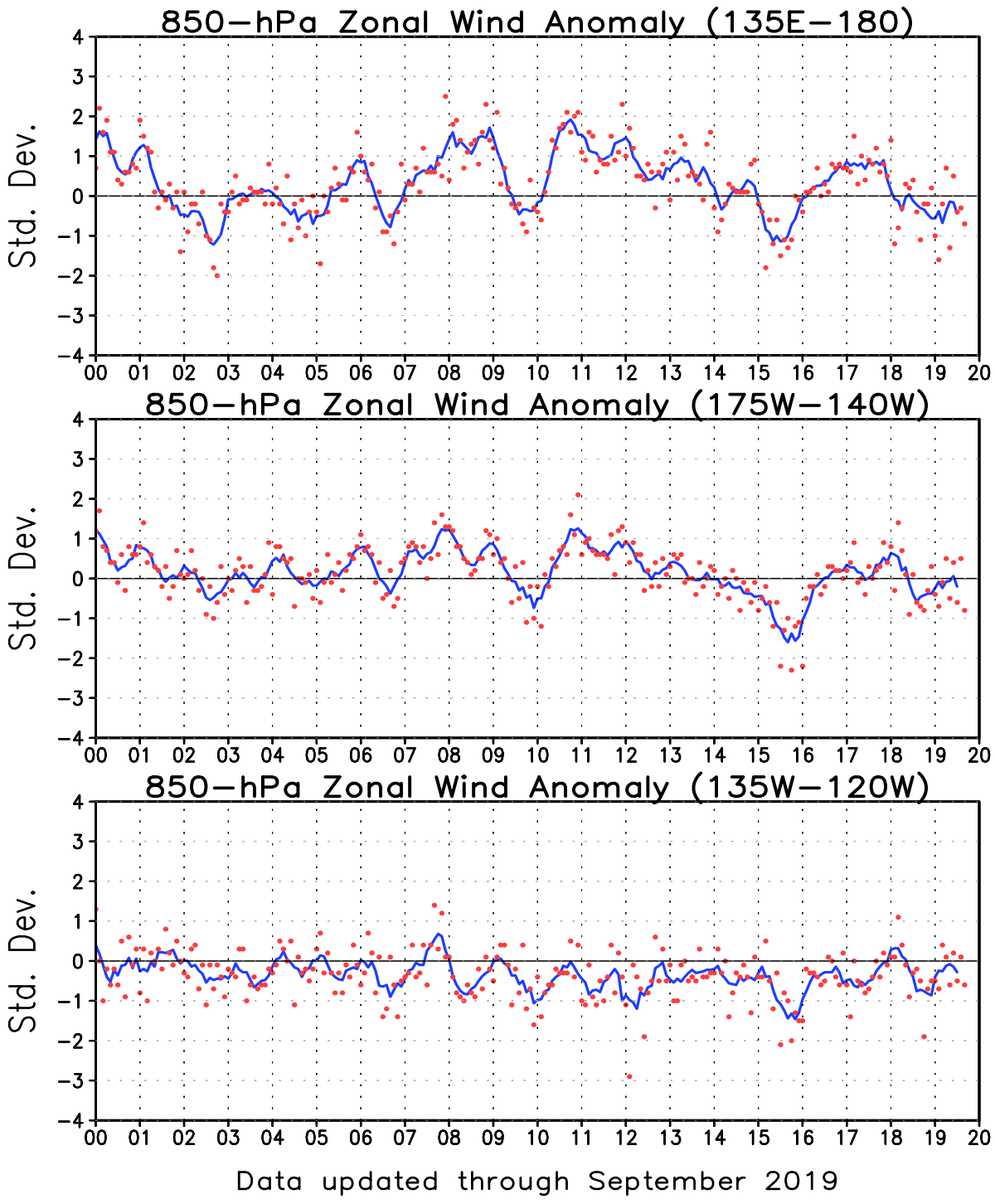


FIGURE T4. Five-month running mean (solid line) and individual monthly mean (dots) of the standardized 850-hPa zonal wind anomaly index in the latitude belt 5N-5S for 135E-180 (top), 175W-140W (middle) and 135W-120W (bottom). Anomalies are departures from the 1981-2010 base period means and are normalized by the mean annual standard deviation.The x-axis labels are centered on January. Positive (negative) values indicate easterly (westerly) anomalies.

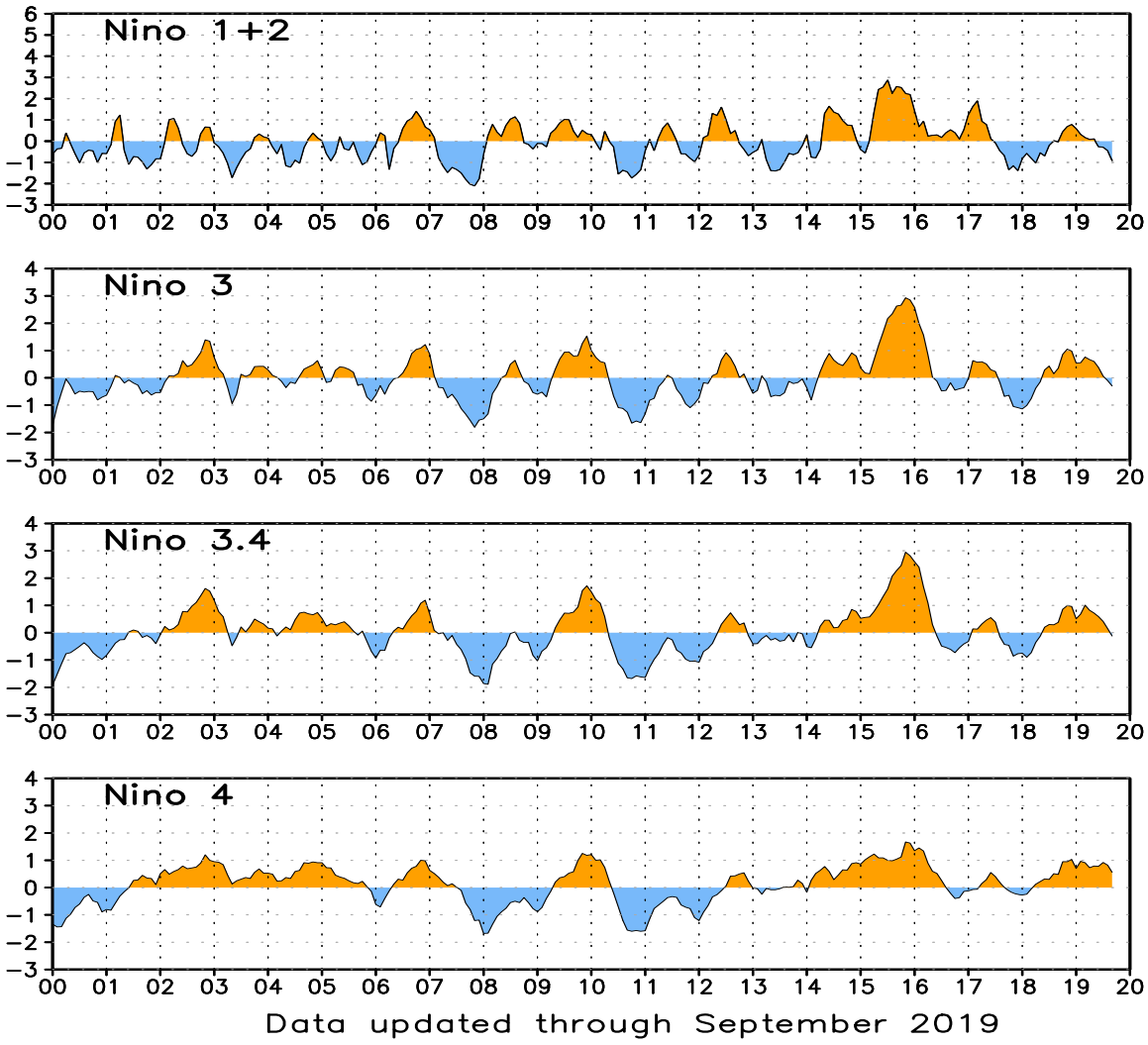


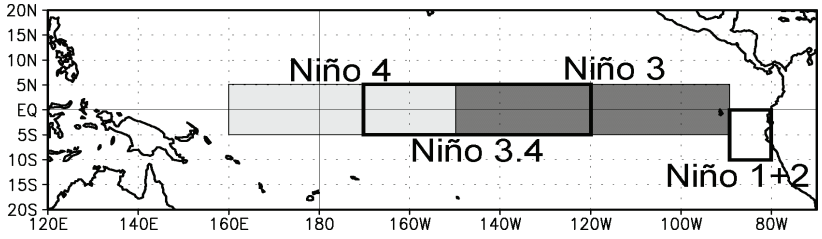


FIGURE T5. Nino region indices, calculated as the area-averaged sea surface temperature anomalies (C) for the specified region. The Nino 1+2 region (top) covers the extreme eastern equatorial Pacific between 0-10S, 90W-80W. The Nino-3 region (2nd from top) spans the eastern equatorial Pacific between 5N-5S, 150W-90W. The Nino 3.4 region 3rd from top) spans the east-central equatorial Pacific between 5N-5S, 170W-120W. The Nino 4 region (bottom) spans the date line and covers the area 5N-5S, 160E-150W. Anomalies are departures from the 1981-2010 base period monthly means *(Smith and Reynolds 1998, J. Climate, 11, 3320-3323)*. Monthly values of each index are also displayed in Table 2.

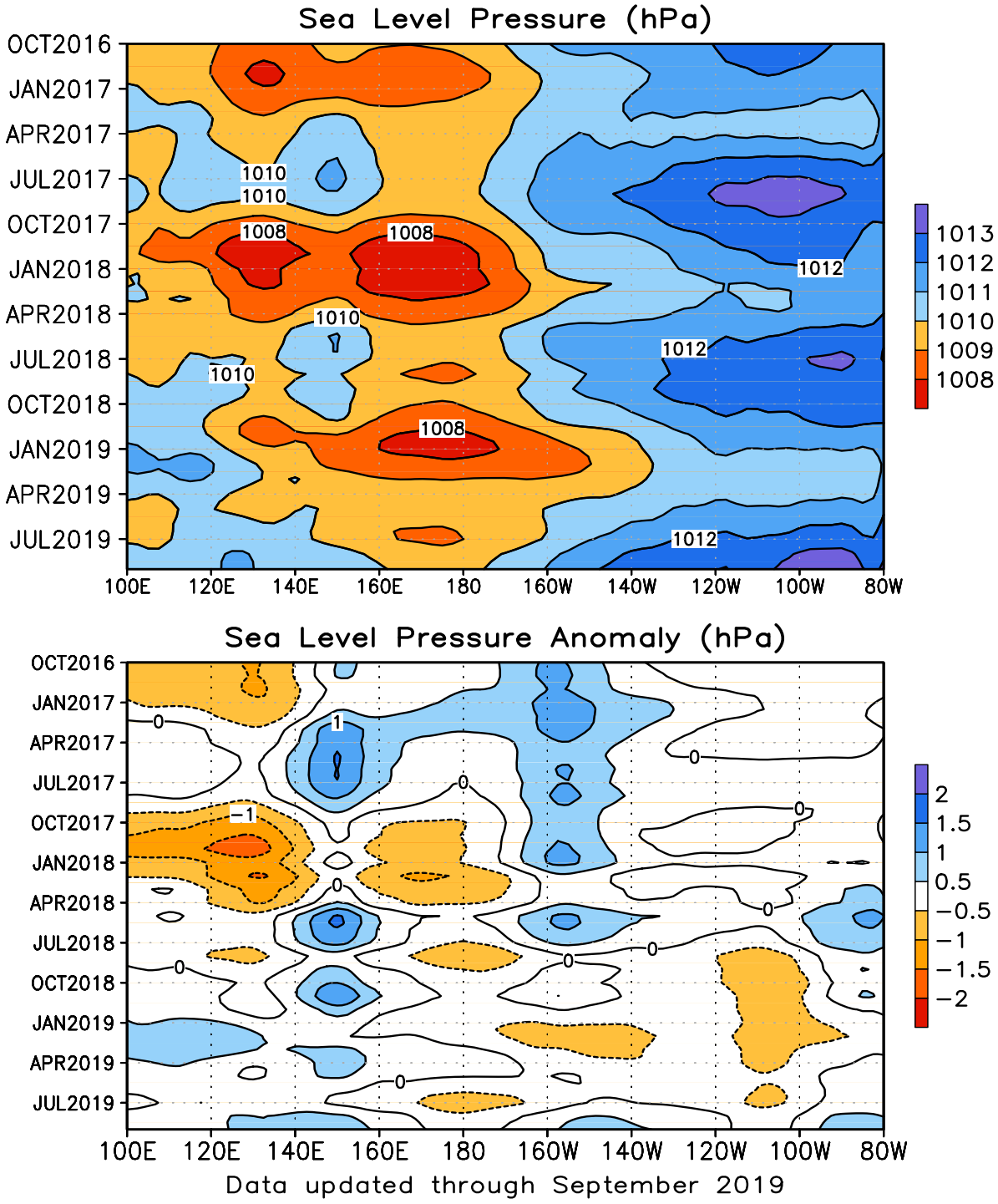


FIGURE T6. Time-longitude section of mean (top) and anomalous (bottom) sea level pressure (SLP) averaged between 5N-5S (CDAS/Reanalysis). Contour interval is 1.0 hPa (top) and 0.5 hPa (bottom). Dashed contours in bottom panel indicate negative anomalies. Anomalies are departures from the 1981-2010 base period monthly means. The data are smoothed temporally using a 3-month running average.

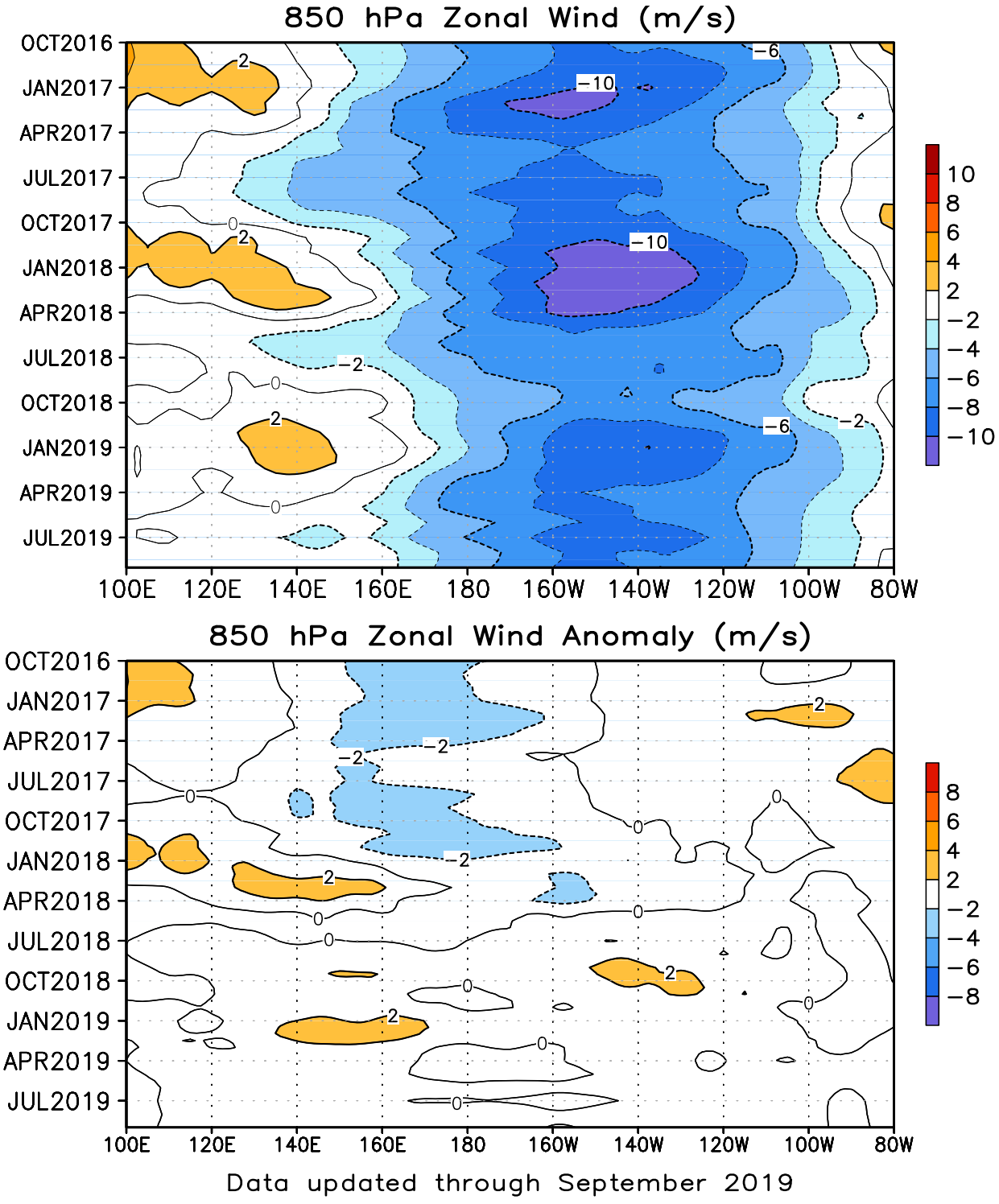


FIGURE T7. Time-longitude section of mean (top) and anomalous (bottom) 850-hPa zonal wind averaged between 5N-5S (CDAS/Reanalysis). Contour interval is 2 $ms^{-1}$. Blue shading and dashed contours indicate easterlies (top) and easterly anomalies (bottom). Anomalies are departures from the 1981-2010 base period monthly means. The data are smoothed temporally using a 3-month running average.

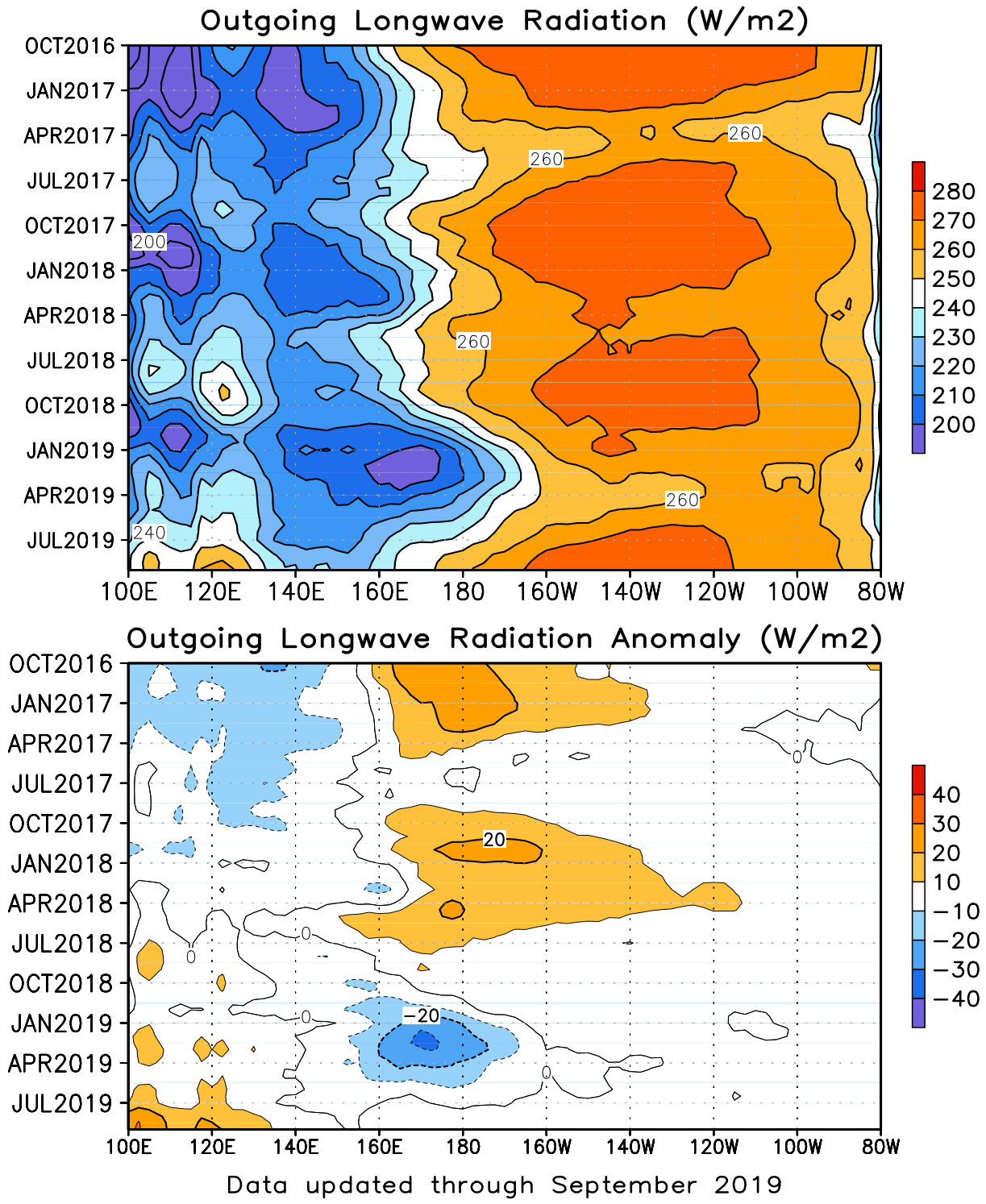


FIGURE T8. Time-longitude section of mean (top) and anomalous (bottom) outgoing longwave radiation (OLR) averaged between 5N-5S. Contour interval is 10 $Wm^{-2}$. Dashed contours in bottom panel indicate negative OLR anomalies. Anomalies are departures from the 1981-2010 base period monthly means. The data are smoothed temporally using a 3-month running average.

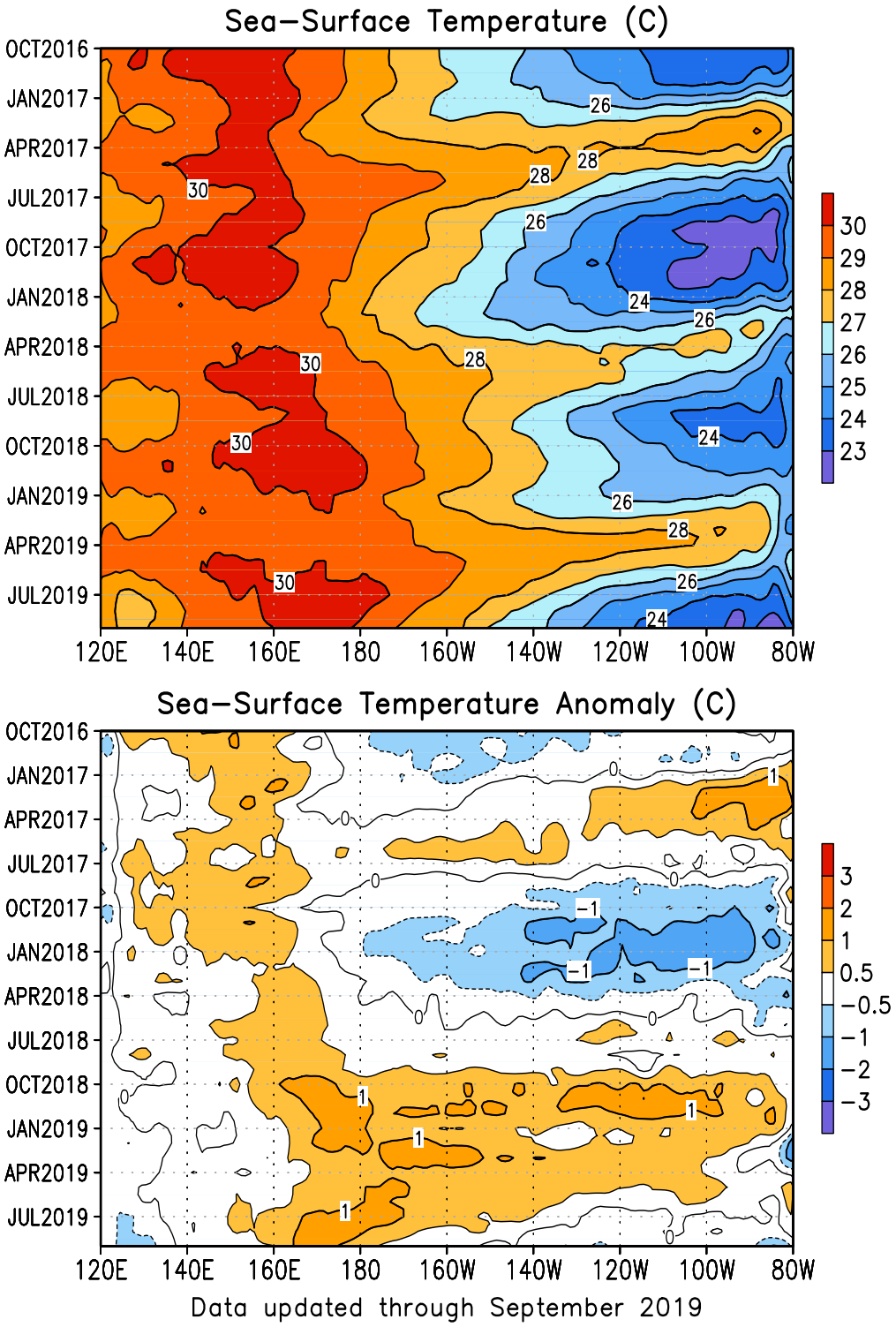


FIGURE T9. Time-longitude section of monthly mean (top) and anomalous (bottom) sea surface temperature (SST) averaged between 5N-5S. Contour interval is 1C (top) and 0.5C (bottom). Dashed contours in bottom panel indicate negative anomalies. Anomalies are departures from the 1981-2010 base period means (Smith and Reynolds 1998, *J. Climate*, **11**, 3320-3323).

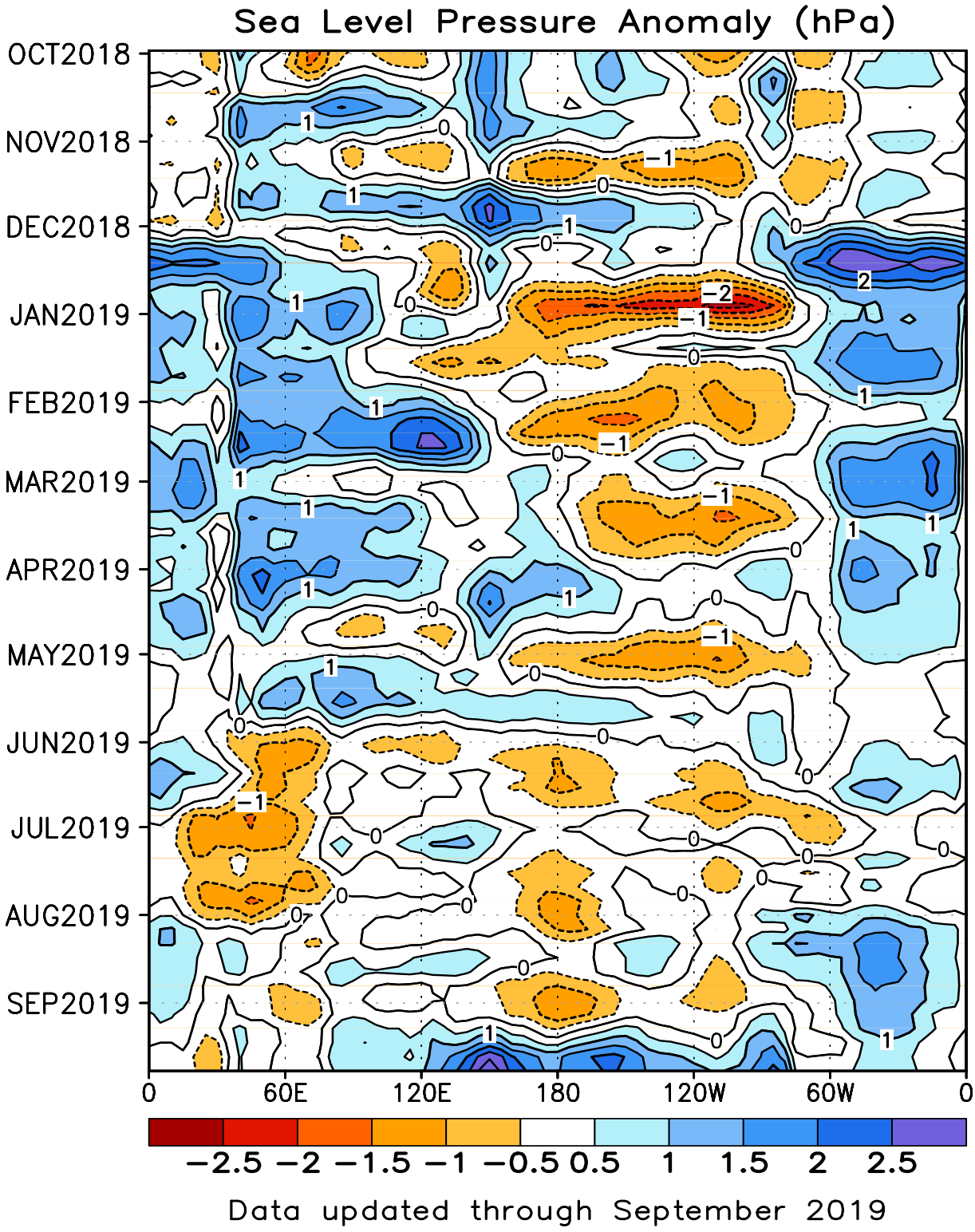


FIGURE T10. Time-longitude section of anomalous sea level pressure (hPa) averaged between 5N-5S (CDAS/Reanaysis). Contour interval is 1 hPa. Dashed contours indicate negative anomalies. Anomalies are departures from the 1981-2010 base period pentad means. The data are smoothed temporally using a 3-point running average.

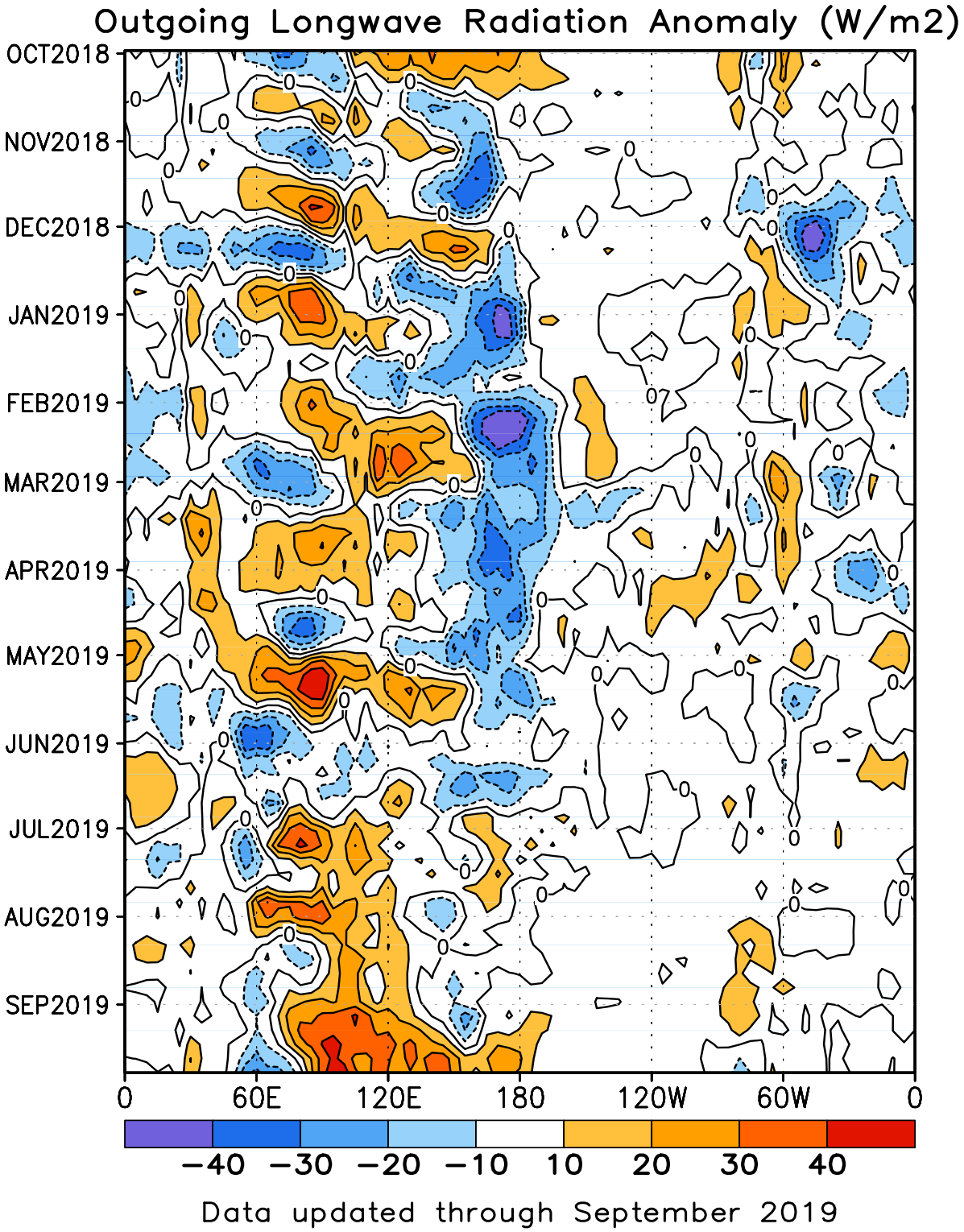


FIGURE T11. Time-longitude section of anomalous outgoing longwave radiation averaged between 5N-5S. Contour interval is 15 $Wm^{-2}$. Dashed contours indicate negative anomalies. Anomalies are departures from the 1981-2010 base period pentad means. The data are smoothed temporally using a 3-point running average.

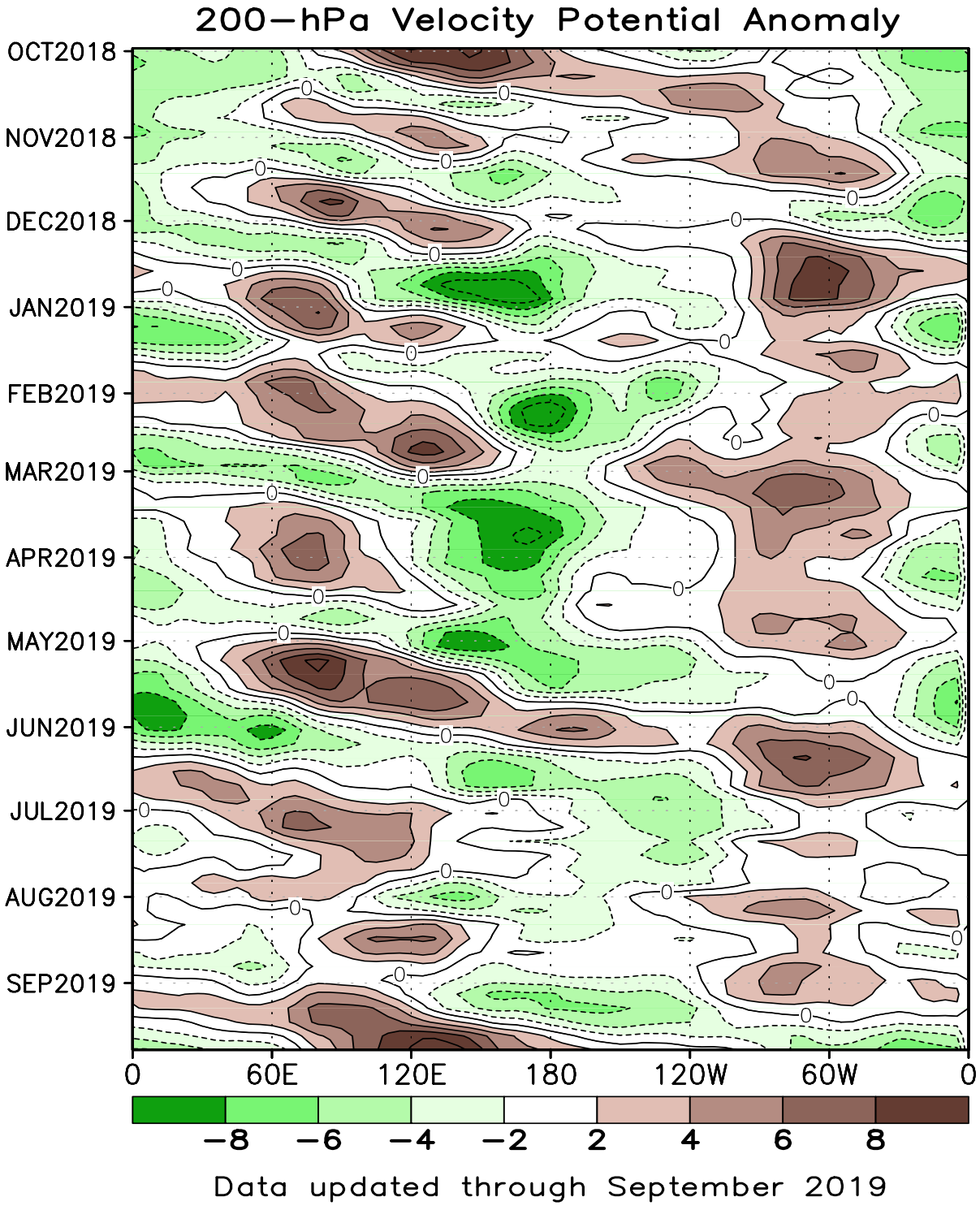


FIGURE T12. Time-longitude section of anomalous 200-hPa velocity potential averaged between 5N-5S (CDAS/Reanalysis). Contour interval is 3 x $10^6$ $m^2s^{-1}$. Dashed contours indicate negative anomalies. Anomalies are departures from the 1981-2010 base period pentad means. The data are smoothed temporally using a 3-point running average.

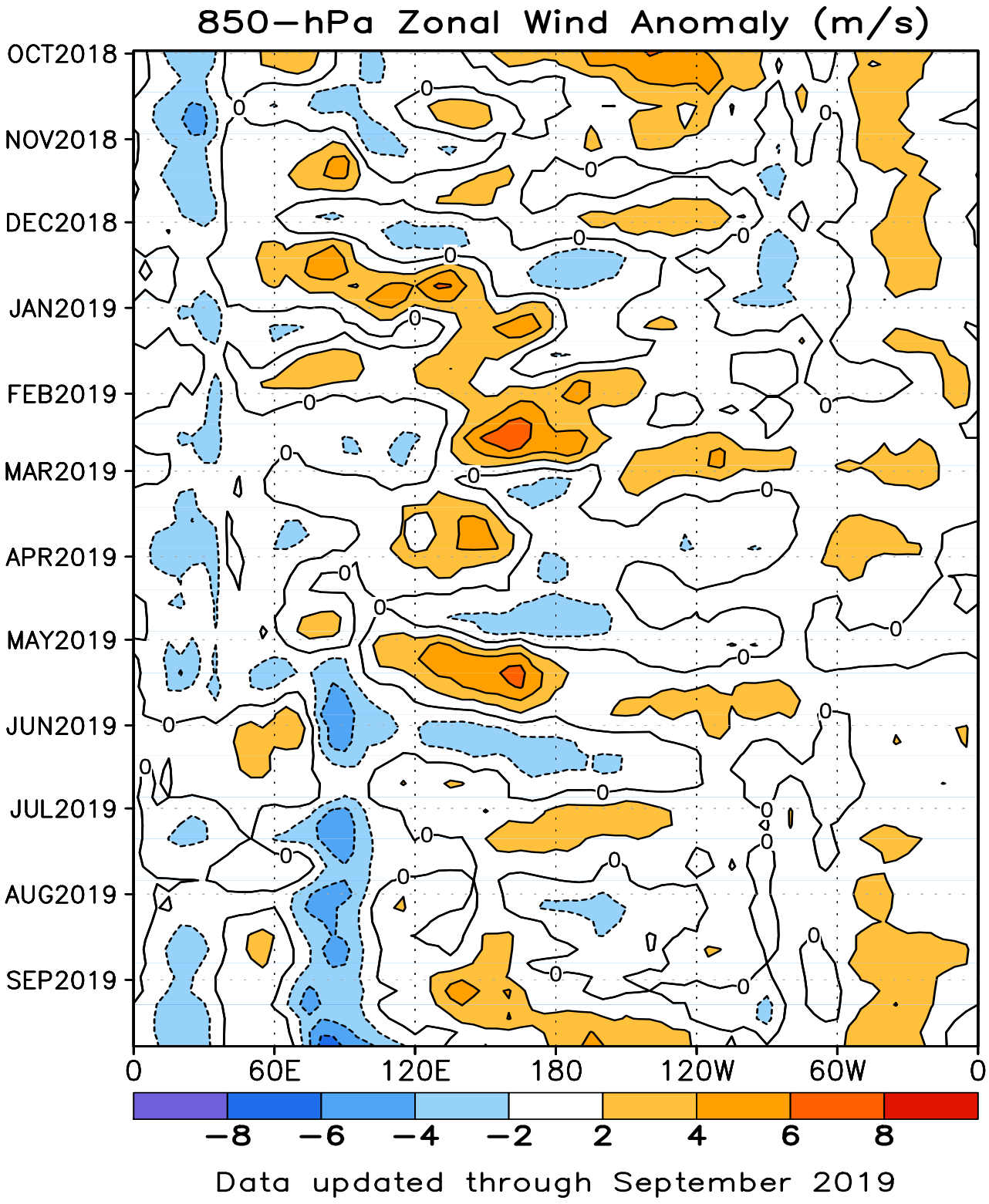


FIGURE T13. Time-longitude section of anomalous 850-hPa zonal wind averaged between 5N-5S (CDAS/Reanalysis). Contour interval is 2 $ms^{-1}$. Dashed contours indicate negative anomalies. Anomalies are departures from the 1981-2010 base period pentad means. The data are smoothed temporally by using a 3-point running average.

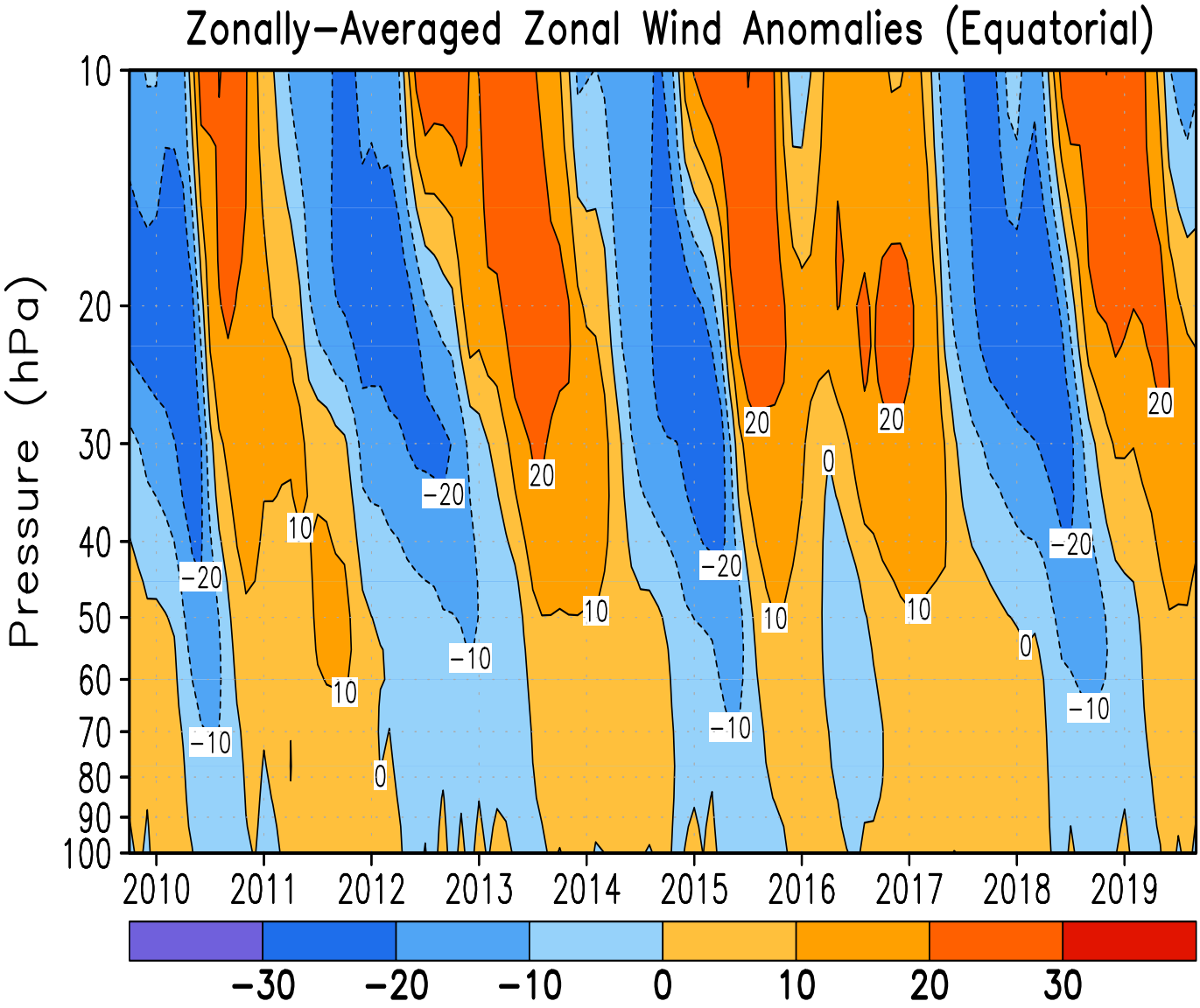


FIGURE T14. Equatorial time-height section of anomalous zonally-averaged zonal wind (m $s^{-1}$) (CDAS/Reanalysis). Contour interval is 10 $ms^{-1}$. Anomalies are departures from the 1981-2010 base period monthly means.

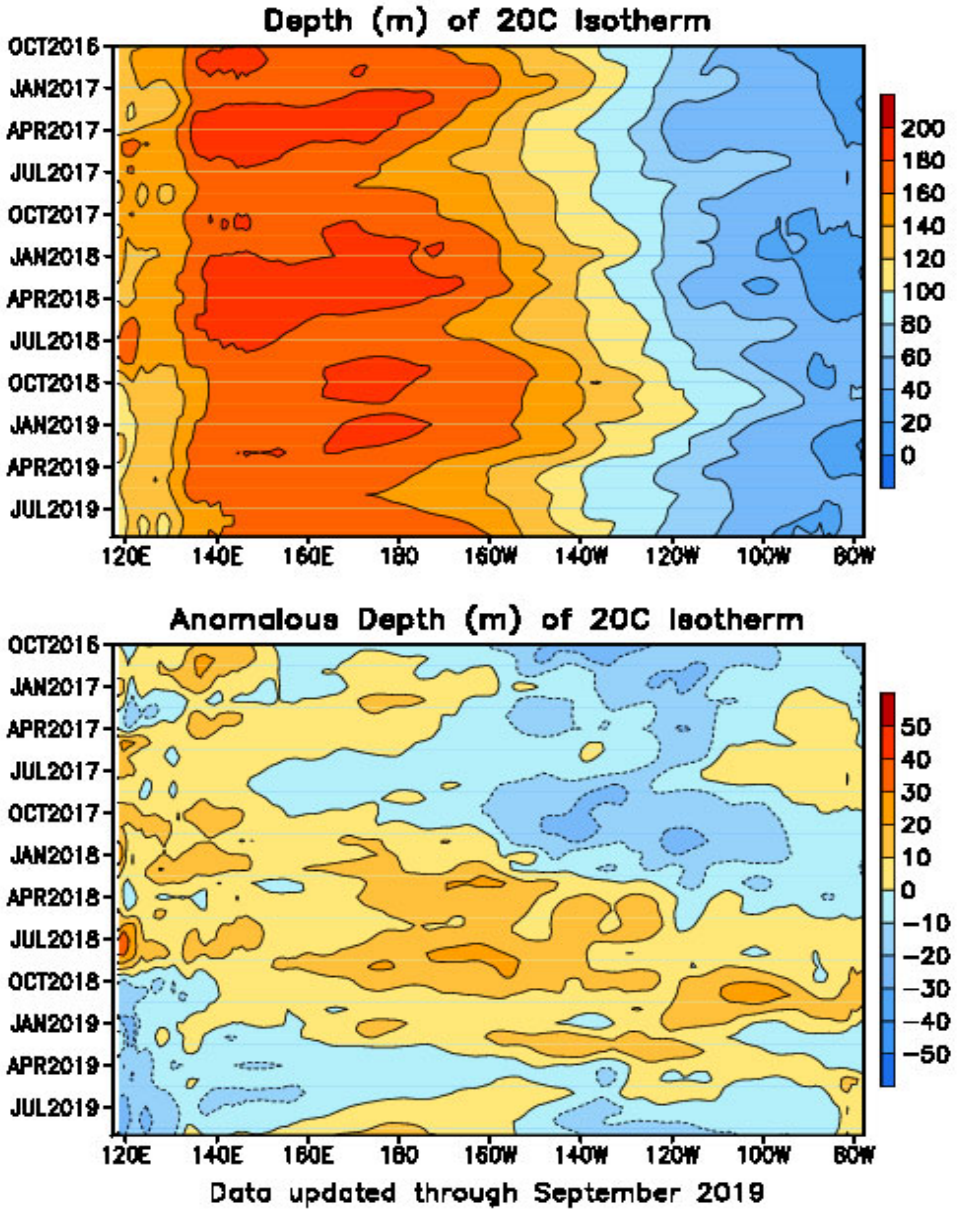


FIGURE T15. Mean (top) and anomalous (bottom) depth of the 20C isotherm averaged between 5N-5S in the Pacific Ocean. Data are derived from the NCEP's global ocean data assimilation system which assimilates oceanic observations into an oceanic GCM (Behringer, D. W., and Y. Xue, 2004: Evaluation of the global ocean data assimilation system at NCEP: The Pacific Ocean. AMS 84th Annual Meeting, Seattle, Washington, 11-15). The contour interval is 10 m. Dashed contours in bottom panel indicate negative anomalies. Anomalies are departures from the 1981-2010 base period means.

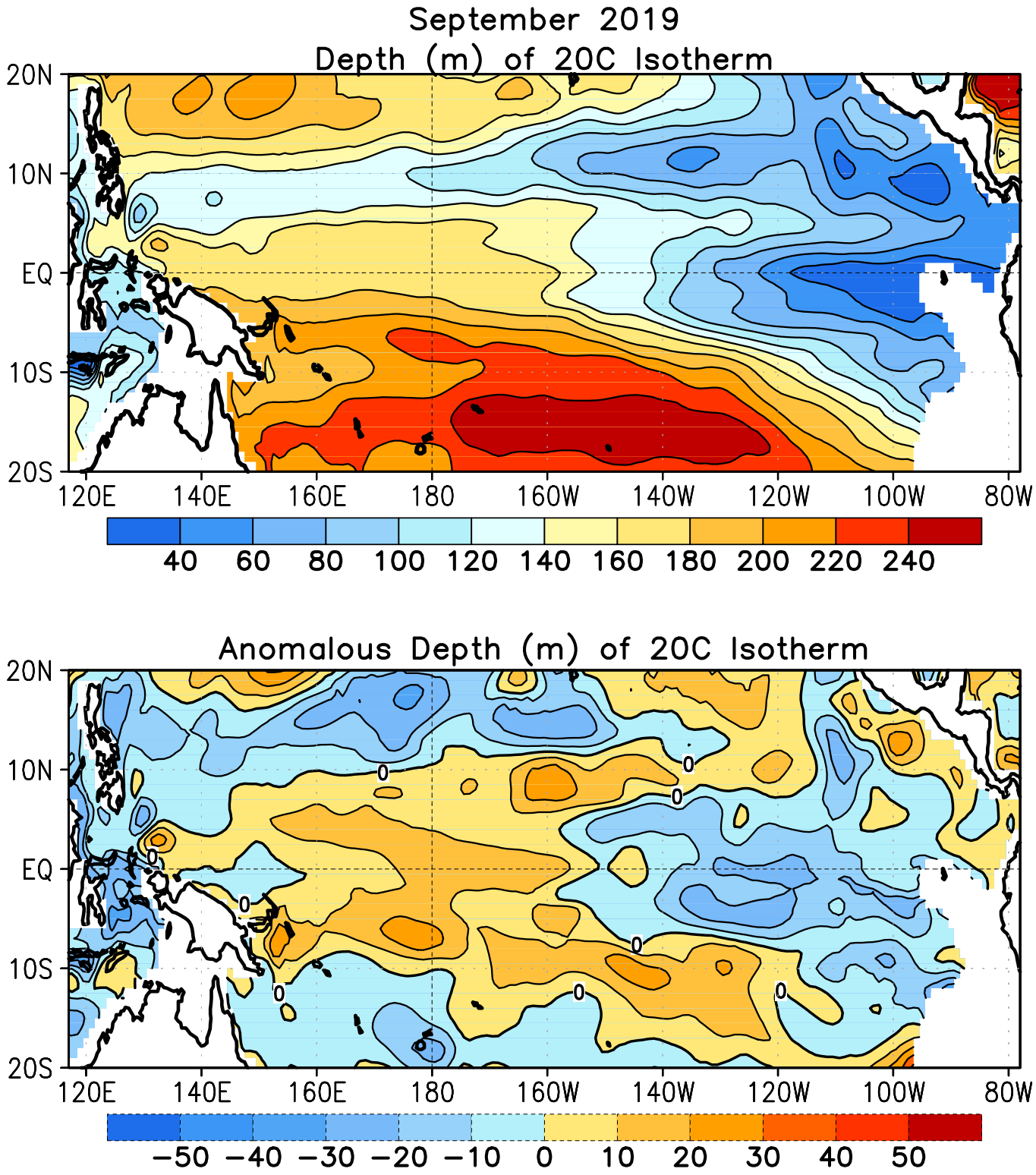


FIGURE T16. Mean (top) and anomalous (bottom) depth of the 20°C isotherm for SEP 2019. Contour interval is 40 m (top) and 10 m (bottom). Dashed contours in bottom panel indicate negative anomalies. Data are derived from the NCEP's global ocean data assimilation system version 2 which assimilates oceanic observations into an oceanic GCM (Xue, Y. and Behringer, D.W., 2006: Operational global ocean data assimilation system at NCEP, to be submitted to BAMS). Anomalies are departures from the 1981–2010 base period means.

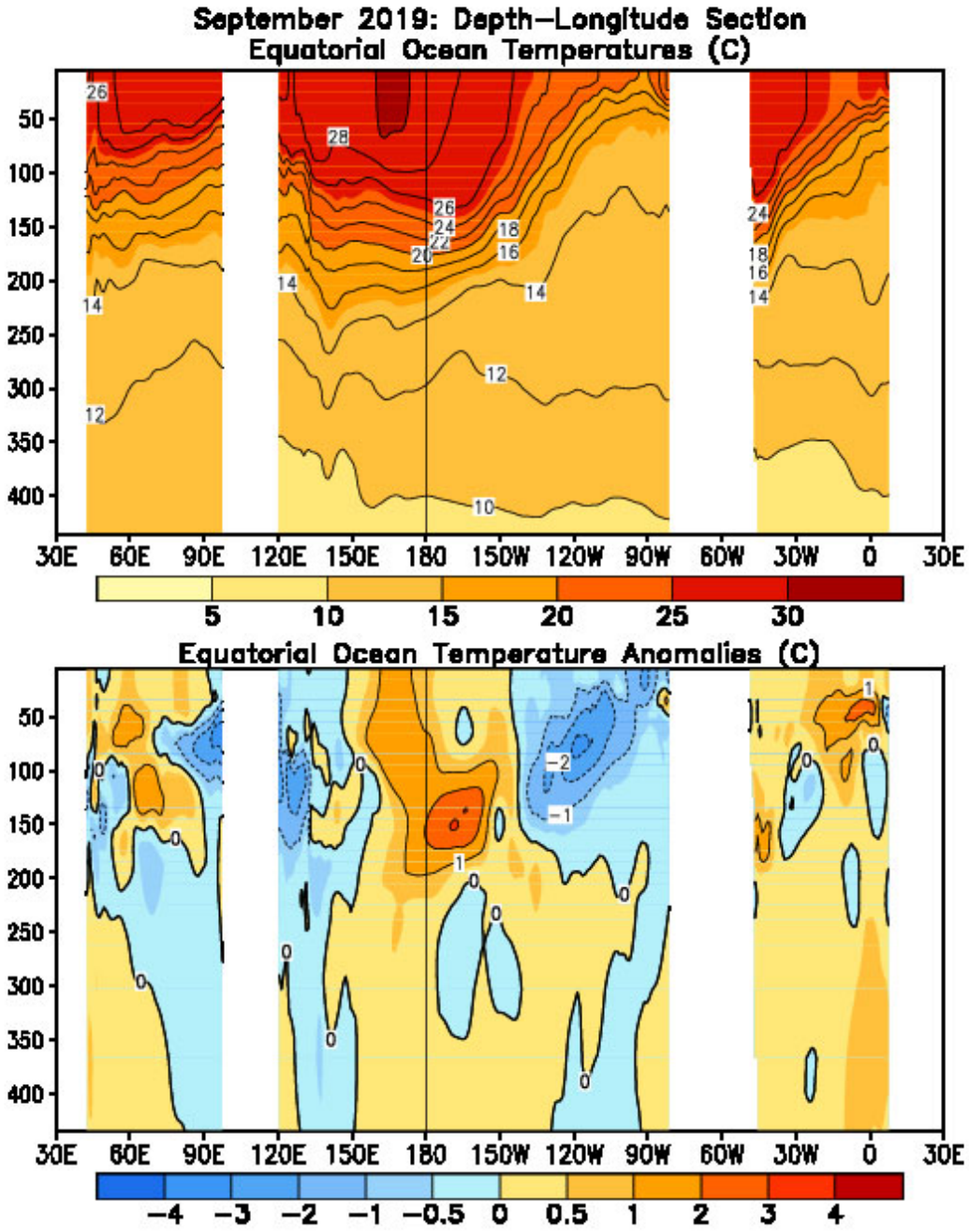


FIGURE T17. Equatorial depth-longitude section of ocean temperature (top) and ocean temperature anomalies (bottom) for SEP 2019. Contour interval is 1°C. Dashed contours in bottom panel indicate negative anomalies. Data are derived from the NCEP's global ocean data assimilation system version 2 which assimilates oceanic observations into an oceanic GCM (Xue, Y. and Behringer, D.W., 2006: Operational global ocean data assimilation system at NCEP, to be submitted to BAMS). Anomalies are departures from the 1981–2010 base period means.

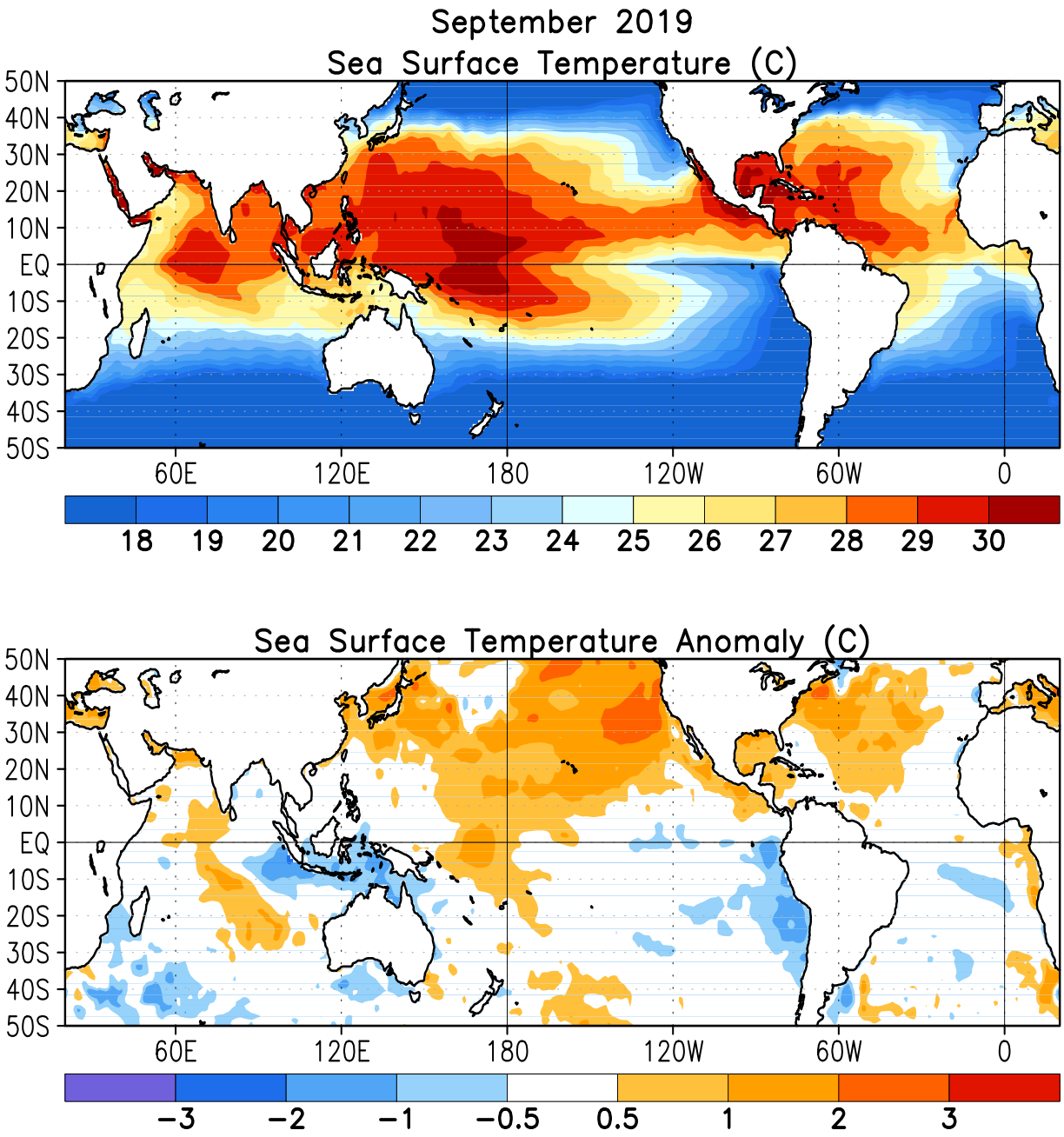


FIGURE T18. Mean (top) and anomalous (bottom) sea surface temperature (SST). Anomalies are departures from the 1981-2010 base period monthly means (Smith and Reynolds 1998, *J. Climate*, **11**, 3320-3323).

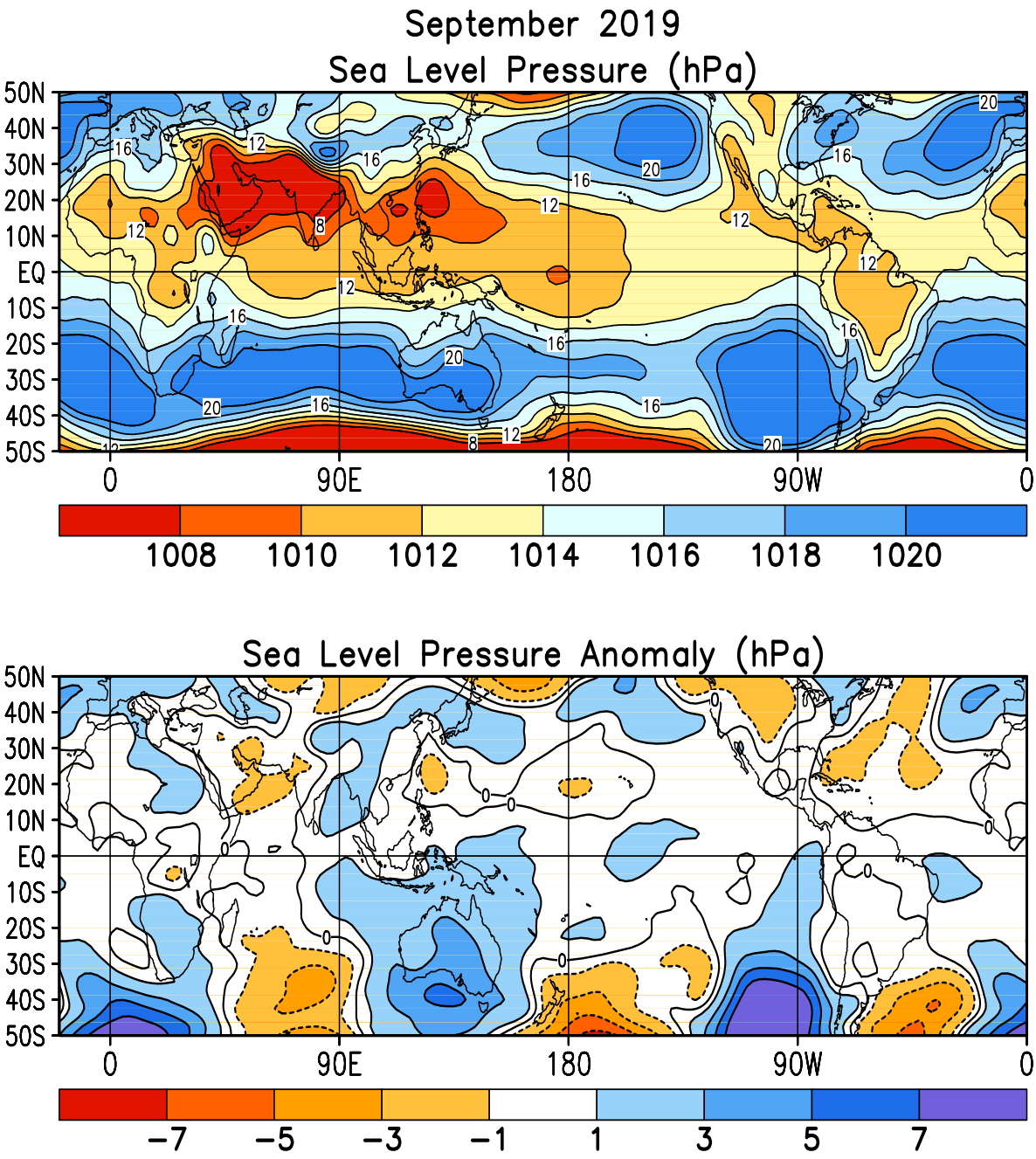


FIGURE T19. Mean (top) and anomalous (bottom) sea level pressure (SLP) (CDAS/Reanalysis). In top panel, 1000 hPa has been subtracted from contour labels, contour interval is 2 hPa, and values below 1000 hPa are indicated by dashed contours. In bottom panel, anomaly contour interval is 1 hPa and negative anomalies are indicated by dashed contours. Anomalies are departures from the 1981-2010 base period monthly means.

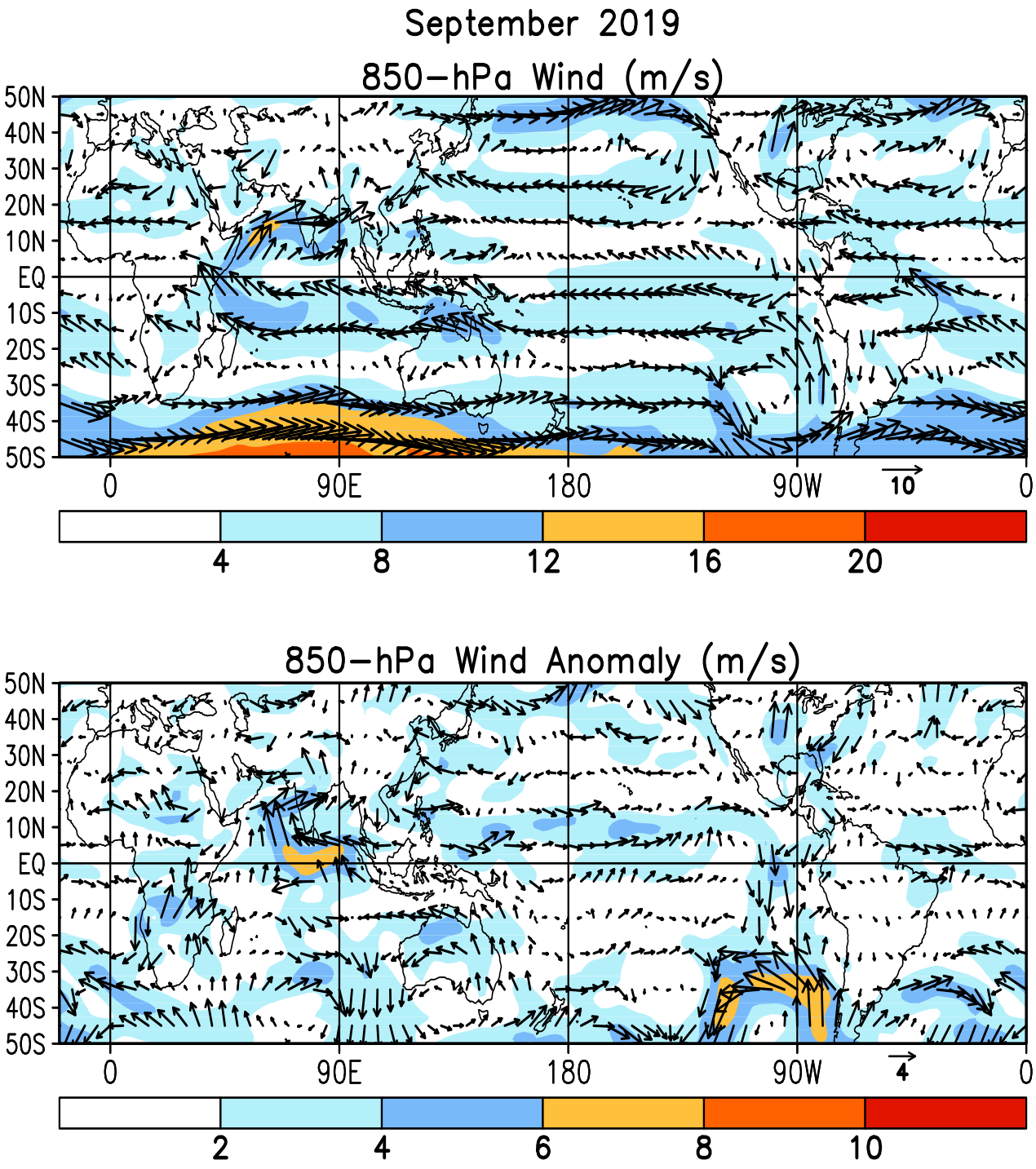


FIGURE T20. Mean (top) and anomalous (bottom) 850-hPa vector wind (CDAS/Reanaysis) for SEP 2019. Contour interval for isotachs is 4 $ms^{-1}$ (top) and 2 $ms^{-1}$ (bottom). Anomalies are departures from the 1981-2010 base period monthly means.

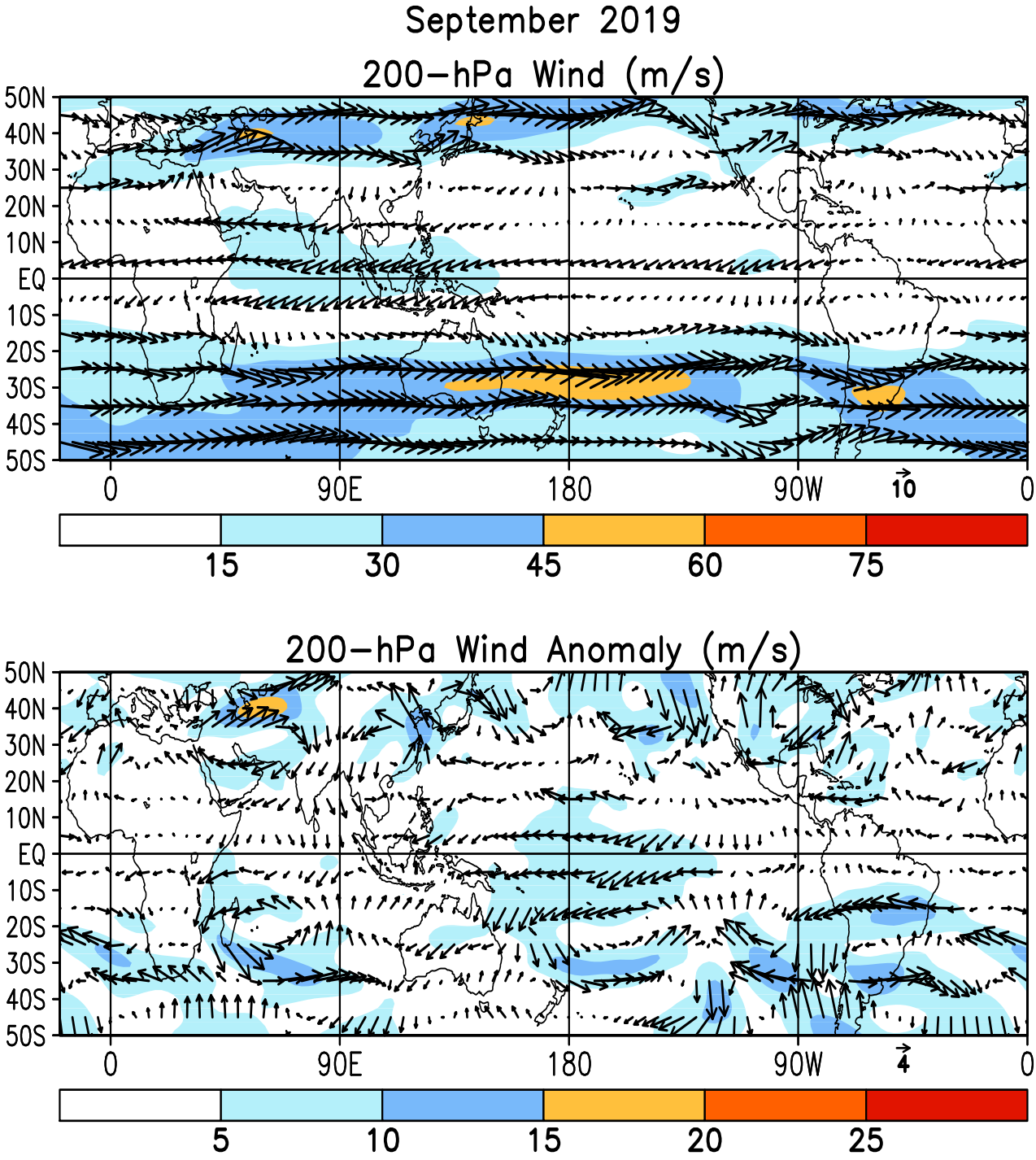


FIGURE T21. Mean (top) and anomalous (bottom) 200-hPa vector wind (CDAS/Reanalysis) for SEP 2019. Contour interval for isotachs is 15 $ms^{-1}$ (top) and 5 $ms^{-1}$ (bottom). Anomalies are departures from 1981-2010 base period monthly means.

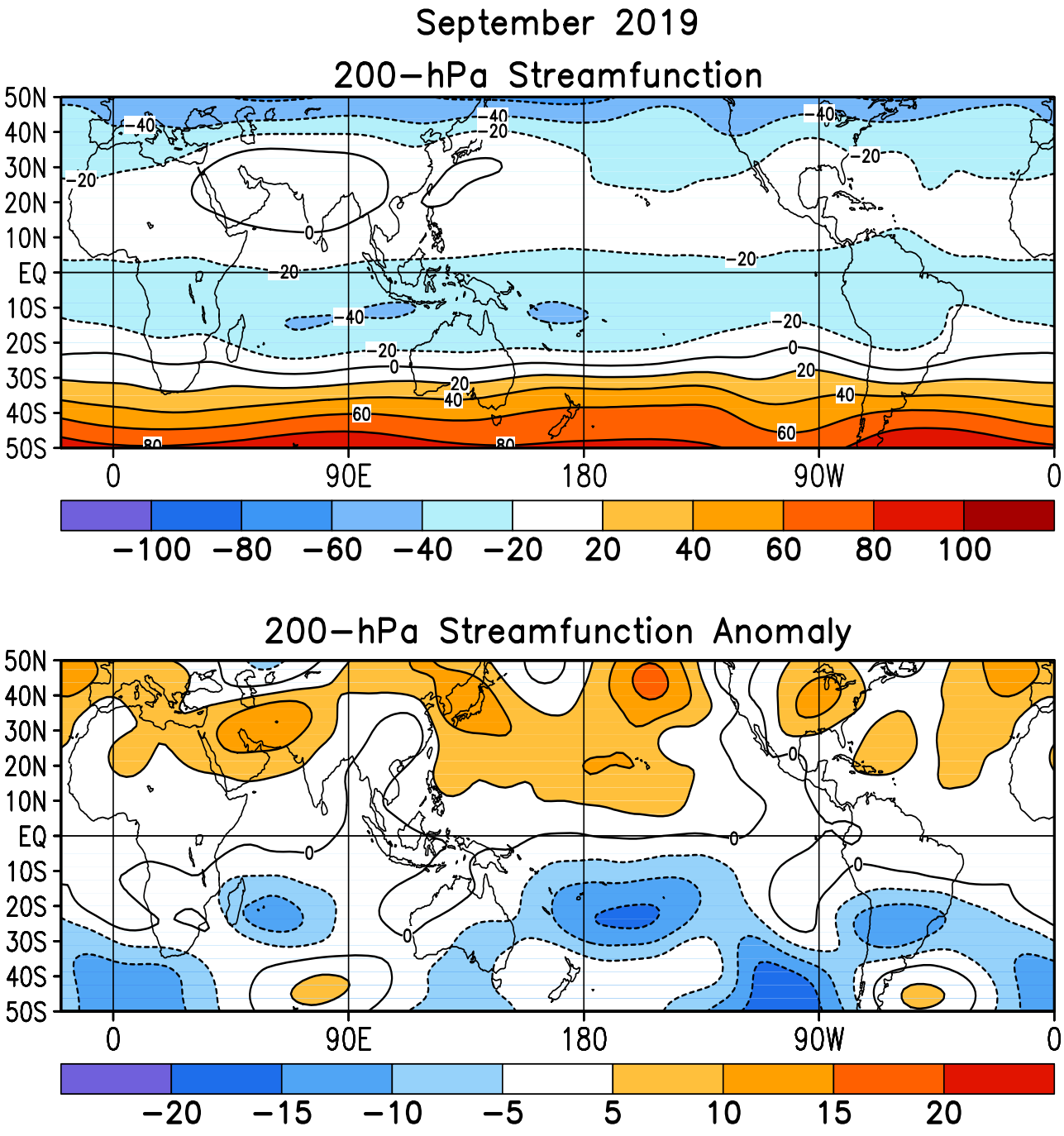


FIGURE T22. Mean (top) and anomalous (bottom) 200-hPa streamfunction (CDAS/Reanalysis). Contour interval is 20 x $10^6$ $m^2s^{-1}$ (top) and 5 x $10^6$ $m^2s^{-1}$ (bottom). Negative (positive) values are indicated by dashed (solid) lines. The non-divergent component of the flow is directed along the contours with speed proportional to the gradient. Thus, high (low) stream function corresponds to high (low) geopotential height in the Northern Hemisphere and to low (high) geopotential height in the Southern Hemisphere. Anomalies are departures from the 1981-2010 base period monthly means.

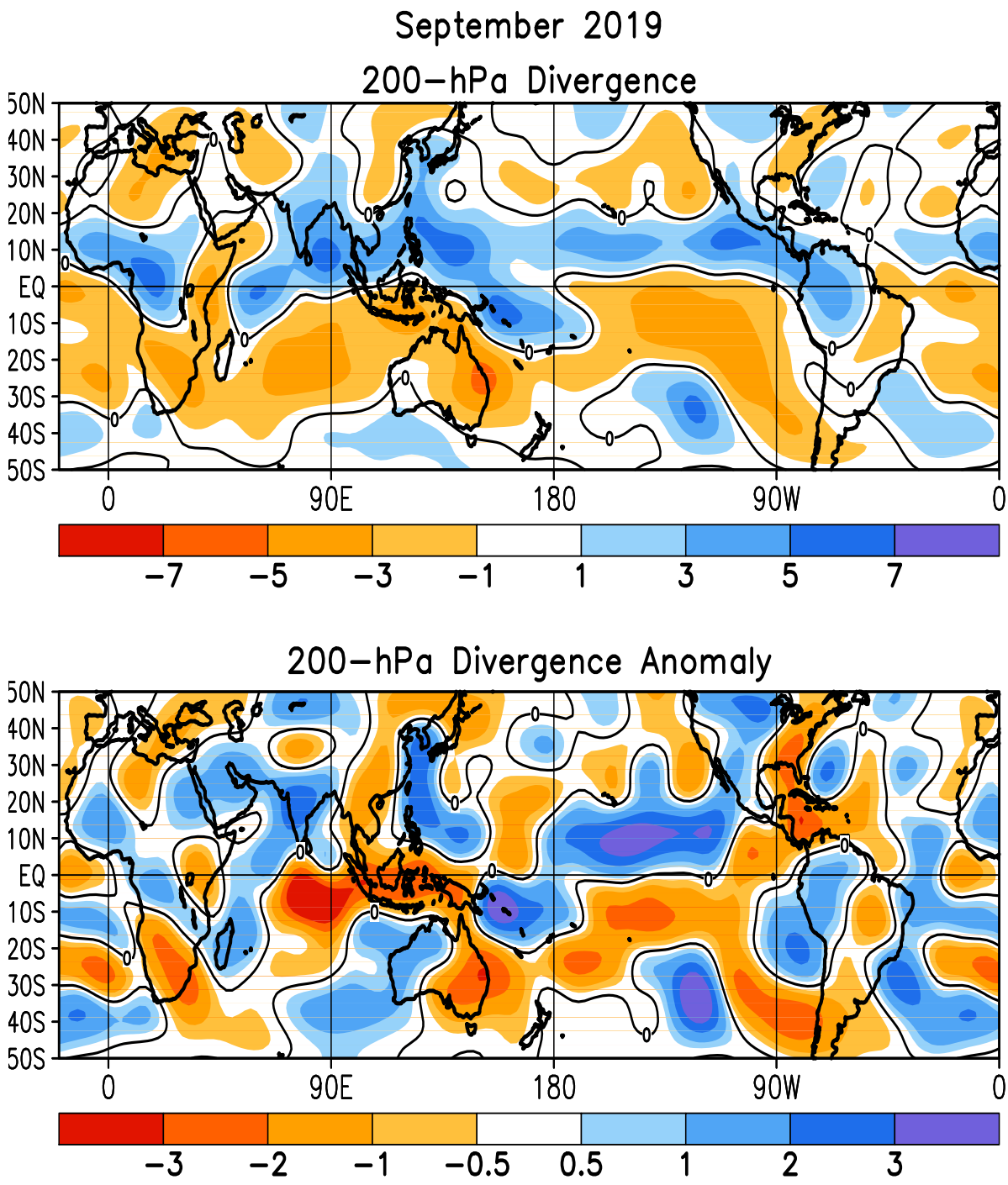


FIGURE T23. Mean (top) and anomalous (bottom) 200-hPa divergence (CDAS/Reanalysis). Divergence and anomalous divergence are shaded blue. Convergence and anomalous convergence are shaded orange. Anomalies are departures from the 1981-2010 base period monthly means.

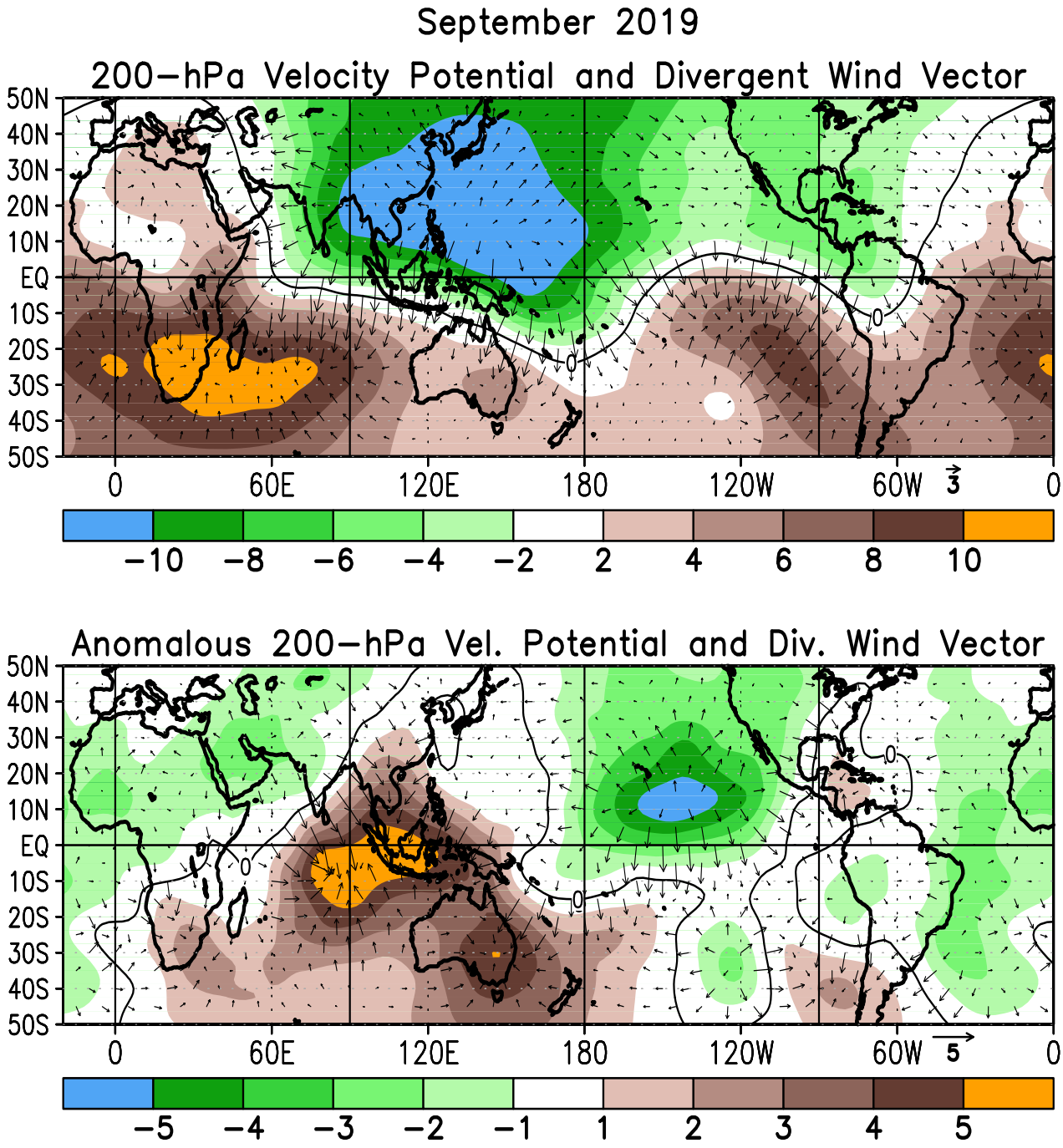


FIGURE T24. Mean (top) and anomalous (bottom) 200-hPa velocity potential ($10^6 m^2 s$) and divergent wind (CDAS/ Reanalysis). Anomalies are departures from the 1981-2010 base period monthly means.

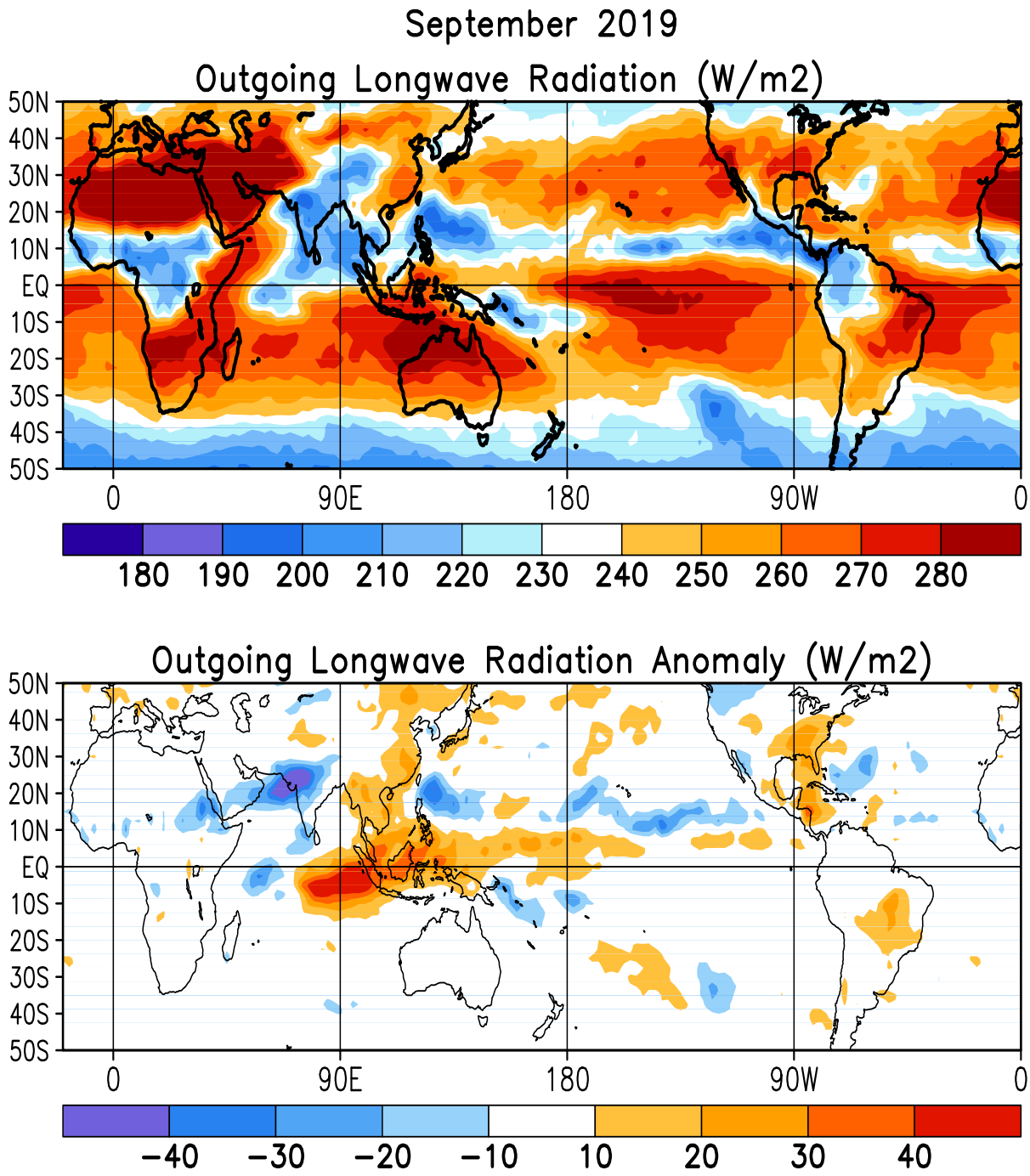


FIGURE T25. Mean (top) and anomalous (bottom) outgoing longwave radiation for SEP 2019 (NOAA 18 AVHRR IR window channel measurements by NESDIS/ORA). OLR contour interval is 20 $Wm^{-2}$ with values greater than 280 $Wm^{-2}$ indicated by dashed contours. Anomaly contour interval is 15 $Wm^{-2}$ with positive values indicated by dashed contours and light shading. Anomalies are departures from the 1981-2010 base period monthly means.

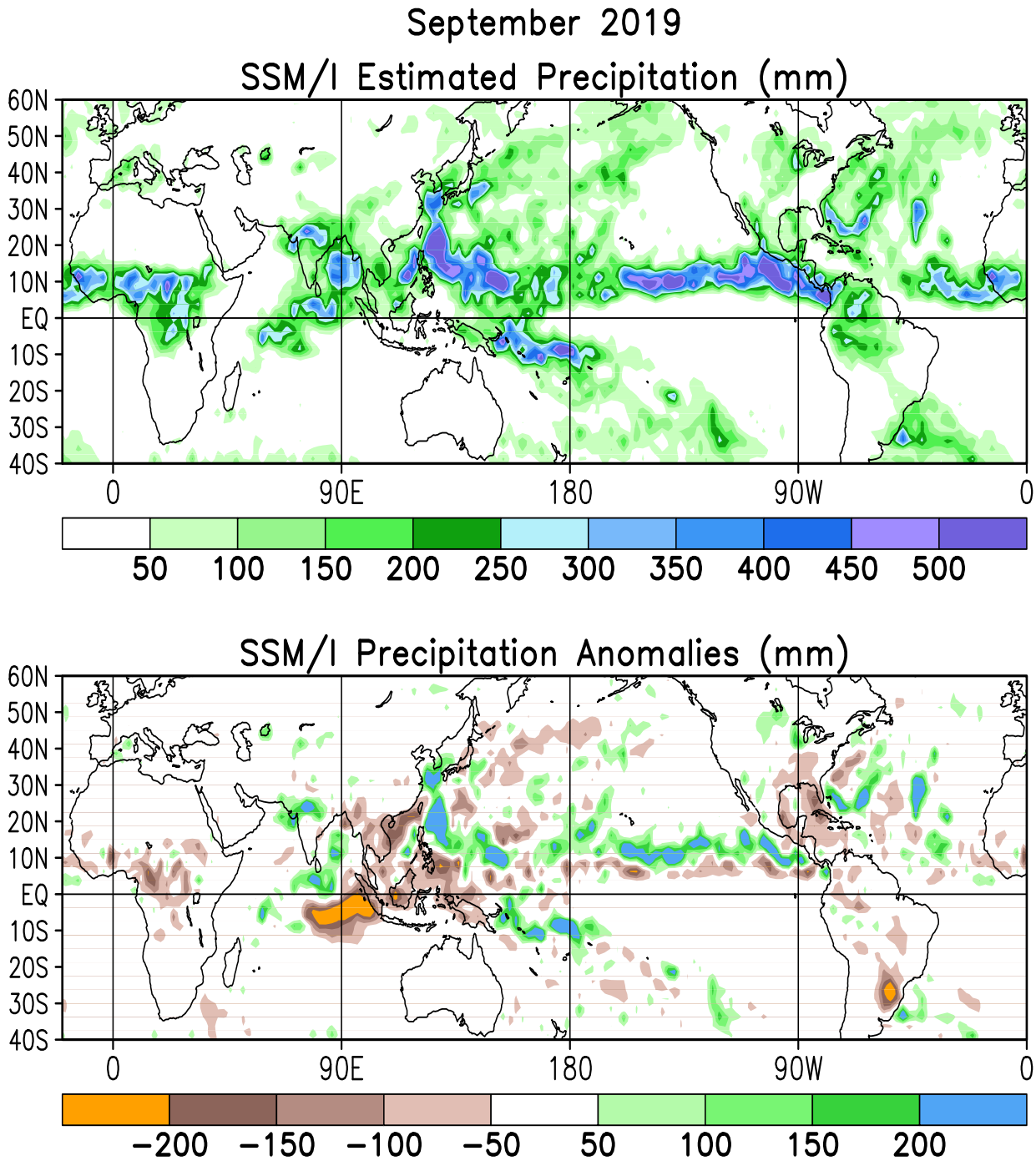


FIGURE T26. Estimated total (top) and anomalous (bottom) rainfall (mm) based on the Special Sensor Microwave/ Imager (SSM/S) precipitation index (Ferraro 1997, *J. Geophys. Res.*, **102**, 16715-16735). Anomalies are computed from the SSM/I 1987-2010 base period monthly means. Anomalies have been smoothed for display purposes.

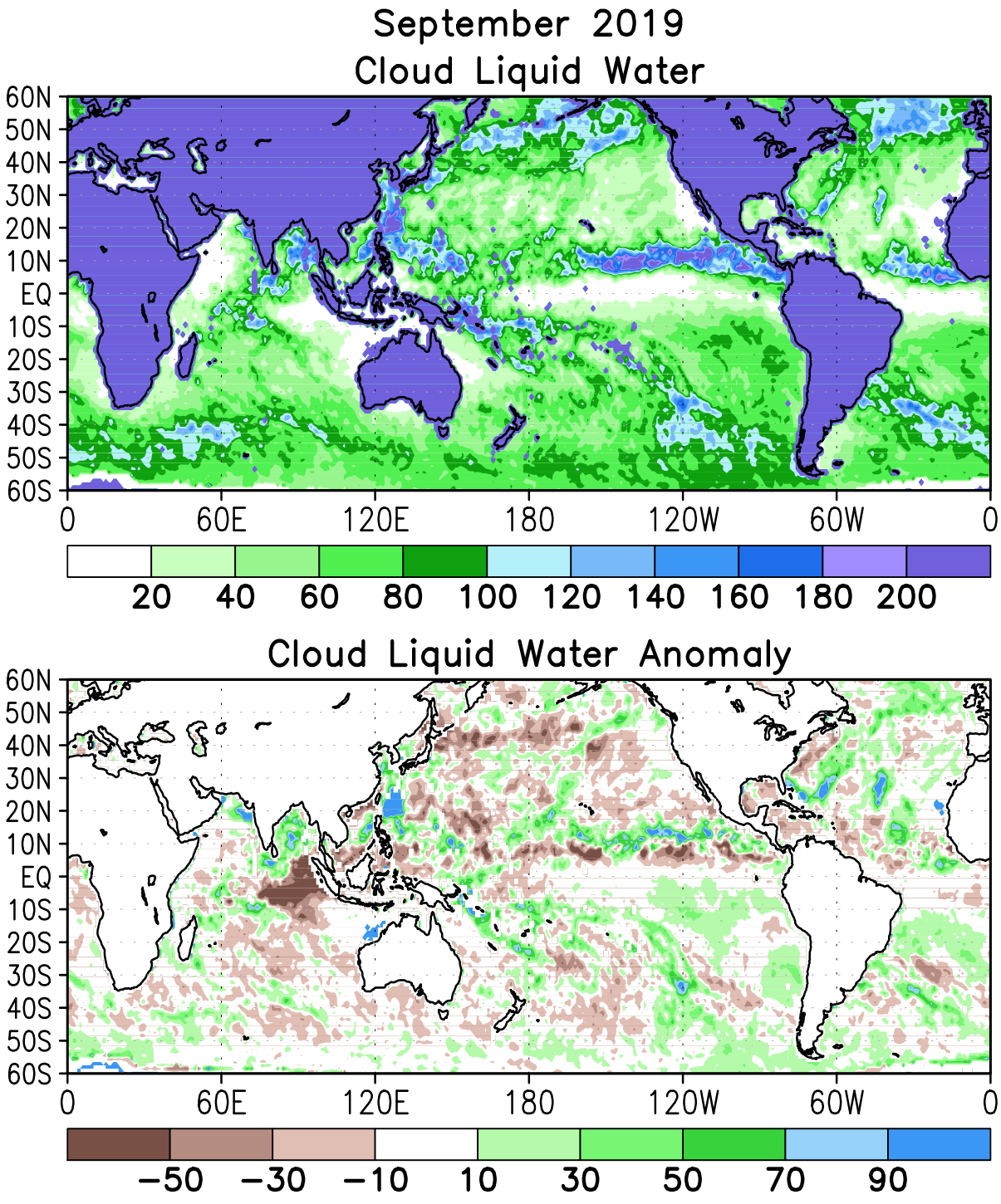


FIGURE T27. Mean (top) and anomalous (bottom) cloud liquid water (g $m^{-2}$) based on the Special Sensor Microwave/ Imager (SSM/I) (Weng et al 1997: *J. Climate*, **10**, 1086-1098). Anomalies are calculated from the 1987-2010 base period means.

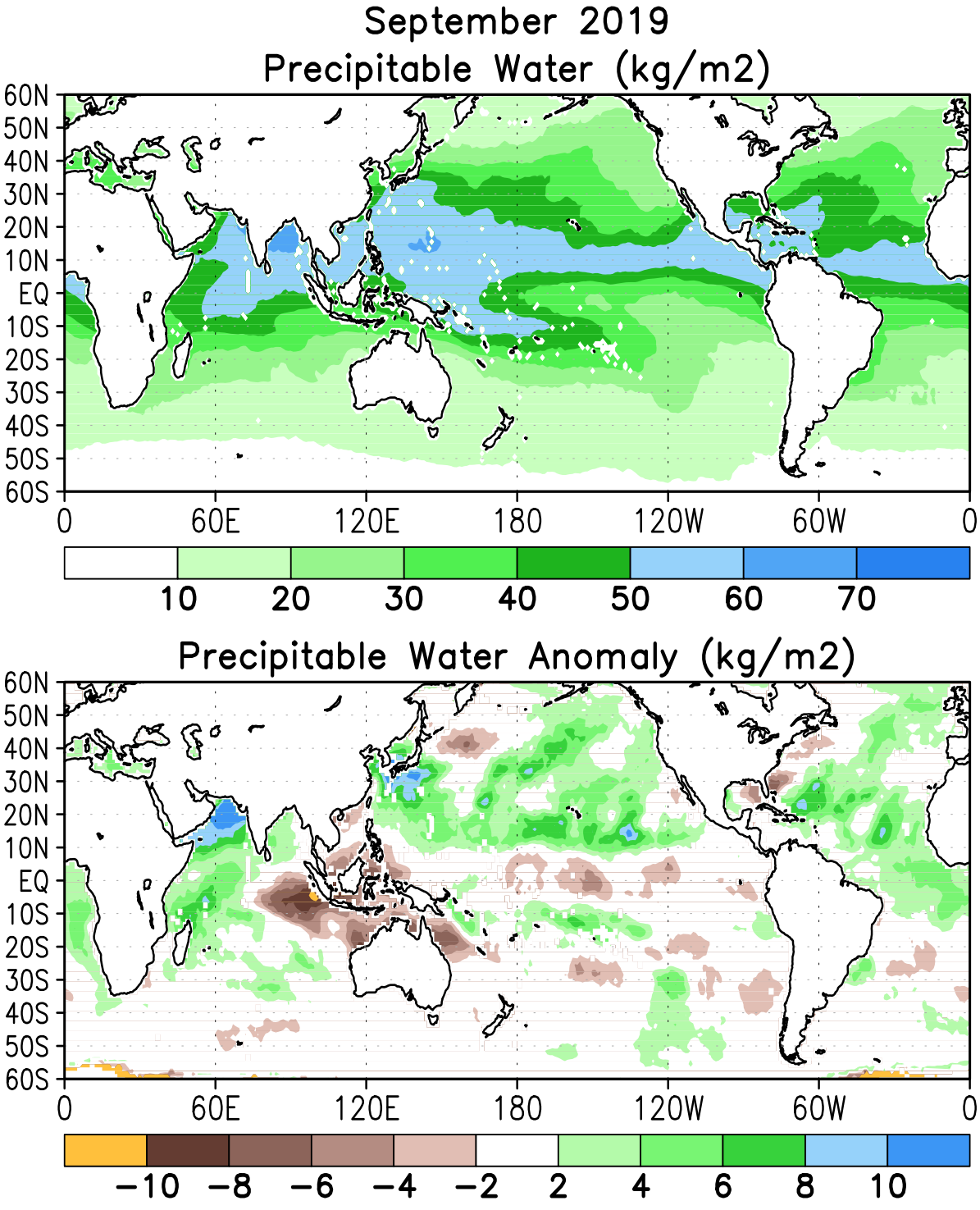


FIGURE T28. Mean (top) and anomalous (bottom) vertically integrated water vapor or precipitable water (kg $m^{-2}$) based on the Special Sensor Microwave/Imager (SSM/I) (Ferraro et. al, 1996: *Bull. Amer. Meteor. Soc.,* **77**, 891-905). Anomalies are calculated from the 1987-2010 base period means.

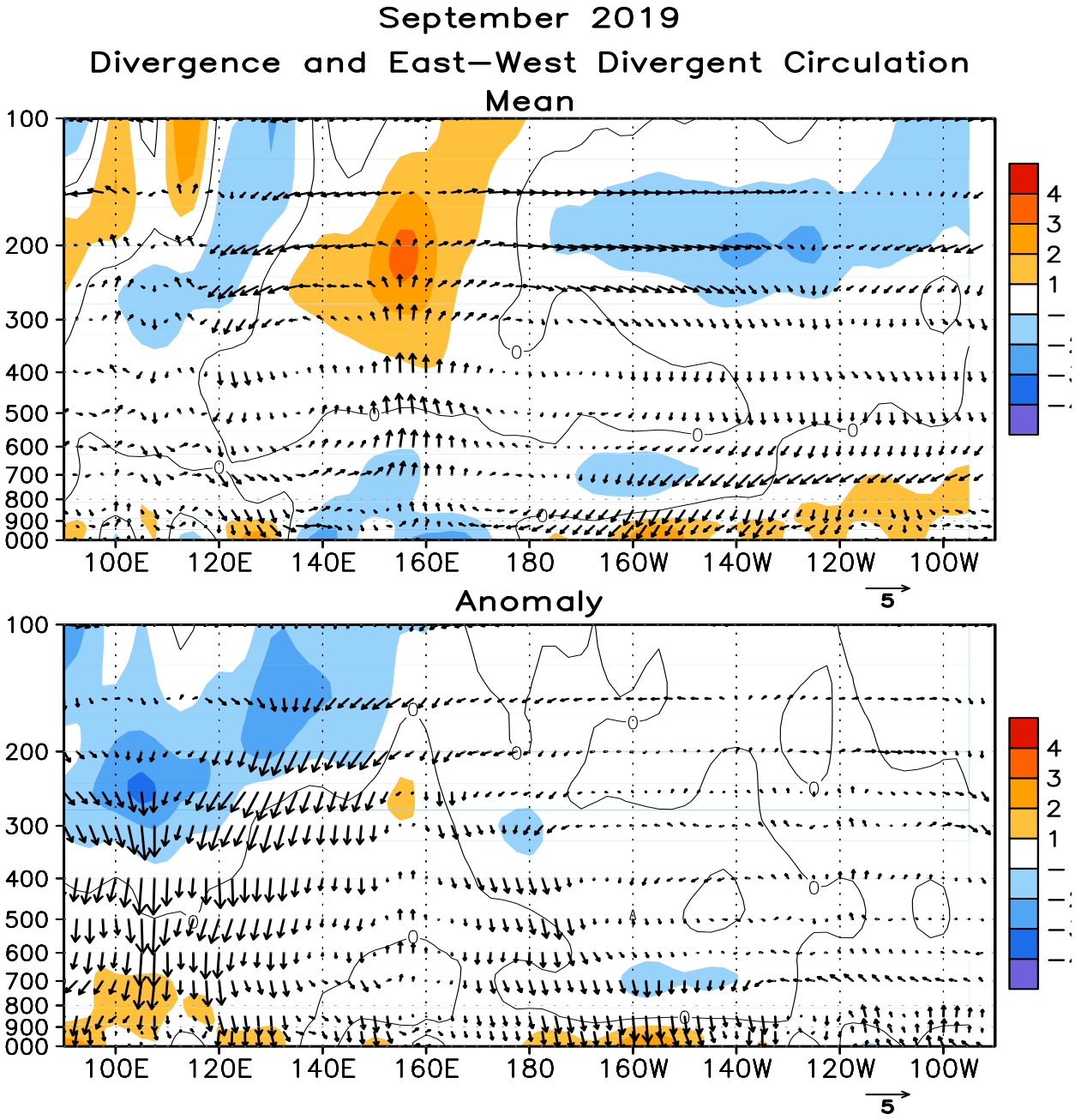


FIGURE T29. Pressure-longitude section (100E-80W) of the mean (top) and anomalous (bottom) divergence (contour interval is 1 x $10^{-6}$ $s^{-1}$) and divergent circulation averaged between 5N-5S. The divergent circulation is represented by vectors of combined pressure vertical velocity and the divergent component of the zonal wind. Red shading and solid contours denote divergence (top) and anomalous divergence (bottom). Blue shading and dashed contours denote convergence (top) and anomalous convergence (bottom). Anomalies are departures from the 1981-2010 base period monthly means.

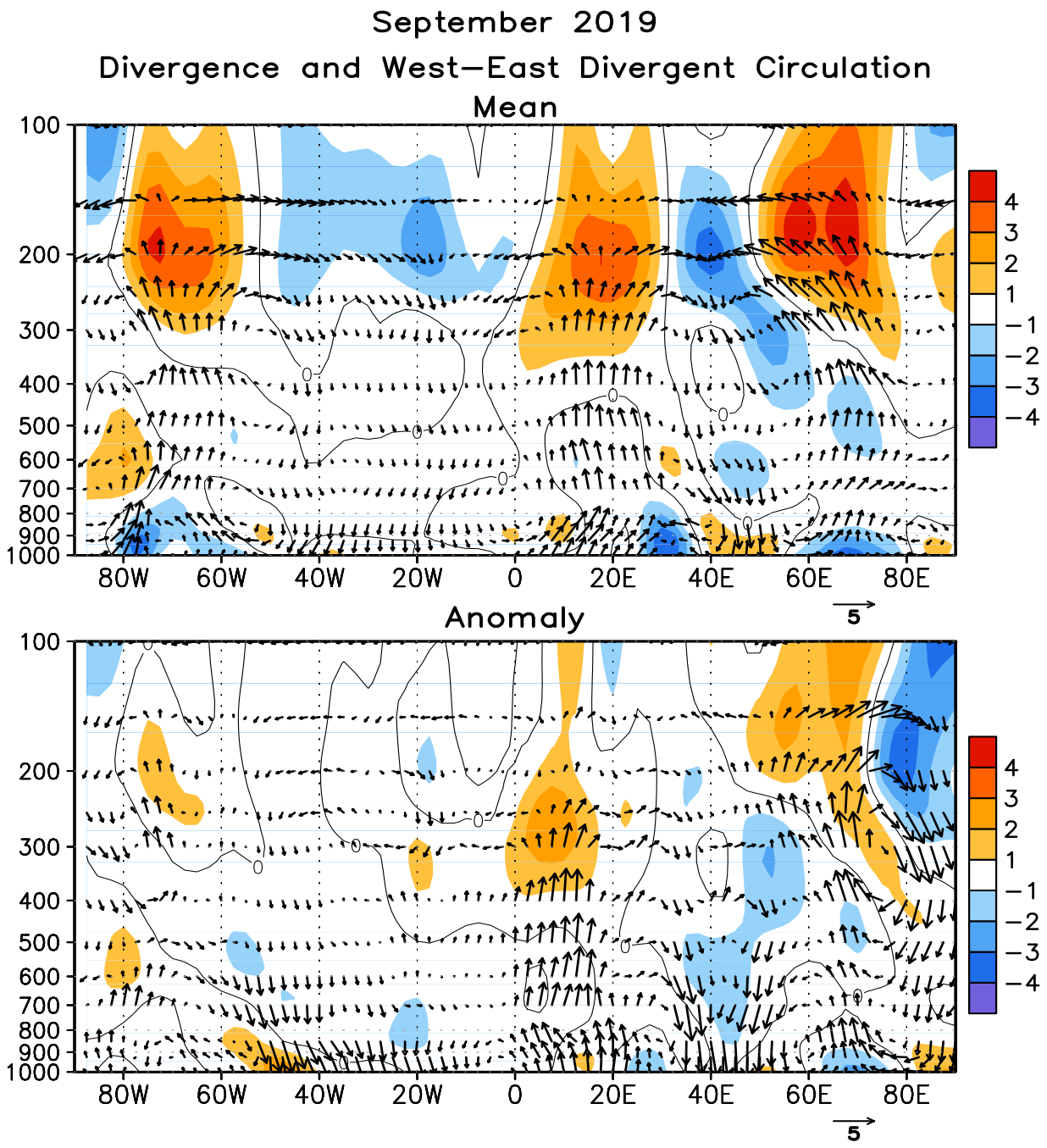


FIGURE T30. Pressure-longitude section (80W-100E) of the mean (top) and anomalous (bottom) divergence (contour interval is 1 x $10^{-6}$ $s^{-1}$) and divergent circulation averaged between 5N-5S. The divergent circulation is represented by vectors of combined pressure vertical velocity and the divergent component of the zonal wind. Red shading and solid contours denote divergence (top) and anomalous divergence (bottom). Blue shading and dashed contours denote convergence (top) and anomalous convergence (bottom). Anomalies are departures from the 1981-2010 base period monthly means.

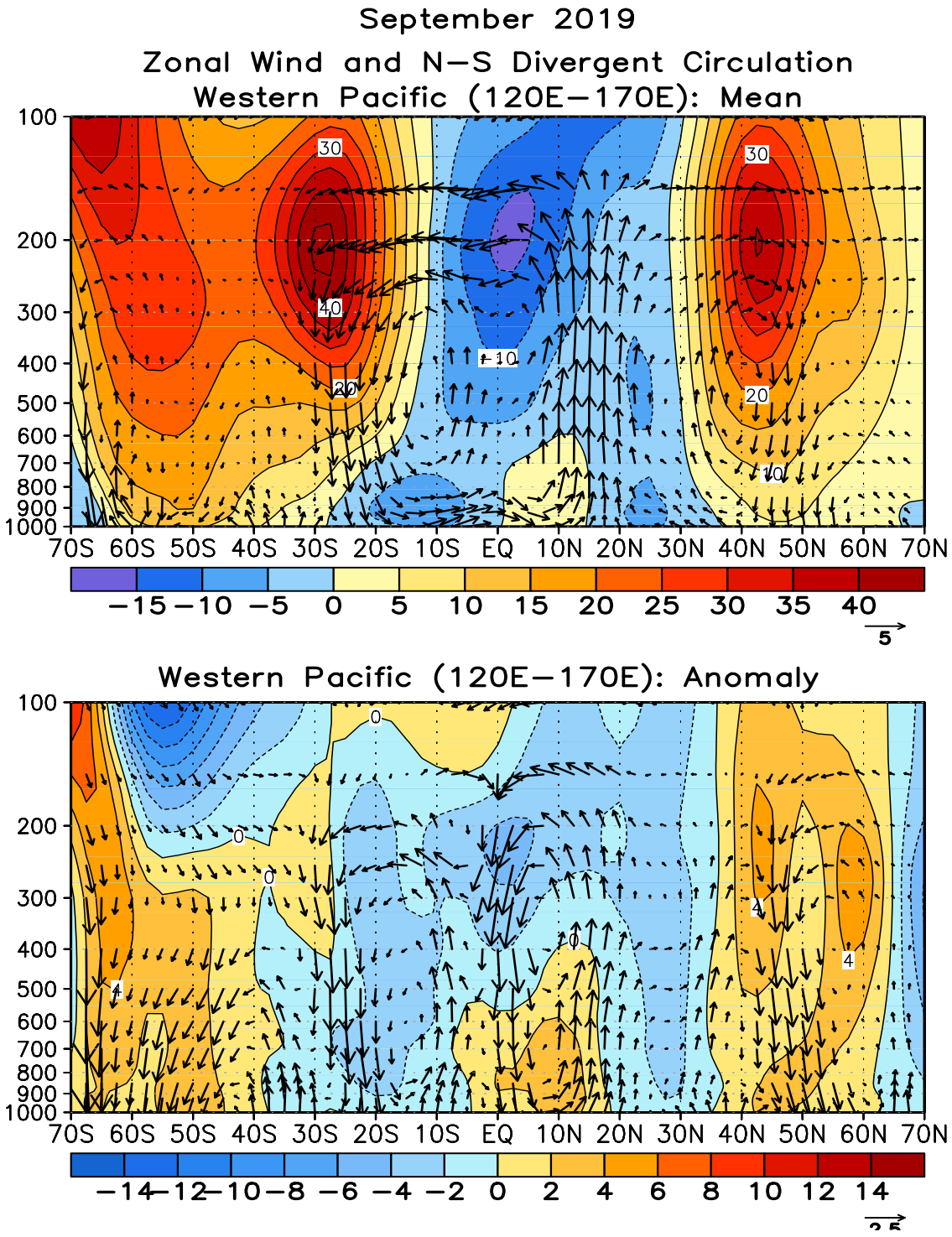


FIGURE T31. Pressure-latitude section of the mean (top) and anomalous (bottom) zonal wind (m $s^{-1}$) and divergent circulation averaged over the west Pacific sector (120E-170E). The divergent circulation is represented by vectors of combined pressure vertical velocity and the divergent component of the meridional wind. Red shading and solid contours denote a westerly (top) or anomalous westerly (bottom) zonal wind. Blue shading and dashed contours denote an easterly (top) or anomalous easterly (bottom) zonal wind. Anomalies are departures from the 1981-2010 base period monthly means.

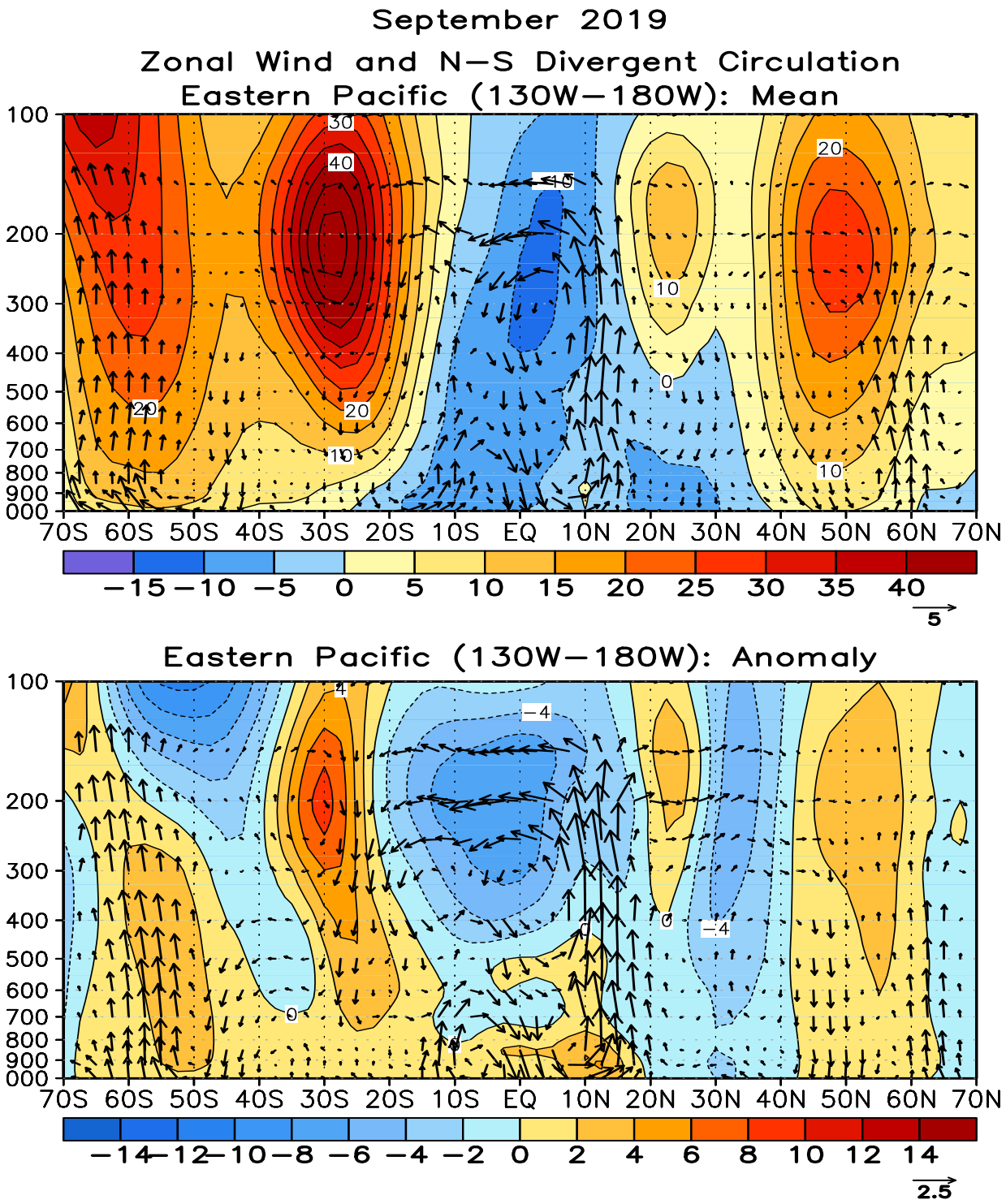


FIGURE T32. Pressure-latitude section of the mean (top) and anomalous (bottom) zonal wind (m $s^{-1}$) and divergent circulation averaged over the central Pacific sector (130W-180W). The divergent circulation is represented by vectors of combined pressure vertical velocity and the divergent component of the meridional wind. Red shading and solid contours denote a westerly (top) or anomalous westerly (bottom) zonal wind. Blue shading and dashed contours denote an easterly (top) or anomalous easterly (bottom) zonal wind. Anomalies are departures from the 1981-2010 base period monthly means.

Tropical Pacific Drifting Buoys R. Lumpkin/M. Pazos, AOML, Miami

During August 2019, 276 satellite-tracked surface drifting buoys were reporting from the tropical Pacific. The drifter array indicated that large-scale currents were close to their climatological July strengths across the basin, although much of the western to central equatorial Pacific was not sampled.

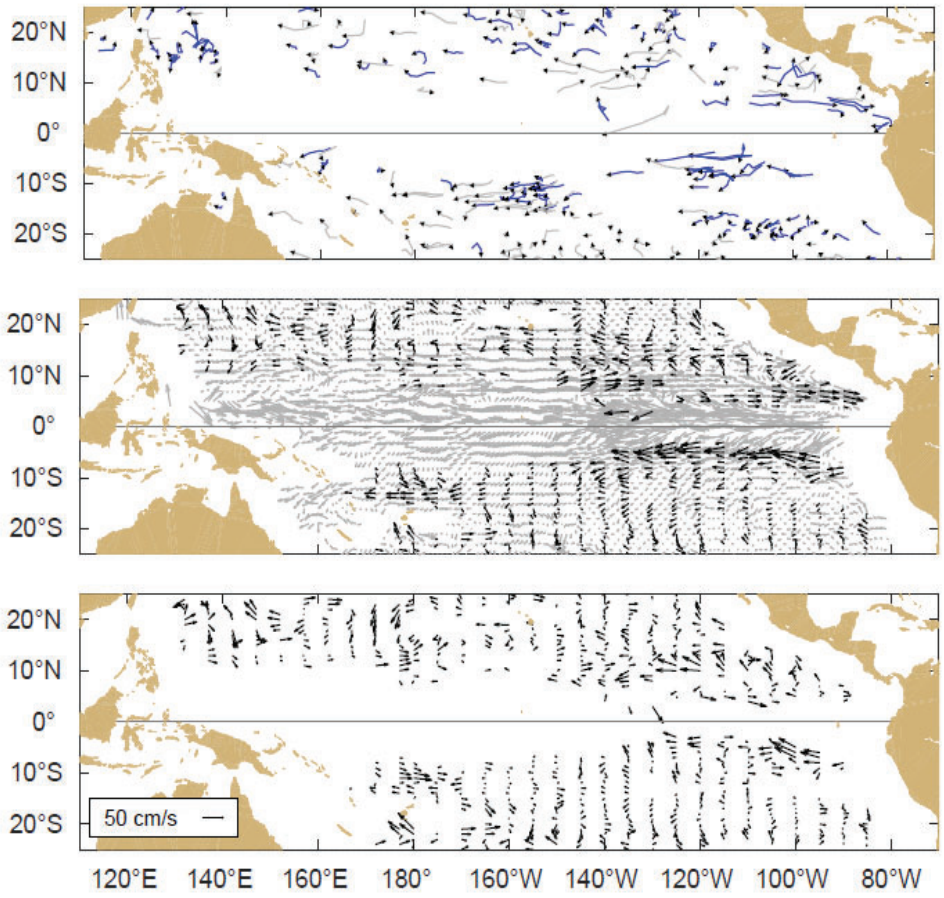


**Figure A1.1 Top:** Movements of drifting buoys in the tropical Pacific Ocean during August 2019. The linear segments of each trajectory represent a one week displacement. Trajectories of buoys which have lost their subsurface drogues are gray; those with drogues are black.
**Middle:** Monthly mean currents calculated from all buoys 1993-2002 (gray), and currents measured by the drogued buoys this month (black) smoothed by an optimal filter.
**Bottom:** Anomalies from the climatological monthly mean currents for this month.

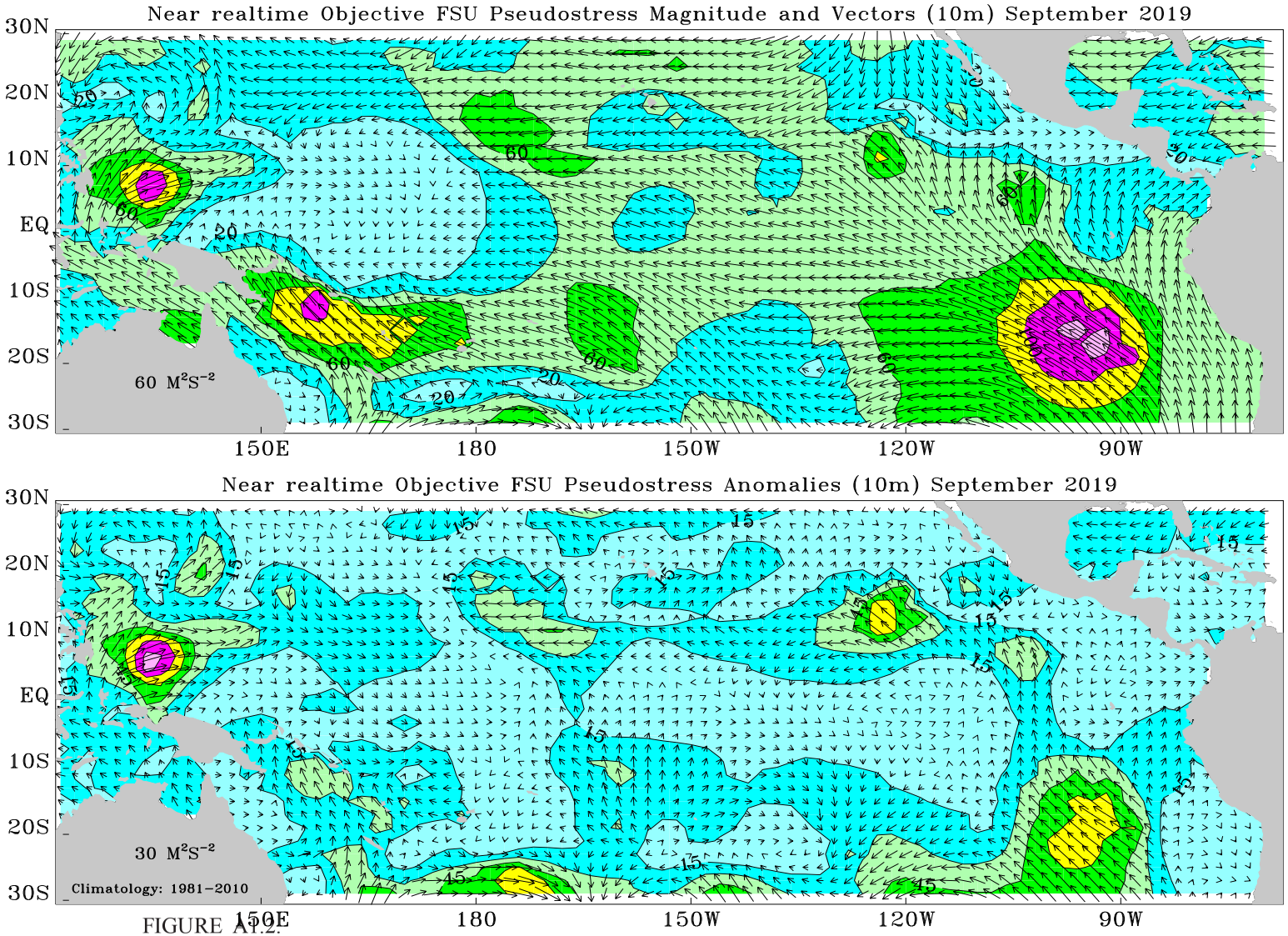


FIGURE A1.2.

FSU SURFACE PSEUDO–STRESS VECTORS AND ANOMALIES: September 2019. Pseudo–stress vectors (top) are objectively analyzed from ship and buoy winds on a 2° grid. Ship and buoy data are independently weighted and the background field is created from the data. Contour interval of the vector magnitudes is 20 $M^2S^{-2}$. Anomalies (bottom) are departures from 1981–2010 mean. The contour interval is 15 $M^2S^{-2}$. For more information, please visit our web site at http://www.coaps.fsu.edu/RVSMDC/html/winds.shtml. Produced by Jeremy Rolph, Mark A. Bourassa, and Shawn R. Smith, Center for Ocean–Atmospheric Prediction Studies, Florida State University, Tallahassee, FL 32306–2840, USA.

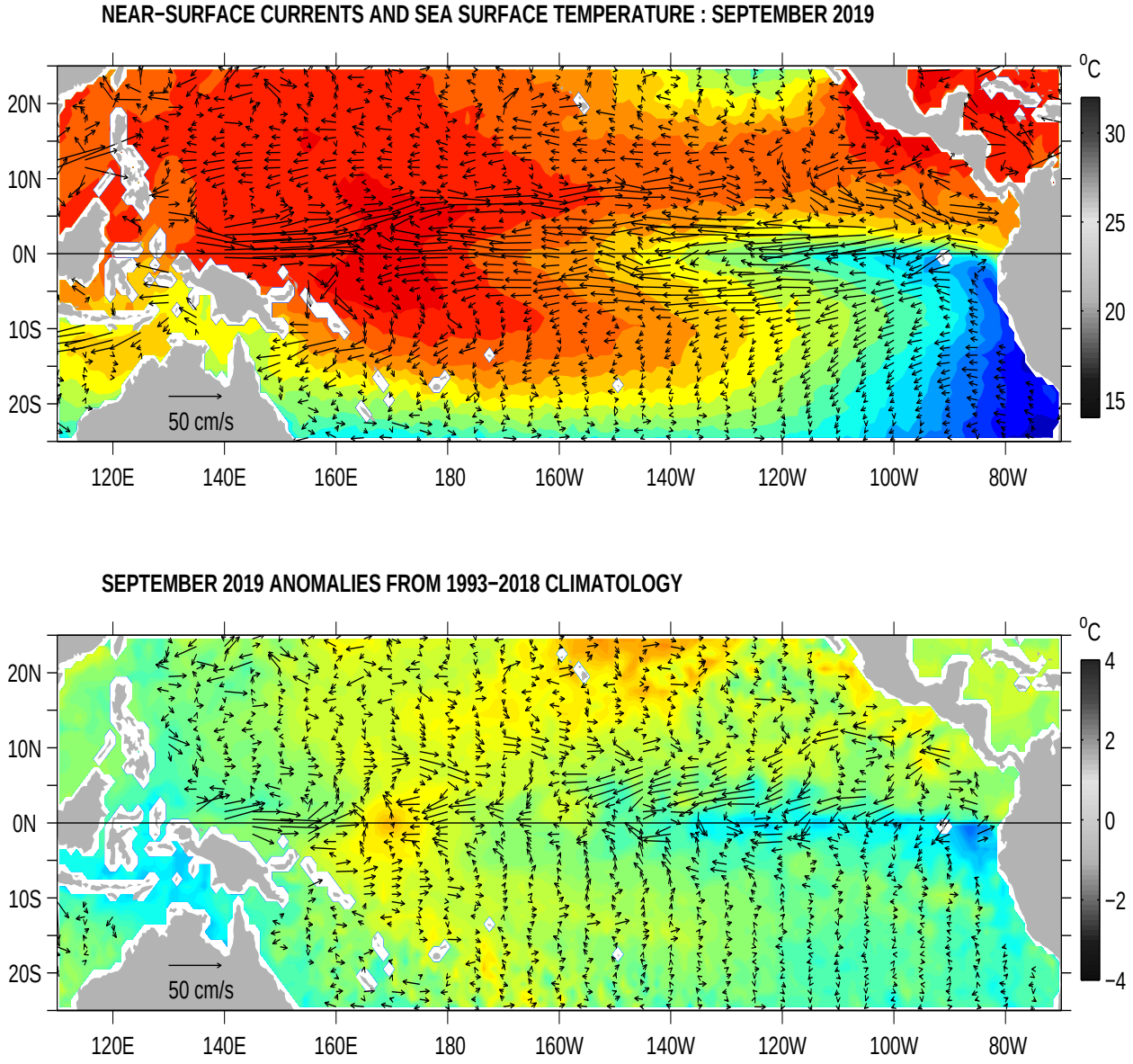


FIGURE A1.3. Ocean Surface Current Analysis-Real-time (OSCAR) for SEP 2019 (Bonjean and Lagerloef 2002, J. Phys. Oceanogr., Vol. 32, No. 10, 2938-2954; Lagerloef et al. 1999, JGR-Oceans, 104, 23313-23326). (top) Total velocity. Surface currents are calculated from satellite data including Jason sea level anomalies and NCEP winds. (bottom) Velocity anomalies. The subtracted climatology was based on SSM/I and QuickScat winds and Topex/ Poseidon and Jason from 1993-2003. See also http://www.oscar.noaa.gov.

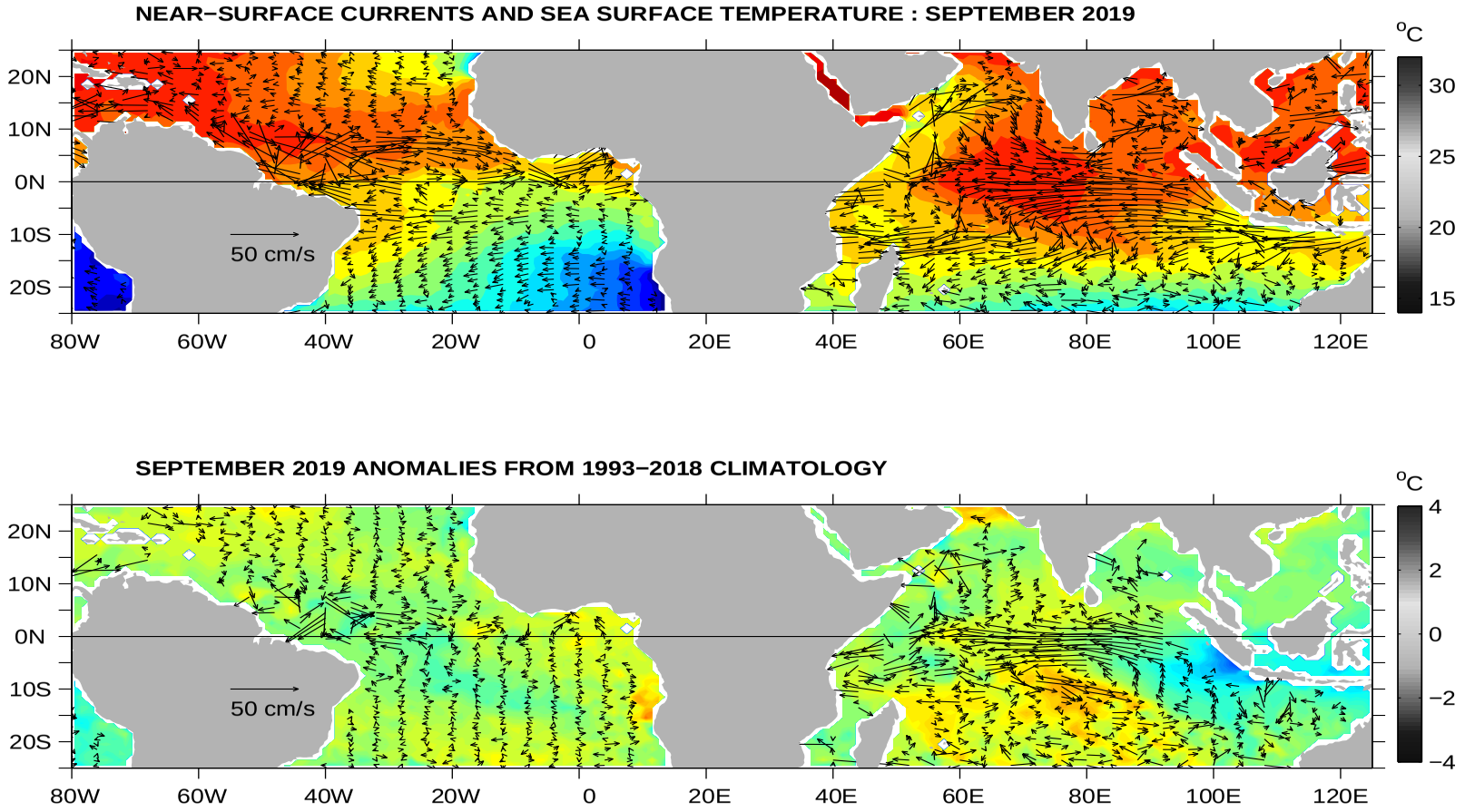


FIGURE A1.4. Ocean Surface Current Analysis-Real-time (OSCAR) for SEP 2019 (Bonjean and Lagerloef 2002, J. Phys. Oceanogr., Vol. 32, No. 10, 2938-2954; Lagerloef et al. 1999, JGR-Oceans, 104, 23313-23326). (top) Total velocity. Surface currents are calculated from satellite data including Jason sea level anomalies and NCEP winds. (bottom) Velocity anomalies. The subtracted climatology was based on SSM/I and QuickScat winds and Topex/Poseidon and Jason from 1993-2003. See also http://www.oscar.noaa.gov.

# Forecast Forum

The canonical correlation analysis (CCA) forecast of SST in the central Pacific (Barnett et al. 1988, *Science*, **241**, 192196; Barnston and Ropelewski 1992, *J. Climate*, **5**, 13161345), is shown in **Figs. F1 and F2.** This forecast is produced routinely by the Prediction Branch of the Climate Prediction Center. The predictions from the National Centers for Environmental Prediction (NCEP) Coupled Forecast System Model (CFS03) are presented in **Figs. F3 and F4a, F4b**. Predictions from the Markov model (Xue, et al. 2000: *J. Climate*, **13**, 849871) are shown in **Figs. F5 and F6.** Predictions from the latest version of the LDEO model (Chen et al. 2000: *Geophys. Res. Let*., **27**, 25852587) are shown in **Figs. F7 and F8**. Predictions using linear inverse modeling (Penland and Magorian 1993: *J. Climate*, **6**, 10671076) are shown in **Figs. F9 and F10.** Predictions from the ENSO CLIPER statistical model (Knaff and Landsea 1997, Wea. Forecasting, 12, 633 652) are shown in **Fig. F11**. Niño 3.4 predictions are summarized in **Fig. F12**, provided by the Forecasting and Prediction Research Group of the IRI.

The CPC and the contributors to the **Forecast Forum** caution potential users of this predictive information that they can expect only modest skill.

# ENSO Alert System Status: Not Active

# Outlook

ENSO-neutral is favored during the Northern Hemisphere fall 2019 (~85% chance), continuing through spring 2020 (55-60% chance).

# Discussion

Near-average sea surface temperatures (SST) were evident in the east-central Pacific Ocean during most of September, though SST anomalies increased during the past couple of weeks (Fig. T18). The monthly SST indices in the westernmost Niño-4 and Niño-3.4 regions were +0.6C and 0.0C, respectively, and the indices in the easternmost Niño-3 and Niño-1+2 regions remained near-to-below average (-0.2C and -0.8C respectively; Table T2). The subsurface temperature anomalies (averaged across 180°-100°W) increased during the month partially because a downwelling oceanic Kelvin wave expanded eastward (Fig. T17). This wave was triggered by low-level westerly wind anomalies across the western and central equatorial Pacific Ocean (Fig. T20). At upper-levels, easterly wind anomalies prevailed over much of the Pacific during September (Fig. T21). Also, the region of suppressed convection over Indonesia intensified and expanded to the Date Line (Fig. T25). Despite the recent warming, the overall oceanic and atmospheric system remained consistent

with ENSO-neutral.

The majority of models in the IRI/CPC plume (Figs. F1-F12) continue to favor ENSO-neutral (Niño-3.4 index between -0.5C and +0.5C) through the Northern Hemisphere spring. Many dynamical forecast models, including the NCEP CFSv2, suggest Niño-3.4 SST index values will remain near +0.5C during the next month or so before decreasing, but remaining above zero. Consequently, forecasters believe the recent oceanic warmth reflects sub-seasonal variability and is not indicative of an evolution toward El Niño. However, chances for El Niño remain between approximately 25-30% through the winter and spring. In summary, ENSO-neutral is favored during the Northern Hemisphere fall 2019 (~85% chance), continuing through spring 2020 (55-60% chance).

Weekly updates of oceanic and atmospheric conditions are available on the Climate Prediction Center homepage (El Niño/La Niña Current Conditions and Expert Discussions).

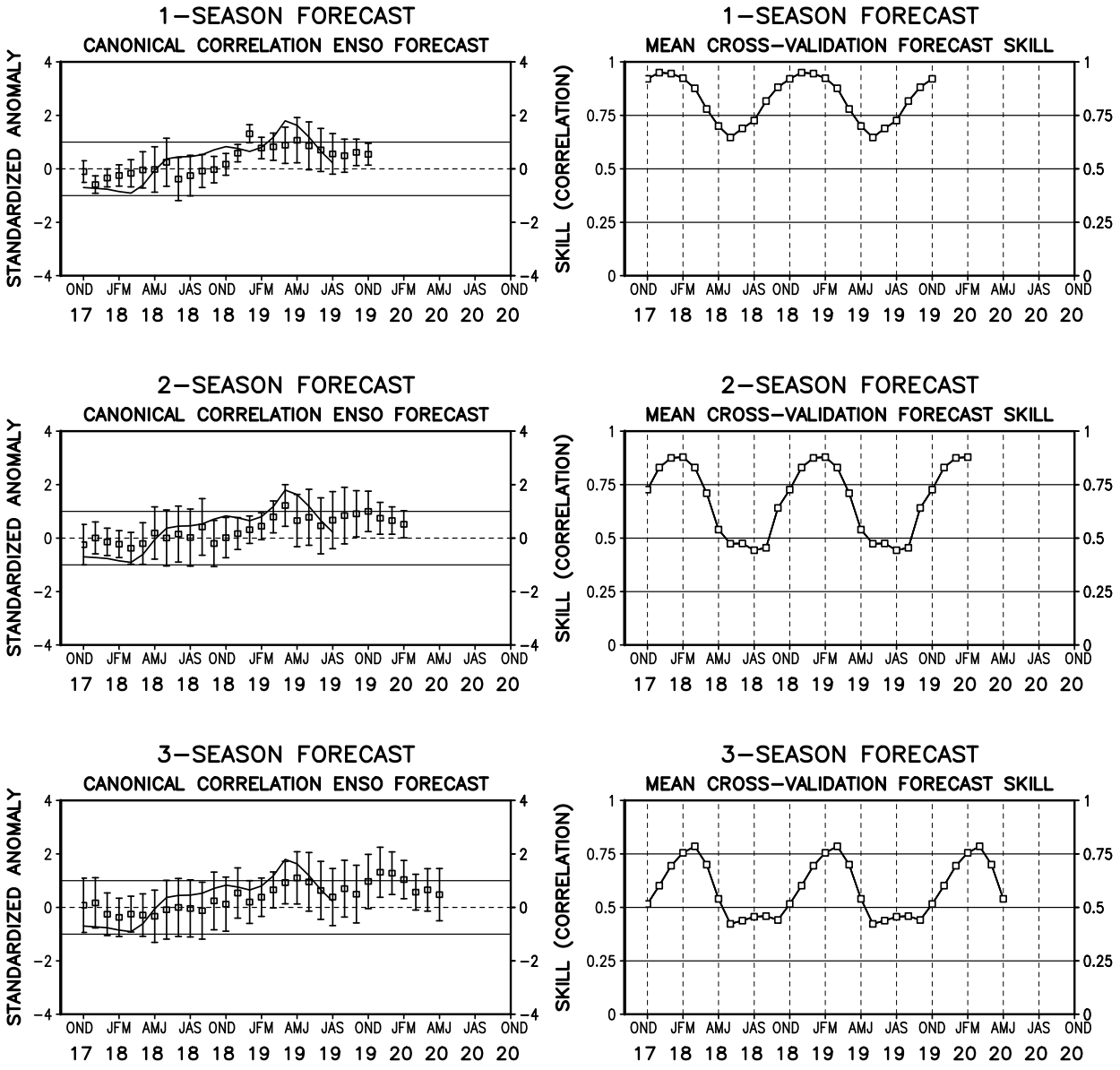


FIGURE F1. Canonical correlation analysis (CCA) sea surface temperature (SST) anomaly prediction for the central Pacific (5˚N to 5˚S, 120˚W to 170˚W (Barnston and Ropelewski, 1992, *J. Climate*, **5**, 1316-1345). The three plots on the left hand side are, from top to bottom, the 1-season, 2-season, and 3-season lead forecasts. The solid line in each forecast represents the observed SST standardized anomaly through the latest month. The small squares at the mid-points of the forecast bars represent the real-time CCA predictions based on the anomalies of quasi-global sea level pressure and on the anomalies of tropical Pacific SST, depth of the 20˚C isotherm and sea level height over the prior four seasons. The vertical lines represent the one standard deviation error bars for the predictions based on past performance. The three plots on the right side are skills, corresponding to the predicted and observed SST. The skills are derived from cross-correlation tests from 1956 to present. These skills show a clear annual cycle and are inversely proportional to the length of the error bars depicted in the forecast time series.

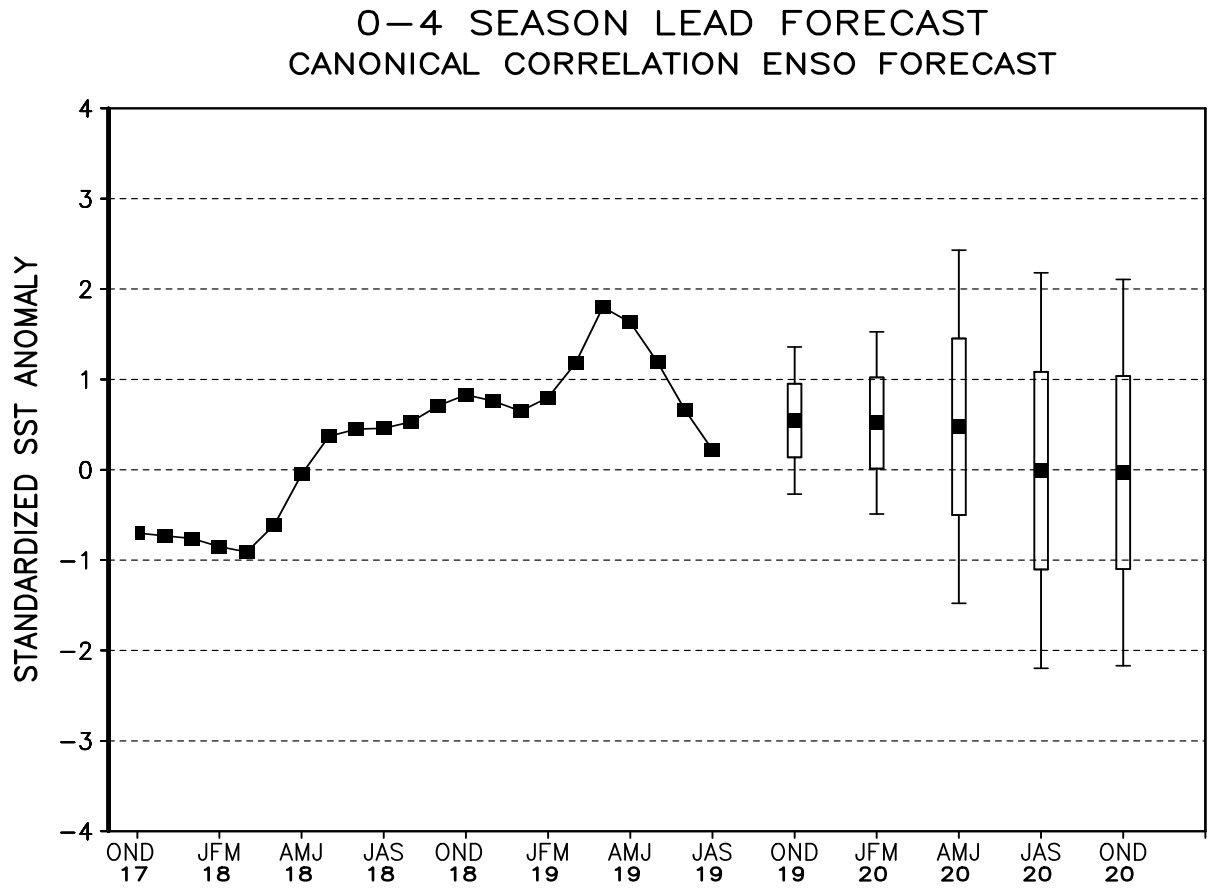


FIGURE F2. Canonical Correlation Analysis (CCA) forecasts of sea-surface temperature anomalies for the Nino 3.4 region (5N-5S, 120W-170W) for the upcoming five consecutive 3-month periods. Forecasts are expressed as standardized SST anomalies. The CCA predictions are based on anomaly patterns of SST, depth of the 20C isotherm, sea level height, and sea level pressure. Small squares at the midpoints of the vertical forecast bars represent the CCA predictions, and the bars show the one (thick) and two (thin) standard deviation errors. The solid continuous line represents the observed standardized three-month mean SST anomaly in the Nino 3.4 region up to the most recently available data.

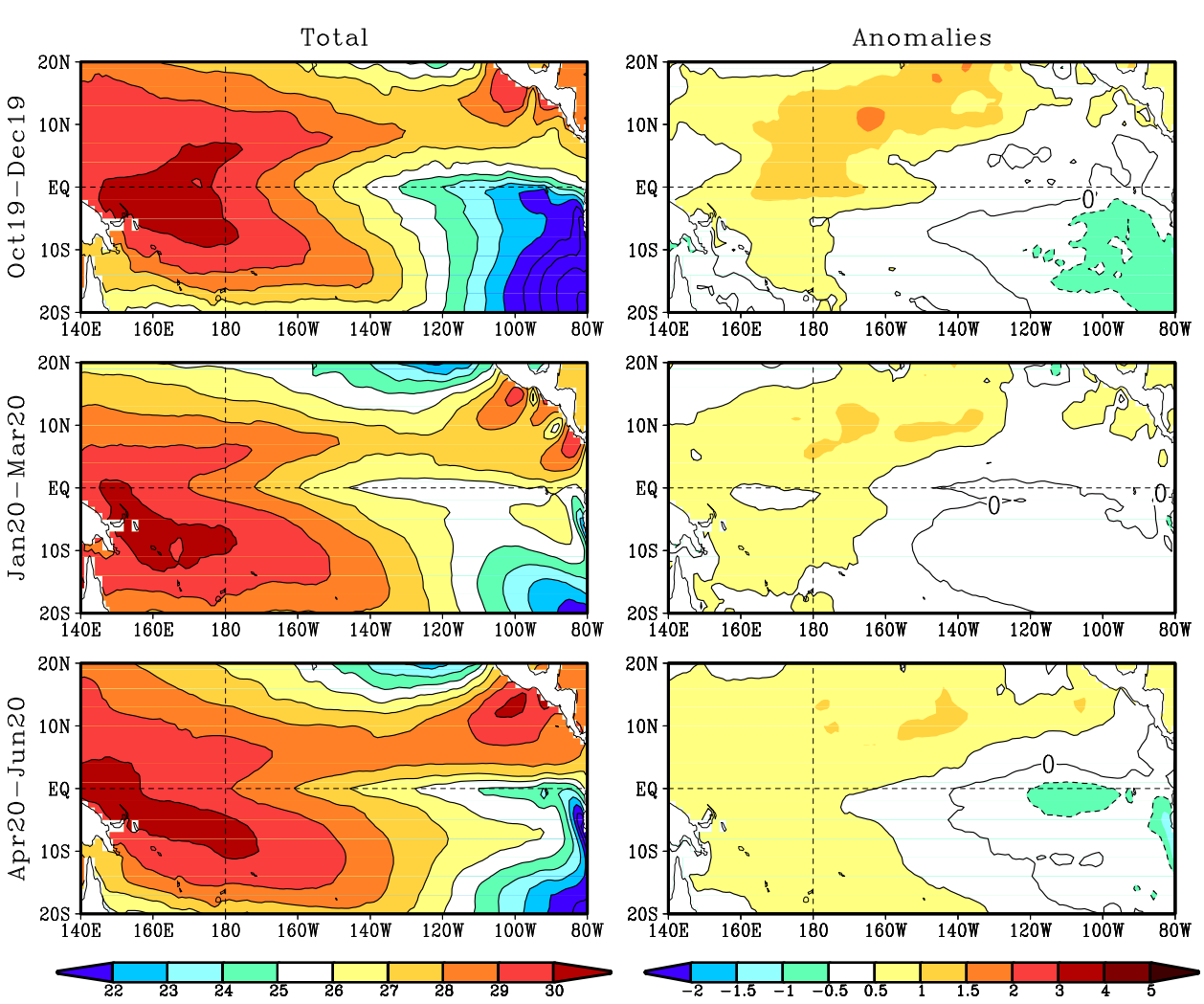


FIGURE F3. Predicted 3-month average sea surface temperature (left) and anomalies (right) from the NCEP Coupled Forecast System Model (CFS03). The forecasts consist of 40 forecast members. Contour interval is 1°C, with additional contours for 0.5°C and -0.5°C. Negative anomalies are indicated by dashed contours.

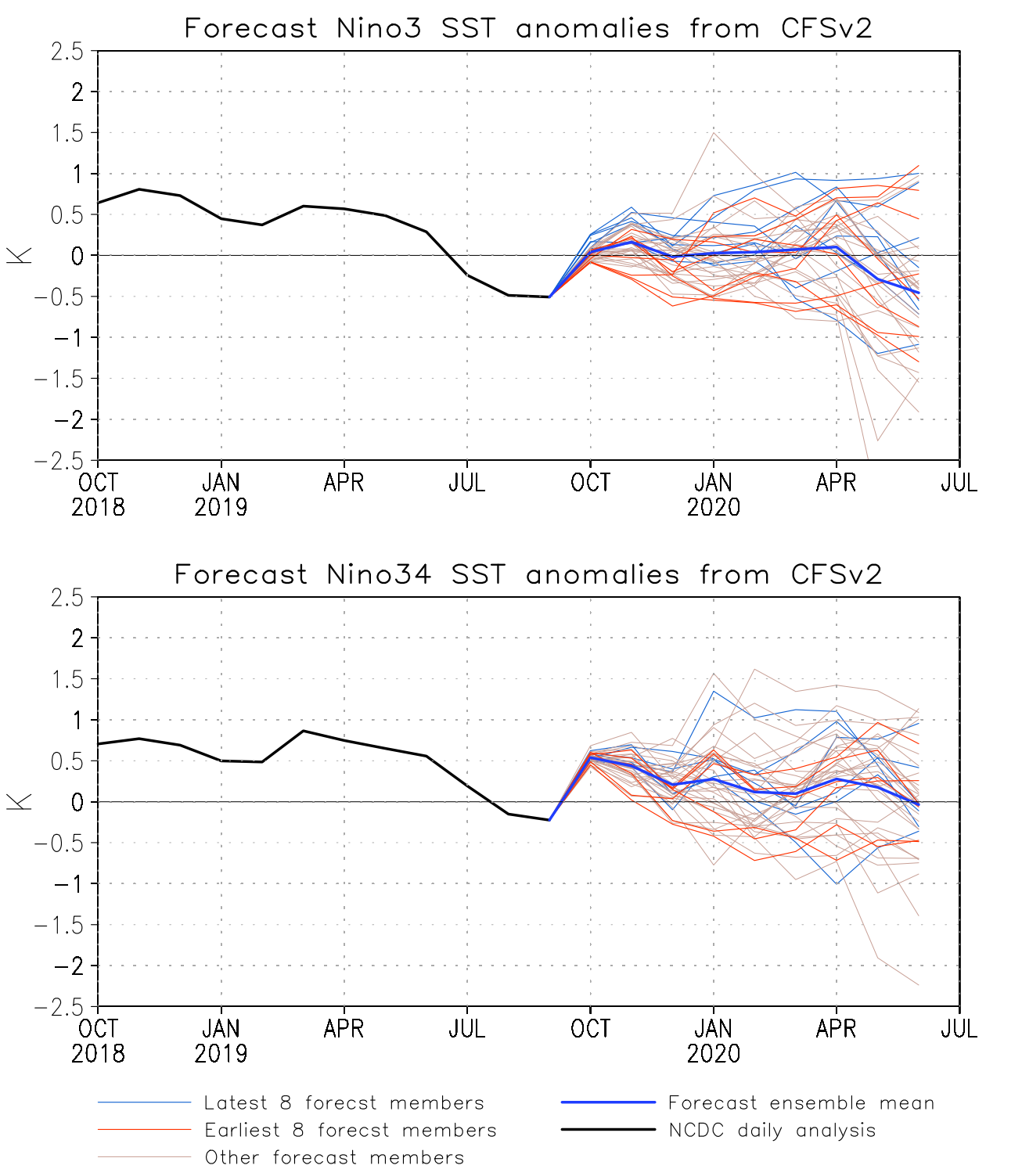


FIGURE F4. Predicted and observed sea surface temperature (SST) anomalies for the Nino 3 (top) and Nino 3.4 (bottom) regions from the NCEP Coupled Forecast System Model (CFS03). The forecasts consist of 40 forecast members. The ensemble mean of all 40 forecast members is shown by the blue line, individual members are shown by thin lines, and the observation is indicated by the black line. The Nino-3 region spans the eastern equatorial Pacific between 5N-5S, 150W-90W. The Nno 3.4 region spans the east-central equatorial Pacific between 5N-5S, 170W-120W.

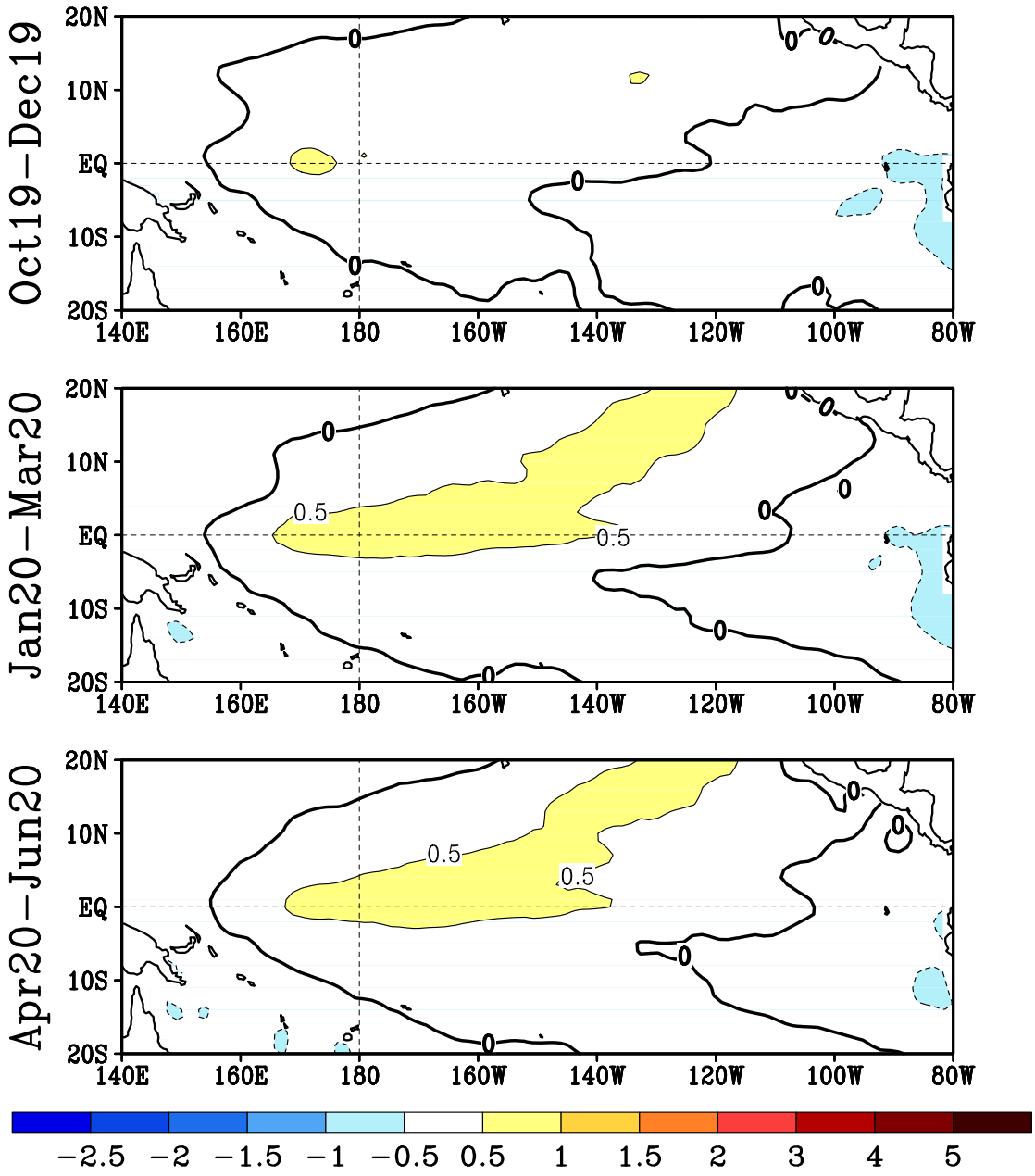


FIGURE F5. Predicted 3-month average sea surface temperature anomalies from the NCEP/CPC Markov model (Xue et al. 2000, *J. Climate*, **13**, 849-871). The forecast is initiated in SEP 2019 . Contour interval is 0.3C and negative anomalies are indicated by dashed contours. Anomalies are calculated relative to the 1971-2000 climatology.

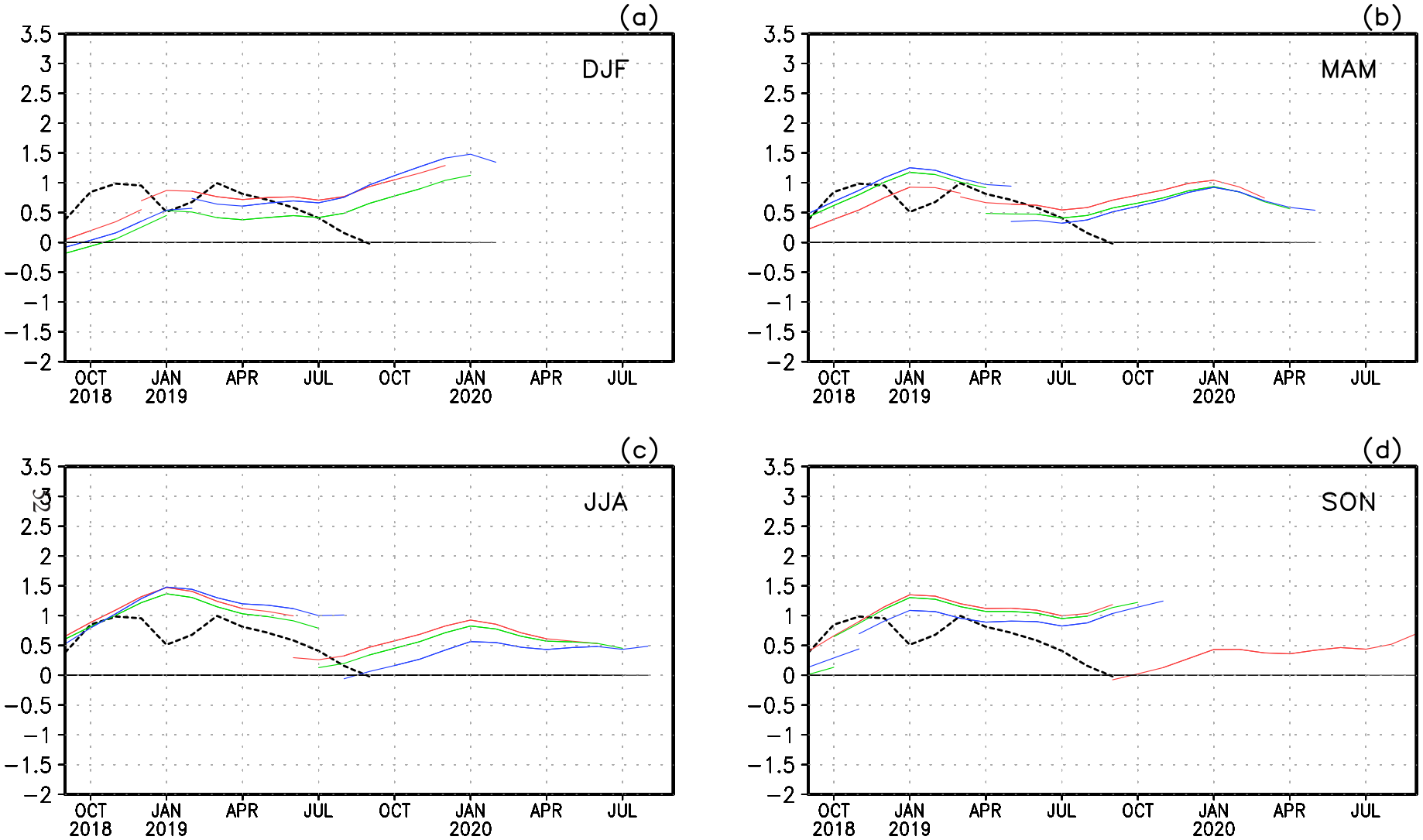


FIGURE F6. Time evolution of observed and predicted SST anomalies in the Nino 3.4 region (up to 12 lead months) by the NCEP/CPC Markov model (Xue et al. 2000, *J. Climate*, **13**, 849-871). Anomalies are calculated relative to the 1971-2000 climatology. Shown in each panel are the forecasts grouped by three consecutive starting months: (a) is for December, January, and February, (b) is for March, April, and May, (c) is for June, July, and August, and (d) is for September, October, and November. The observed Nino 3.4 SST anomalies are indicated by the black dashed lines. The Nino 3.4 region spans the east-central equatorial Pacific between 5N-5S, 170W-120W.

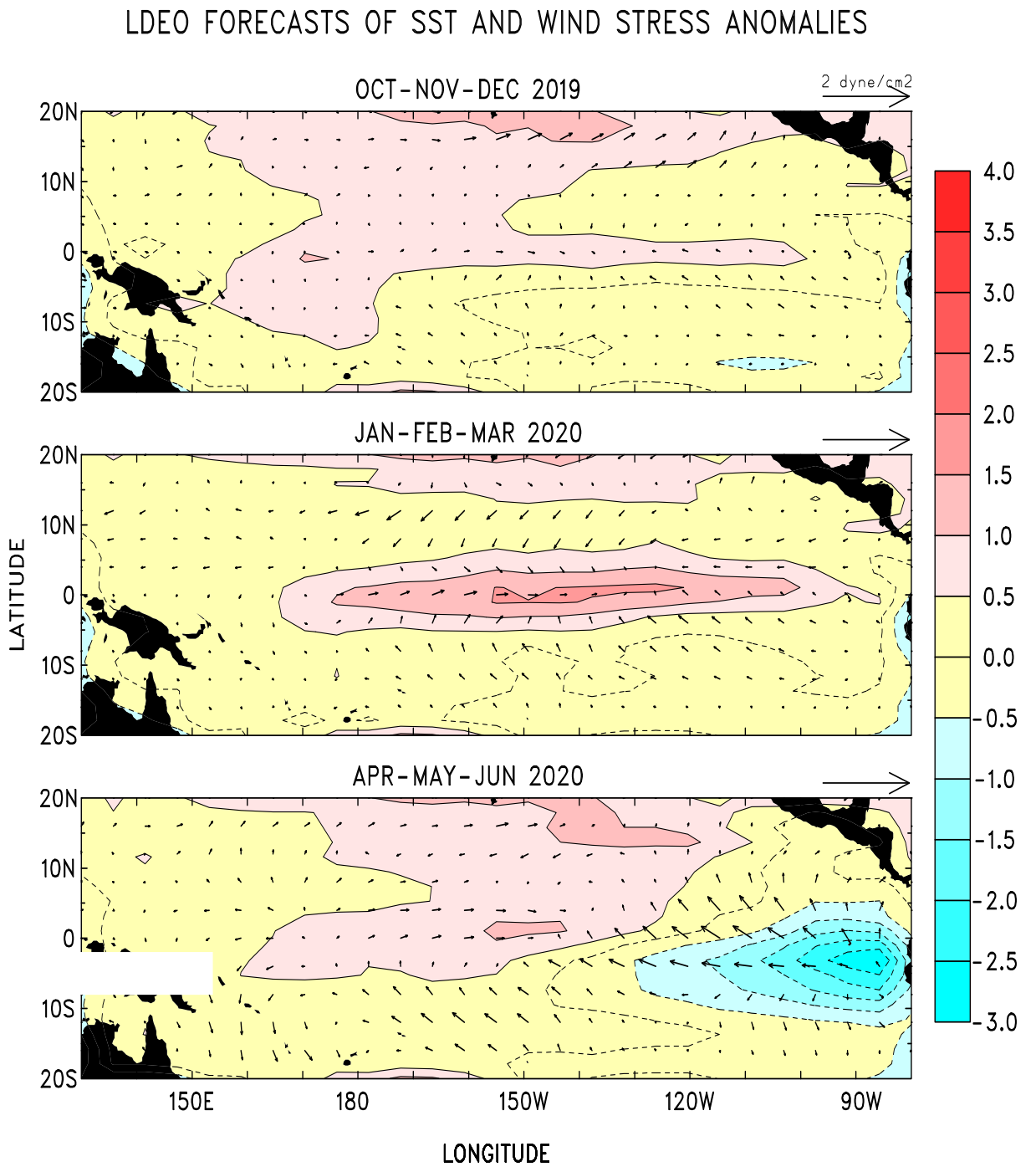


**FIGURE F7.** Forecasts of the tropical Pacific Predicted SST (shading) and vector wind anomalies for the next 3 seasons based on the LDEO model. Each forecast represents an ensemble average of 3 sets of predictions initialized during the last three consecutive months (see Figure F8).

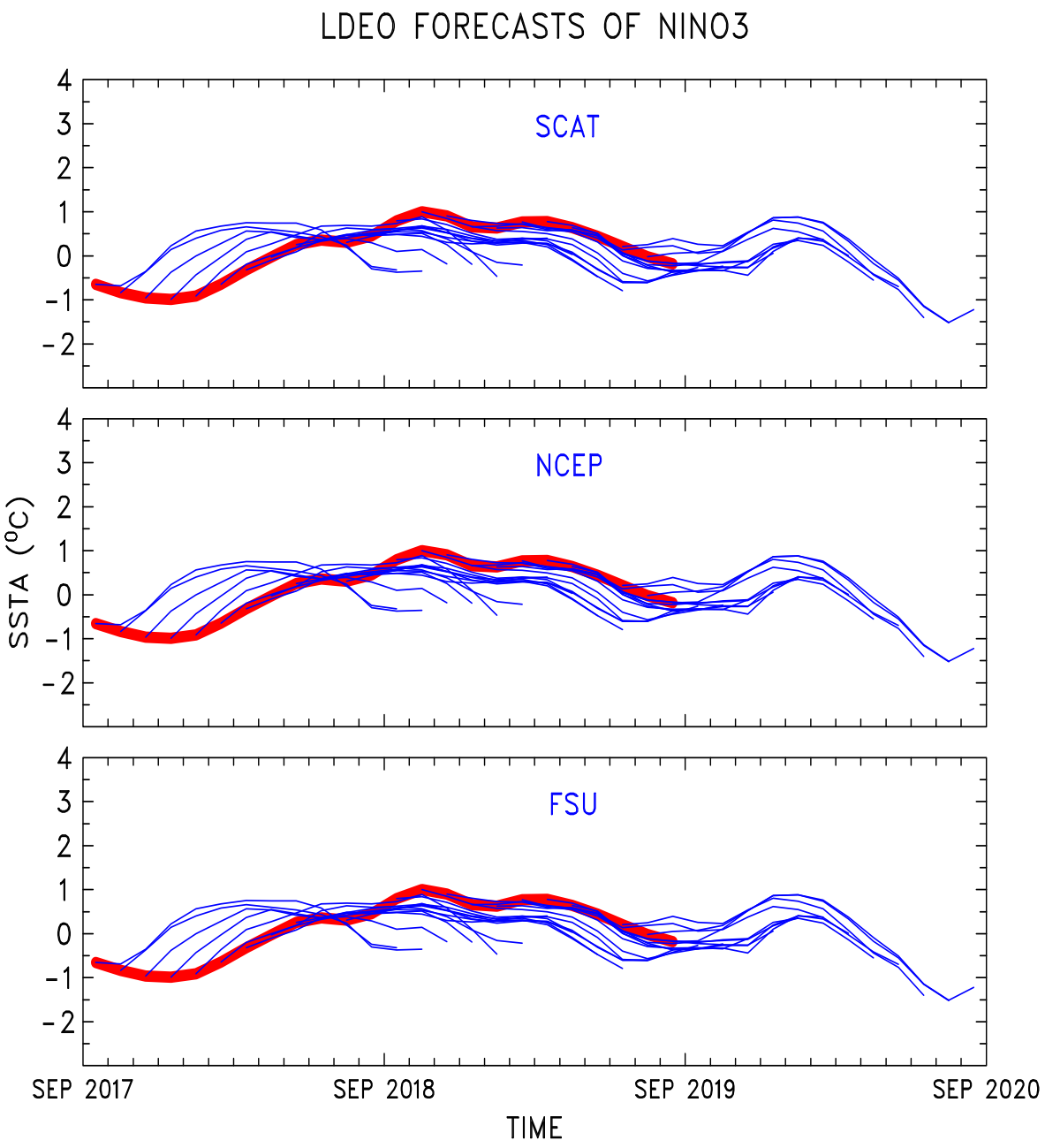


**FIGURE F8.** LDEO forecasts of SST anomalies for the Nino 3 region using wind stresses obtained from (top) QuikSCAT, (middle) NCEP, and (bottom) Florida State Univ. (FSU), along with SSTs (obtained from NCEP), and sea surface height data (obtained from TOPEX/POSEIDON) data. Each thin blue line represents a 12-month forecast, initialized one month apart for the past 24 months. Observed SST anomalies are indicated by the thick red line. The Nino-3 region spans the eastern equatorial Pacific between 5N-5S, 150W-90W.

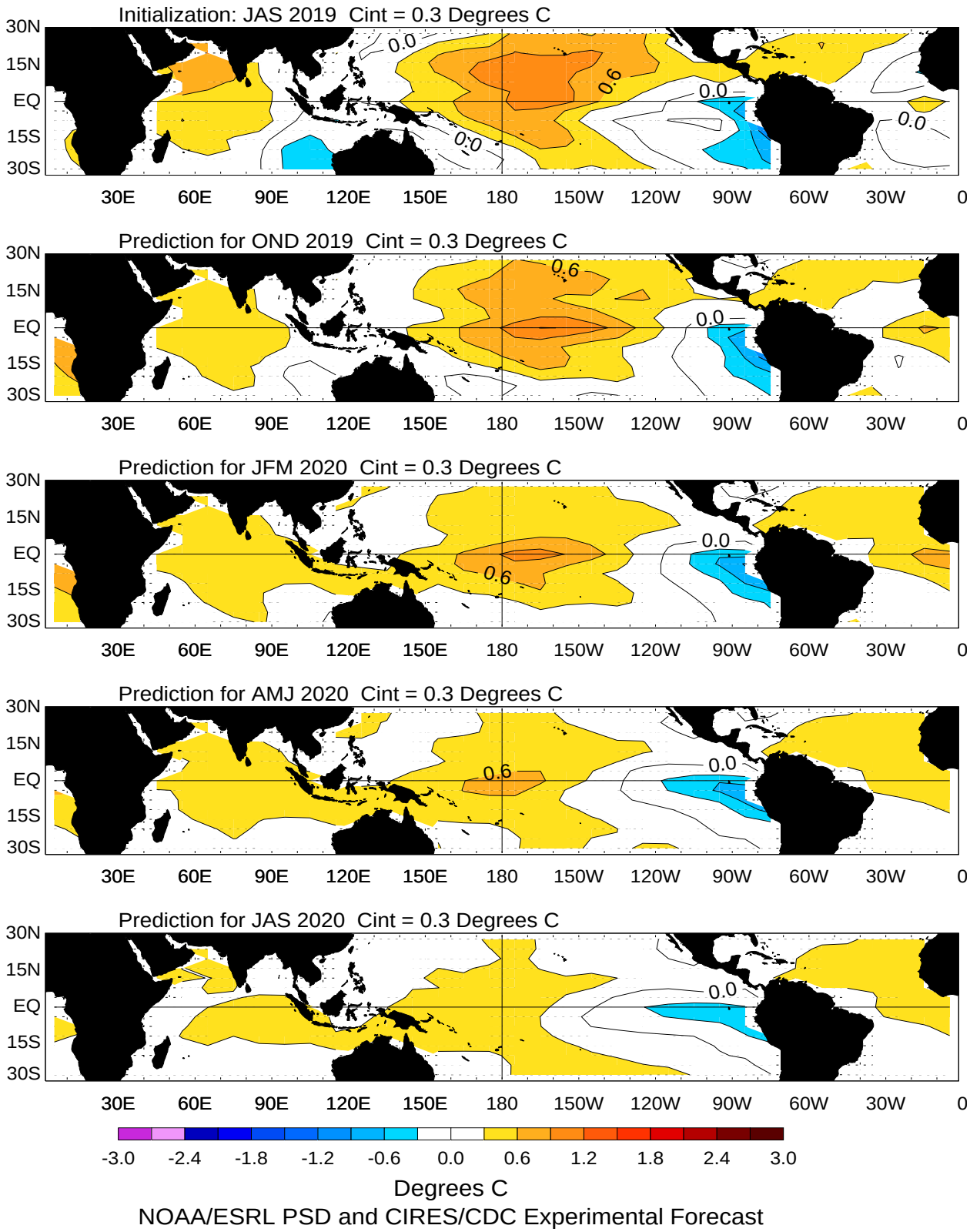


FIGURE F9. Forecast of tropical SST anomalies from the Linear Inverse Modeling technique of Penland and Magorian (1993: *J. Climate*, **6**, 1067-1076). The contour interval is 0.3C. Anomalies are calculated relative to the 1981-2010 climatology and are projected onto 20 leading EOFs.

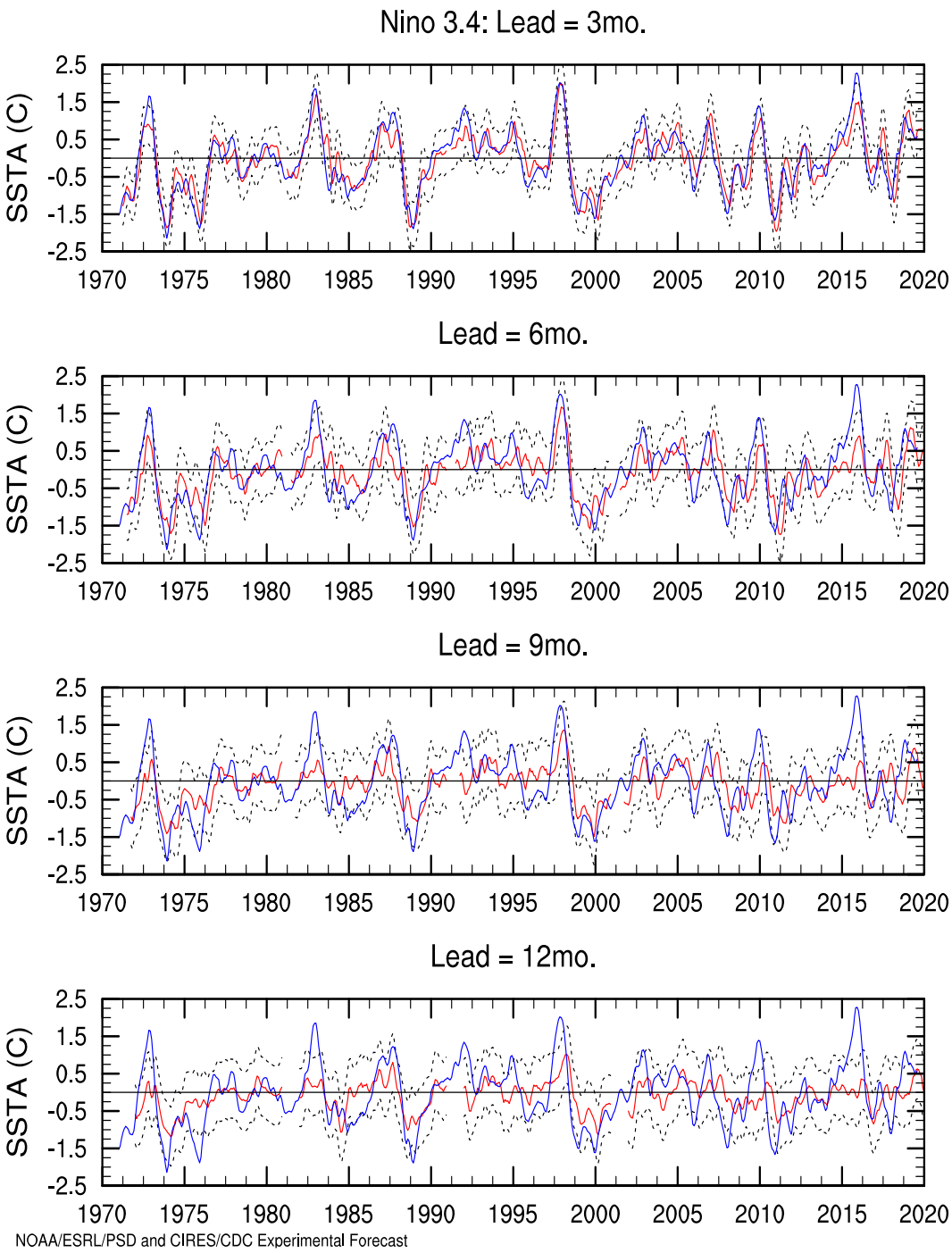


FIGURE F10. Predictions of Niño 3.4 SSTA (blue solid line) and verification (solid red line). The Niño3.4 Index was calculated in the area 6N-6S, 170W-120W. The 1980-2010 climatology was subtracted from ERSST data between 1950 and 2010, after which they were projected onto 20 EOFs containing 90% of thevariance. Significant 1950-2010 trends were subtracted from the corresponding PCs, the forecast was made on the detrended anomalies, after which the trend was added to the forecast. The dotted lines indicate the one standard deviation confidence interval for the forecasts based on a perfect adherence to assumption.

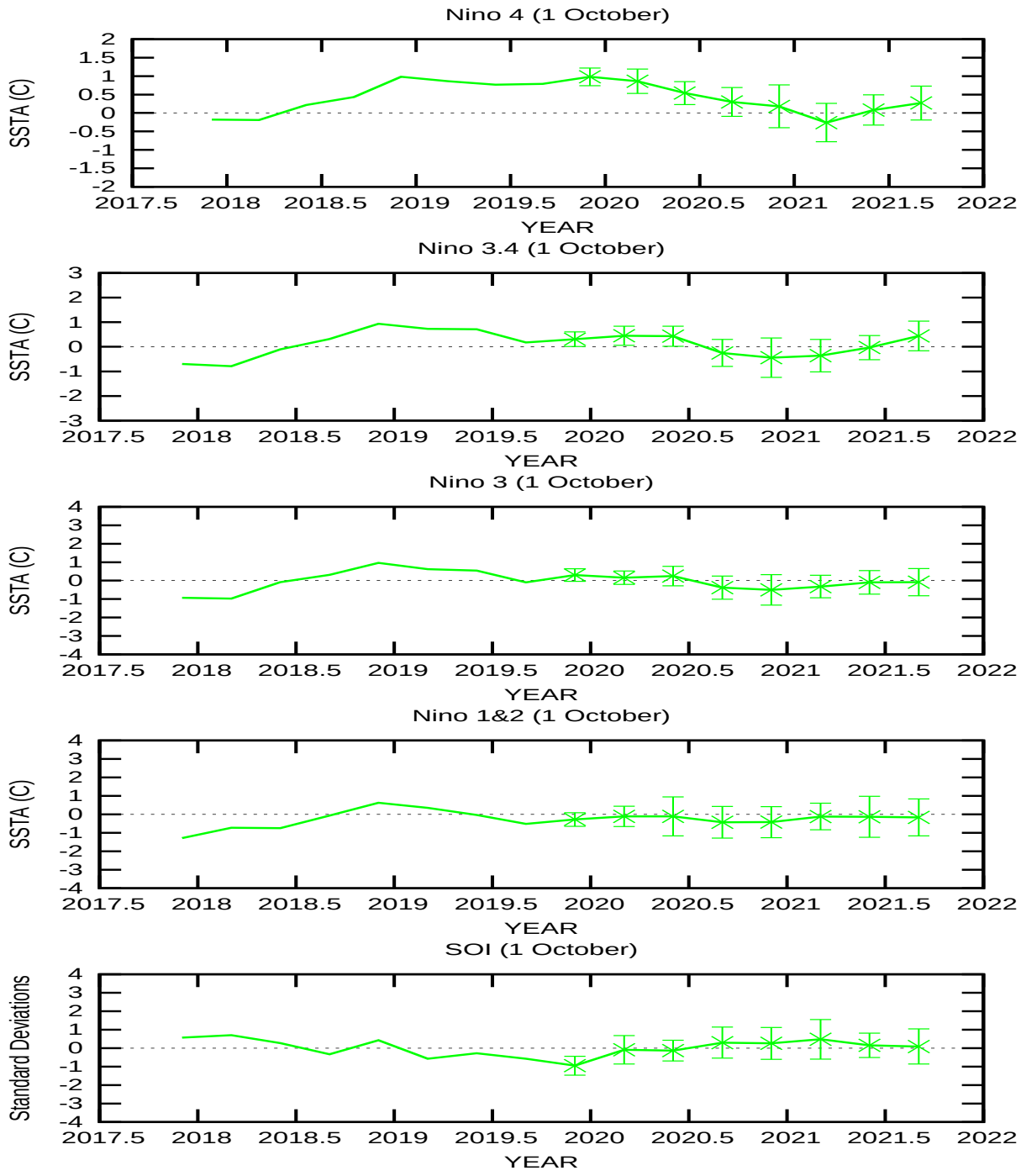


FIGURE F11. ENSO-CLIPER statistical model forecasts of three-month average sea surface temperature anomalies (green lines, deg. C) in (top panel) the Nino 4 region (5N-5S, 160E-150W), (second panel) the Nino 3.4 region (5N-5S, 170W-120W), (third panel) the Nino 3 region (5N-5S, 150W-90W), and (fourth panel) the Nino 1+2 region (0-10S, 90W-80W) (Knaff and Landsea 1997, *Wea. Forecasting*, **12**, 633-652). Bottom panel shows predictions of the three-month standardized Southern Oscillation Index (SOI, green line). Horizontal bars on green line indicate the adjusted root mean square error (RMSE). The Observed three-month average values are indicated by the thick blue line. SST anomalies are departures from the 1981-2010 base period means, and the SOI is calculated from the 1951-1980 base period means.

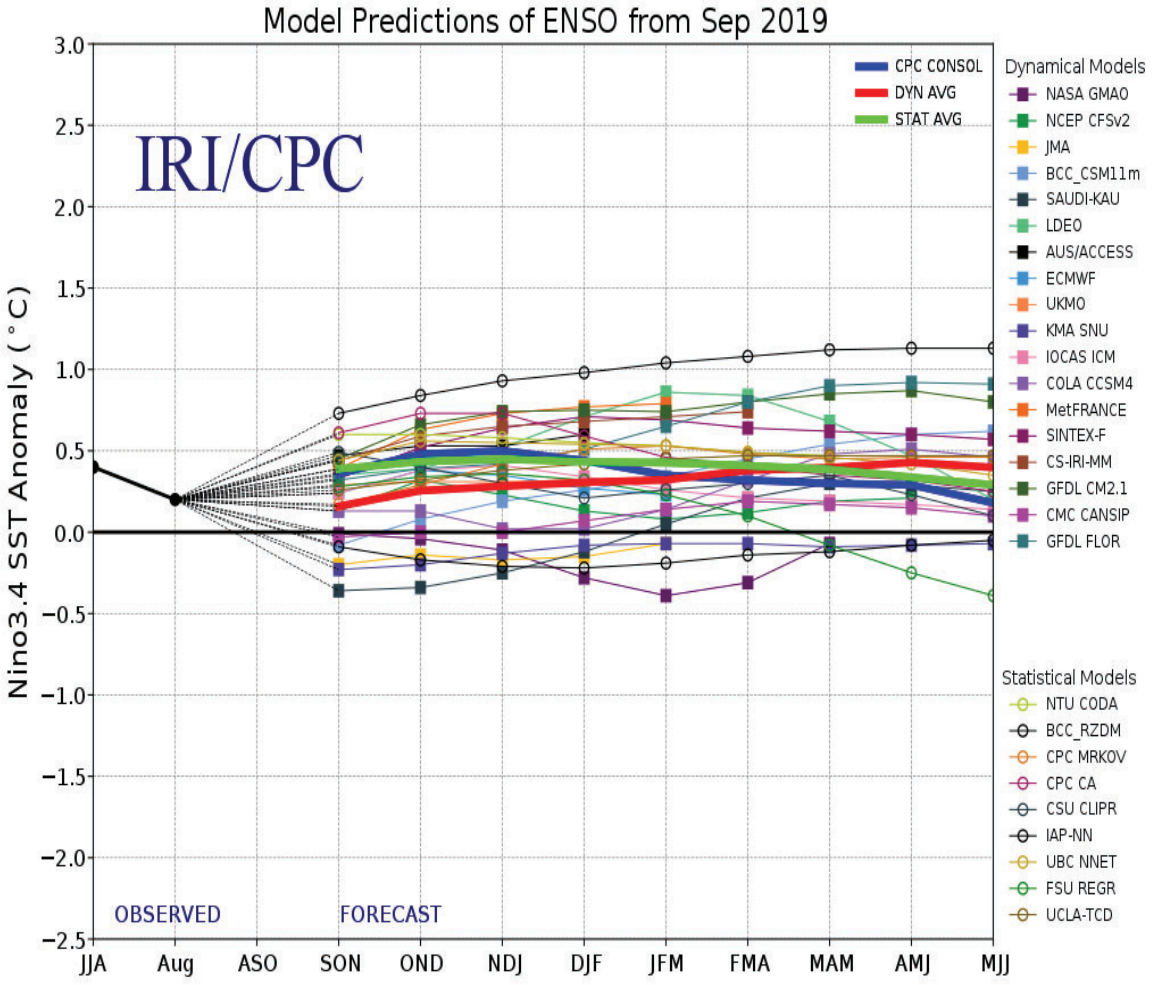


FIGURE F12. Time series of predicted sea surface temperature anomalies for the Nino 3.4 region (deg. C) from various dynamical and statistical models for nine overlapping 3-month periods. The Nino 3.4 region spans the east-central equatorial Pacific between 5N-5S, 170W-120W. Figure provided by the International Research Institute (IRI).

# Extratropical Highlights – September 2019

1. Northern Hemisphere

The 500-hPa circulation during September featured above-average heights over the eastern North Pacific Ocean, the eastern U.S., southern Europe, and the polar region, and below-average heights over the northwestern U.S. and central Russia (Fig. E9). The main land-surface temperature signals included above-average temperatures in Alaska, across the central and eastern U.S., in much of Europe, and in most of China (Fig. E1). The main precipitation signals included above-average totals across the northern tier of the U.S. and below-average totals in the eastern U.S. (Fig. E3).

a. North America

The 500-hPa circulation during September featured an anomalous wave pattern extending from the eastern North Pacific to the eastern U.S. (Fig. E9). This pattern reflected amplified ridges over the eastern North Pacific and the eastern U.S., and an amplified trough in the northwestern U.S.. These conditions contributed to above-average surface temperatures in Alaska, and across most of the U.S. east of the Rocky Mountains (Fig. E1).

The anomalous trough contributed to above-average precipitation in the northern tier of the U.S. (Fig. E3), with area-averaged totals exceeding the 90th percentile of occurrences in both the Pacific Northwest and Great Plains regions (Fig. E5). Conversely, in the eastern U.S., the anomalous ridge contributed to well below-average rainfall, with area-averaged totals in the lowest 10th percentile of occurrences in the Ohio Valley, Gulf Coast, and Mid-Atlantic regions (Fig. E5).

b. West African monsoon

The west African monsoon extends from June through September, with a peak during July-September. During September 2019, the west African monsoon system was enhanced (Fig. E3, Fig. T23, Fig. T24). For the July-September 2019 period as a whole, the monsoon was enhanced, with area-average rainfall totals above the 90th percentile of occurrences in both July and August (see Sahel region, Fig. E4).

.

2. Southern Hemisphere

The 500-hPa height field during September featured above-average heights over southern Australia, the high latitudes of the eastern South Pacific, and in the area south of Africa, and below-average heights over the central South Pacific and central Indian Ocean (Fig. E15). In southern Australia, the anomalous ridge contributed to warmer (Fig. E1) and drier (Fig. E3) than average conditions. In South America, the anomalous upstream ridge contributed to exceptionally dry conditions over much of the continent.

The Antarctic ozone hole typically develops during August and reaches peak size in September. The ozone hole then gradually decreases during October and November, and dissipates on average in early December (Fig. S8). By the end of September 2019, the size of the ozone hole was only about 7.5 million square kilometers, which is well below the 2008-2017 average size of 20 million square kilometers. This significantly reduced size of the ozone hole reflected a markedly reduced size of the polar vortex (22 million square kilometers compared to the average of 32 million), along with a complete disappearance of polar stratospheric clouds (PSCs) (Fig. S8). On average, the PSC area covers about 15 million square kilometers by the end of September. These highly anomalous stratospheric conditions were associated with a pronounced stratospheric warming (Fig. S4) and with well above-average heights throughout the polar stratosphere at levels above 50-hPa (Fig. S1).

# TELECONNECTION INDICES

| Month | North Atlantic | | | North Pacific | | | EURASIA | | |
|---|---|---|---|---|---|---|---|---|---|
| | NAO | EA | WP | EP-NP | PNA | TNH | EATL/ WRUS | SCAND | POLEUR |
| SEP 19 | -0.0 | 2.2 | 0.9 | -1.5 | 1.6 | --- | 0.8 | -0.5 | -0.1 |
| AUG 19 | -1.6 | 1.9 | -2.2 | -1.2 | 1.2 | --- | -1.7 | -2.1 | 0.3 |
| JUL 19 | -1.4 | 0.1 | -0.3 | 0.1 | 0.6 | --- | 1.0 | -0.7 | -1.5 |
| JUN 19 | -0.8 | 1.3 | -1.9 | 1.7 | 0.2 | --- | 0.3 | -0.2 | -0.5 |
| MAY 19 | -2.4 | -0.6 | -0.6 | 0.3 | -0.2 | --- | -0.7 | -0.1 | -0.8 |
| APR 19 | 0.4 | -1.0 | -1.3 | 0.7 | -0.8 | --- | 0.8 | 2.1 | -0.4 |
| MAR 19 | 0.9 | 0.9 | 0.9 | 2.1 | -0.1 | --- | -1.1 | -0.9 | 0.9 |
| FEB 19 | -0.1 | -0.1 | 2.1 | 1.2 | -1.7 | 1.6 | 0.5 | -0.4 | 0.7 |
| JAN 19 | 0.2 | -1.7 | 1.0 | 1.1 | 0.4 | 0.3 | 0.7 | -0.1 | 0.1 |
| DEC 18 | 0.5 | 1.4 | 0.1 | --- | 0.6 | -0.6 | -0.4 | 1.3 | 1.5 |
| NOV 18 | -0.3 | 0.3 | -0.6 | 1.4 | 0.2 | --- | 1.5 | 1.9 | 0.8 |
| OCT 18 | 1.5 | -0.4 | -1.1 | 1.2 | 0.4 | --- | 0.4 | -1.1 | -1.3 |
| SEP 18 | 1.8 | 0.1 | -1.8 | -0.8 | 1.2 | --- | -1.8 | -0.7 | 0.5 |

TABLE E1-Standardized amplitudes of selected Northern Hemisphere teleconnection patterns for the most recent thirteen months (computational procedures are described in Fig. E7). Pattern names and abbreviations are North Atlantic Oscillation (NAO); East Atlantic pattern (EA);West Pacific pattern (WP); East Pacific - North Pacific pattern (EP-NP); Pacific/North American pattern (PNA); Tropical/Northern Hemisphere pattern (TNH);East Atlantic/Western Russia pattern (EATL/WRUS-called Eurasia-2 pattern by Barnston and Livezey, 1987, *Mon. Wea. Rev.*, **115**, 1083-1126); Scandanavia pattern (SCAND-called Eurasia-1 pattern by Barnston and Livezey 1987); and Polar Eurasia pattern (POLEUR). No value is plotted for calendar months in which the pattern does not appear as a leading mode.

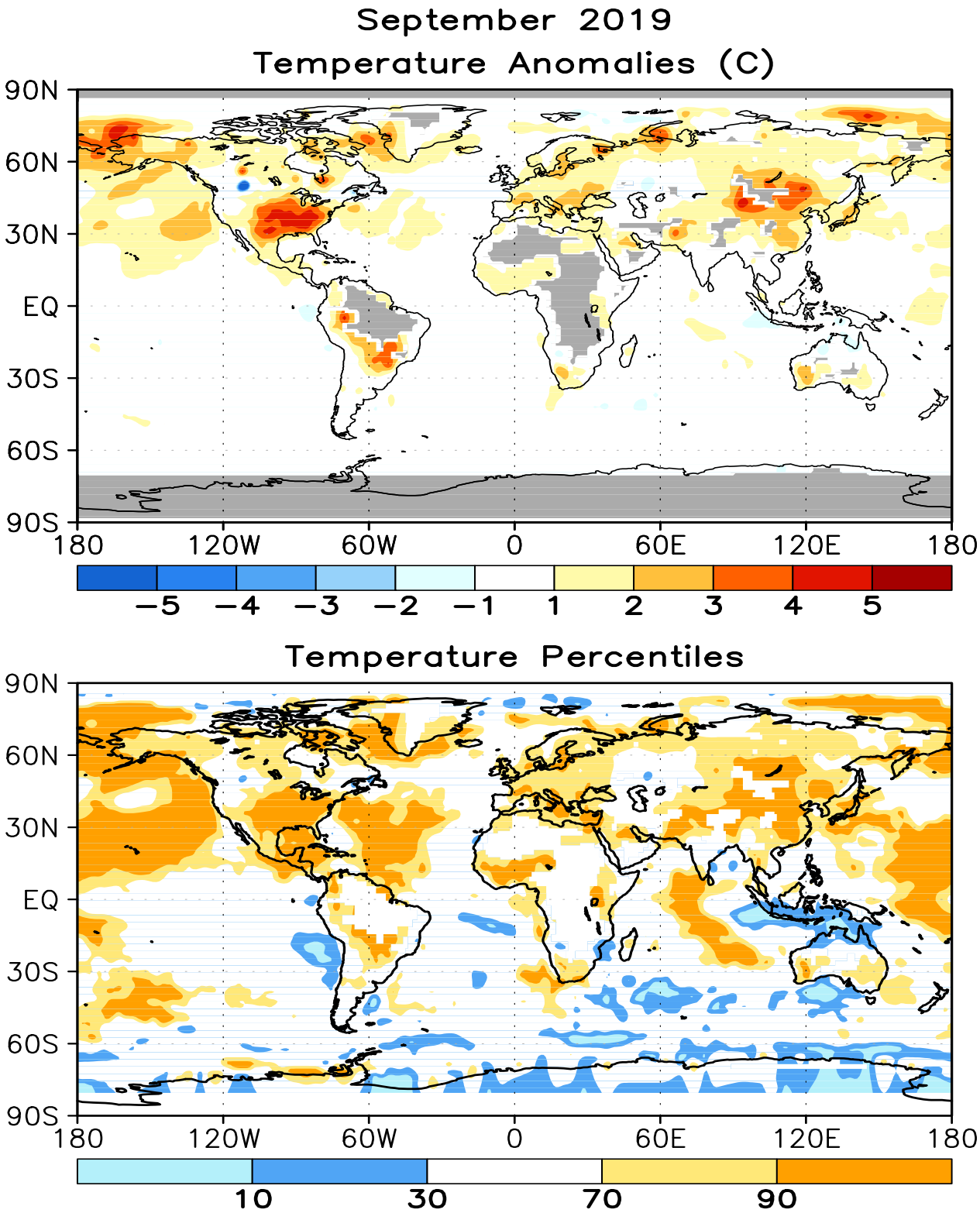


FIGURE E1. Surface temperature anomalies (°C, top) and surface temperature expressed as percentiles of the normal (Gaussian) distribution fit to the 1981–2010 base period data (bottom) for SEP 2019. Analysis is based on station data over land and on SST data over the oceans (top). Anomalies for station data are departures from the 1981–2010 base period means, while SST anomalies are departures from the 1981–2010 adjusted OI climatology. (Smith and Reynolds 1998, *J. Climate*, **11**, 3320-3323). Regions with insufficient data for analysis in both figures are indicated by shading in the top figure only.

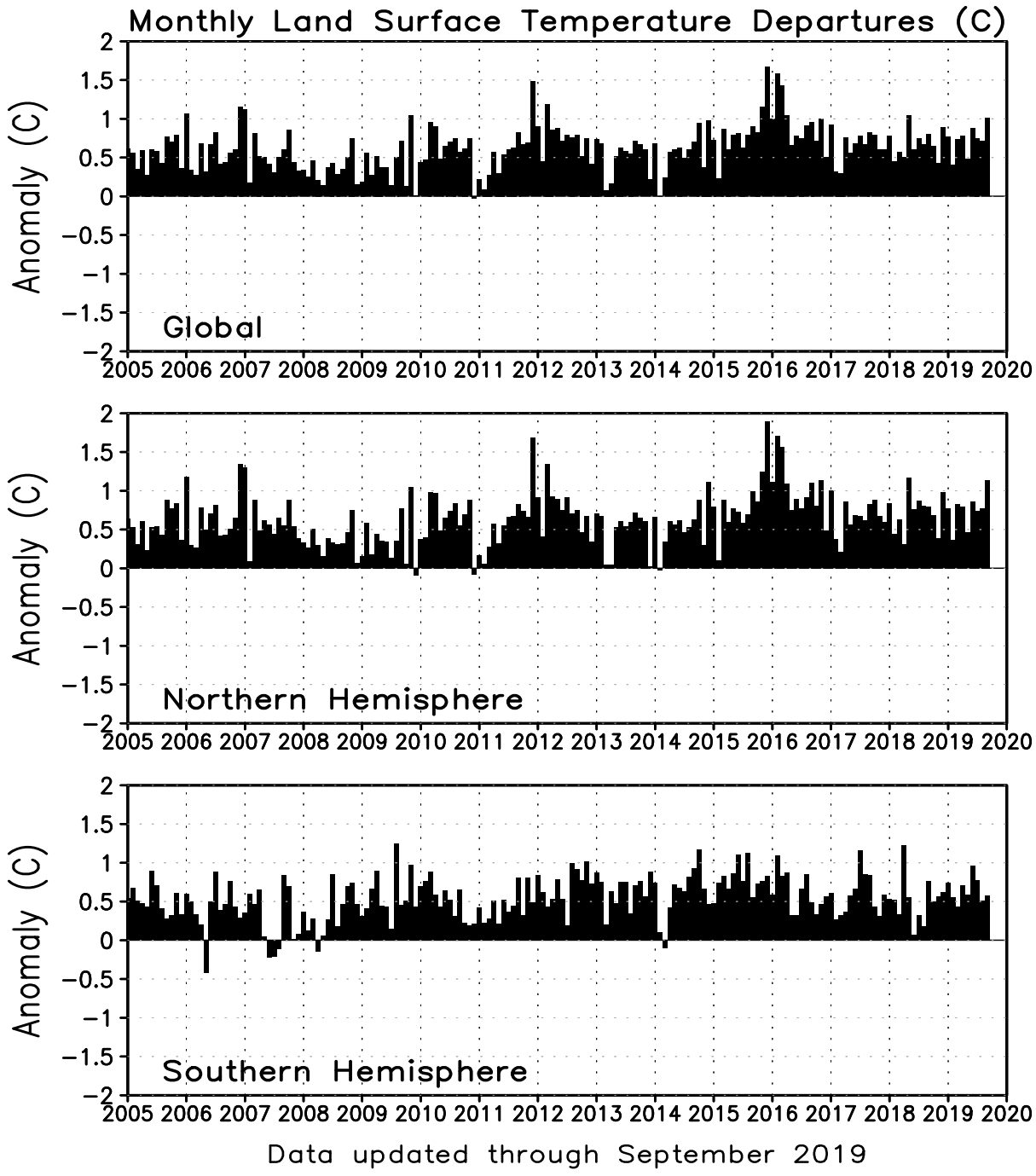


FIGURE E2. Monthly global (top), Northern Hemisphere (middle), and Southern Hemisphere (bottom) surface temperature anomalies (land only, ˚C) from January 1990 - present, computed as departures from the 1981–2010 base period means.

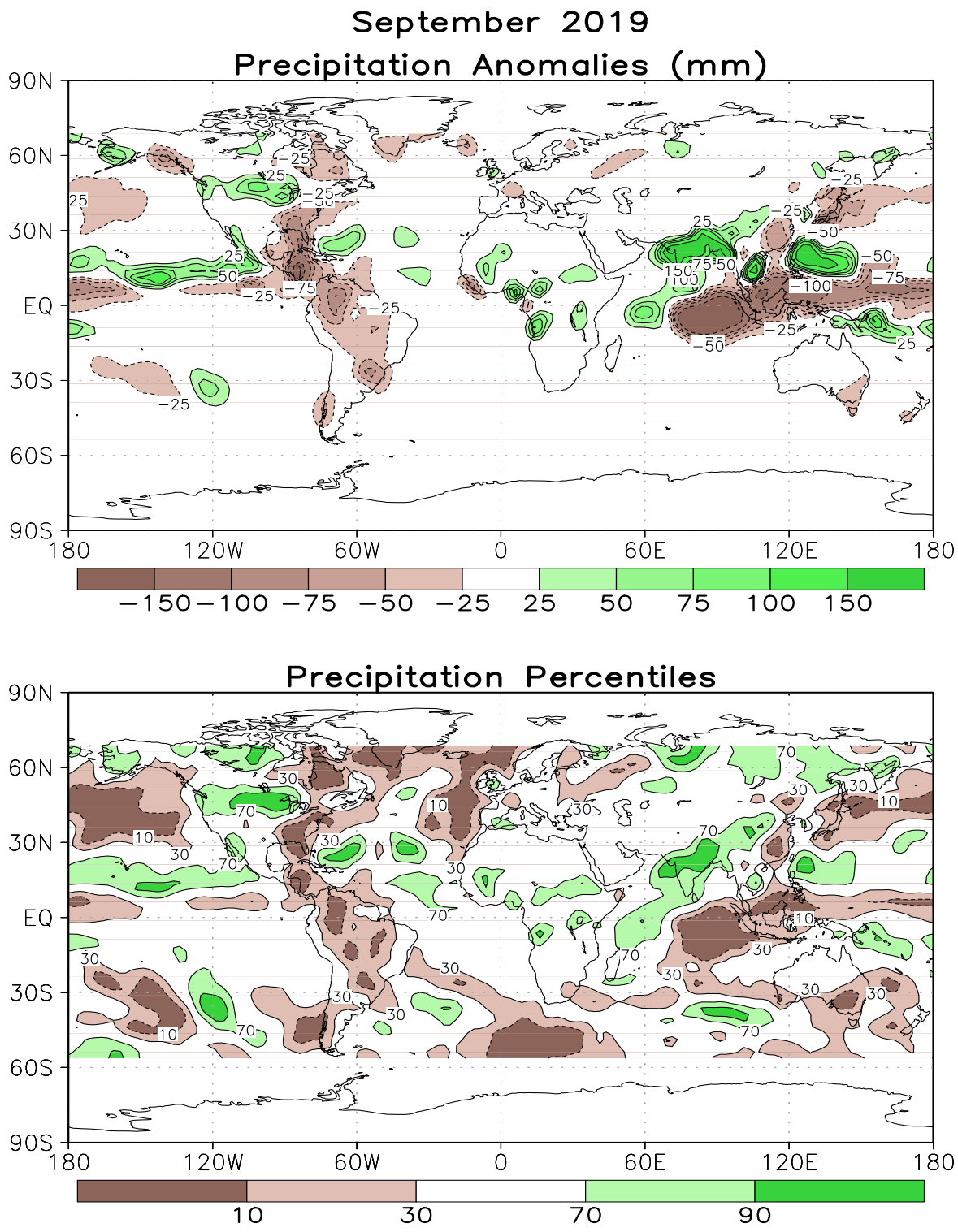


FIGURE E3. Anomalous precipitation (mm, top) and precipitation percentiles based on a Gamma distribution fit to the 1981–2010 base period data (bottom) for SEP 2019. Data are obtained from a merge of raingauge observations and satellite-derived precipitation estimates (Janowiak and Xie 1999, *J. Climate*, **12**, 3335–3342). Contours are drawn at 200, 100, 50, 25, -25, -50, -100, and -200 mm in top panel. Percentiles are not plotted in regions where mean monthly precipitation is <5mm/month.

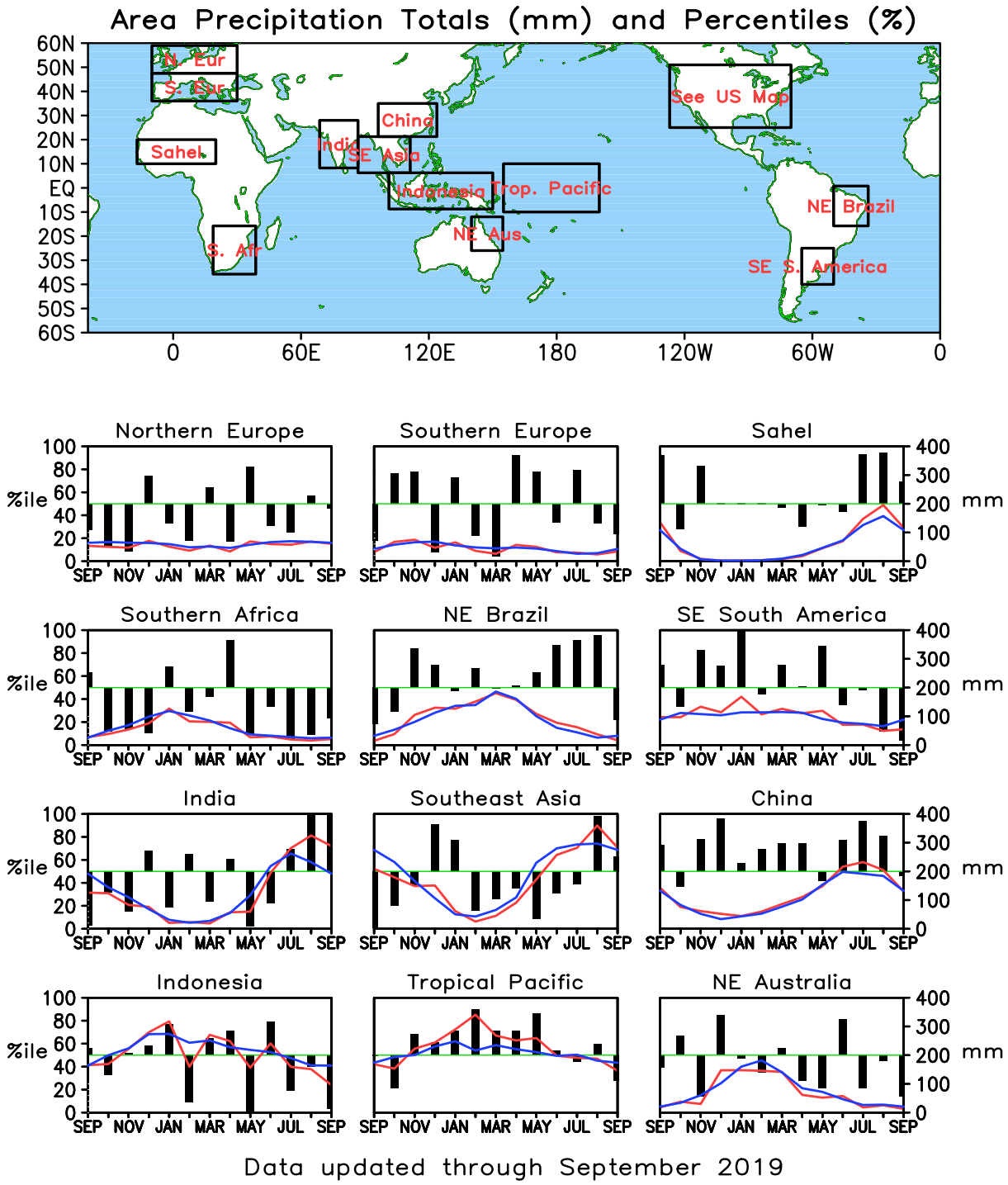


FIGURE E4. Areal estimates of monthly mean precipitation amounts (mm, solid lines) and precipitation percentiles (%, bars) for the most recent 13 months obtained from a merge of raingauge observations and satellite-derived precipitation estimates (Janowiak and Xie 1999, *J. Climate*, **12**, 3335–3342). The monthly precipitation climatology (mm, dashed lines) is from the 1981–2010 base period monthly means. Monthly percentiles are not shown if the monthly mean is less than 5 mm.

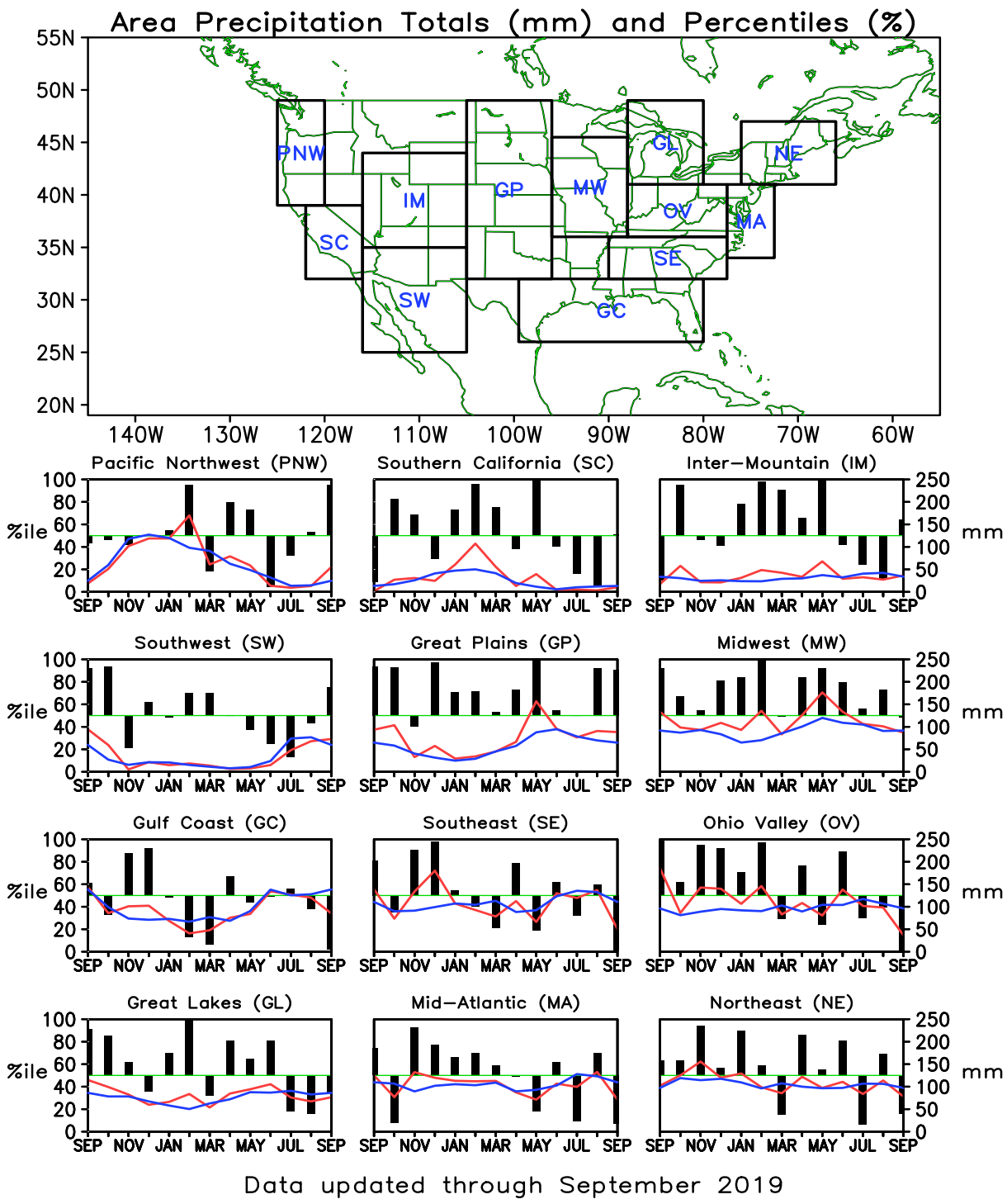


FIGURE E5. Areal estimates of monthly mean precipitation amounts (mm, solid lines) and precipitation percentiles (%, bars) for the most recent 13 months obtained from a merge of raingauge observations and satellite-derived precipitation estimates (Janowiak and Xie 1999, *J. Climate*, **12**, 3335–3342). The monthly precipitation climatology (mm, dashed lines) is from the 1981–2010 base period monthly means. Monthly percentiles are not shown if the monthly mean is less than 5 mm.

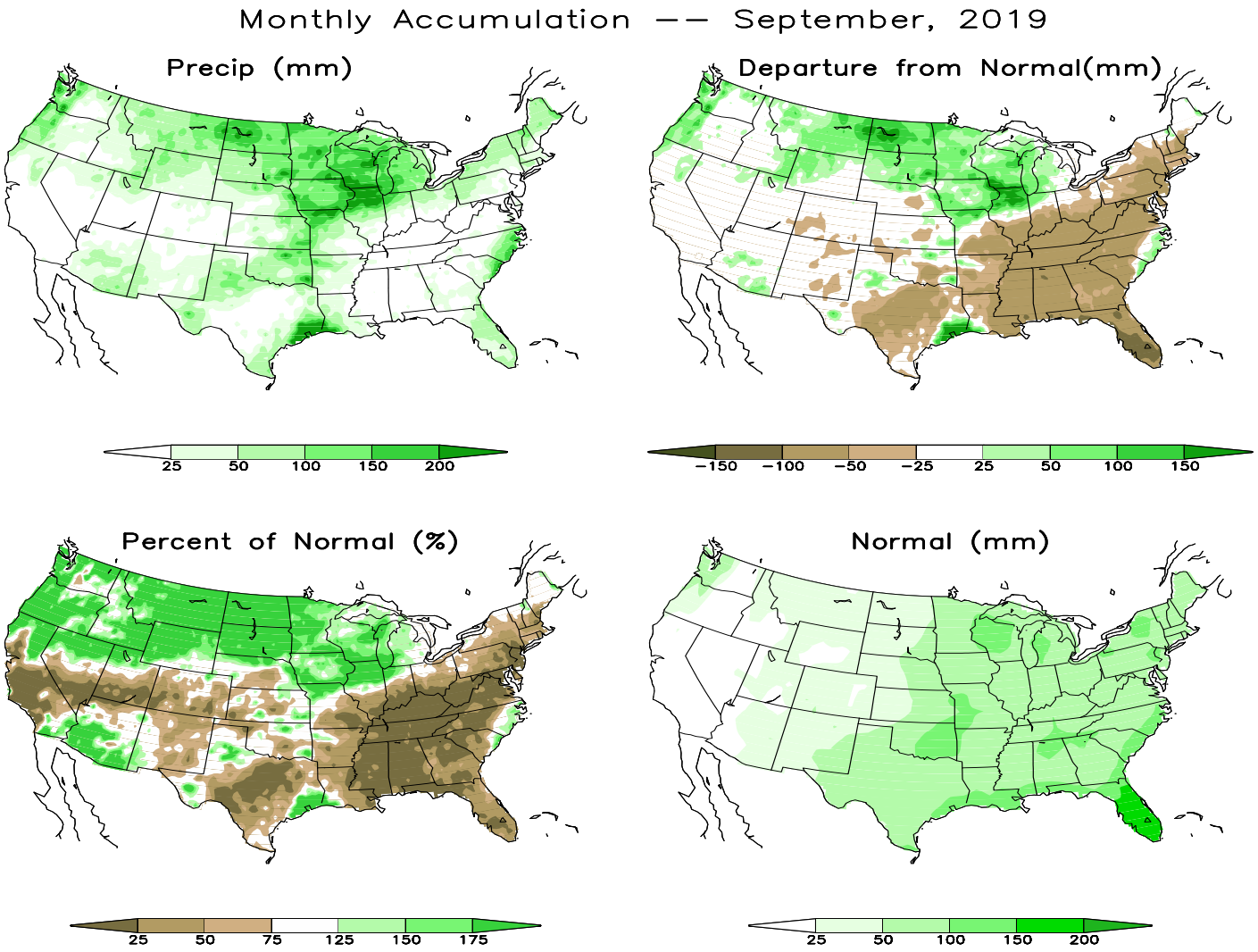


FIGURE E6. Observed precipitation (upper left), departure from average (upper right), percent of average (lower left), and average precipitation (lower right) for SEP 2019. The units are given on each panel. Base period for averages is 1981–2010. Results are based on CPC's U. S. daily precipitation analysis, which is available at http://www.cpc.ncep.noaa.gov/prodcuts/precip/realtime.

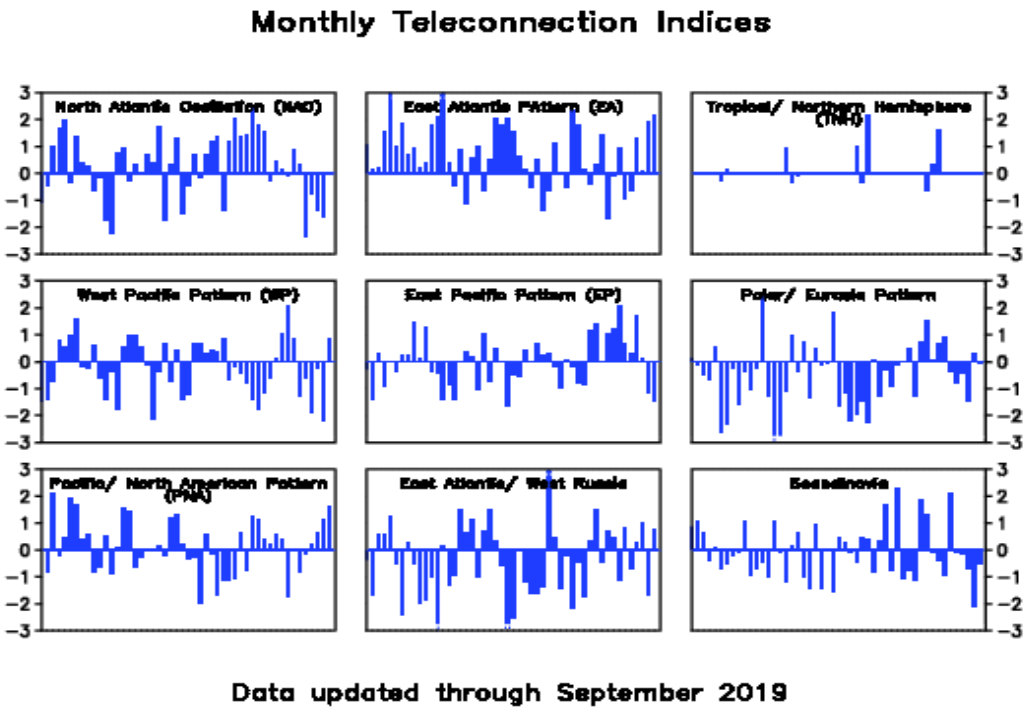


FIGURE E7. Standardized monthly Northern Hemisphere teleconnection indices. The teleconnection patterns are calculated from a Rotated Principal Component Analysis (RPCA) applied to monthly standardized 500-hPa height anomalies during the 1981-2010 base period. To obtain these patterns, ten leading un-rotated modes are first calculated for each calendar month by using the monthly height anomaly fields for the three-month period centered on that month: [i.e., The July modes are calculated from the June, July, and August standardized monthly anomalies]. A Varimax spatial rotation of the ten leading un-rotated modes for each calendar month results in 120 rotated modes (12 months x 10 modes per month) that yield ten primary teleconnection patterns.The teleconnection indices are calculated by first projecting the standardized monthly anomalies onto the teleconnection patterns corresponding to that month (eight or nine teleconnection patterns are seen in each calendar month). The indices are then solved for simultaneously using a Least-Squares approach. In this approach, the indices are the solution to the Least-Squares system of equations which explains the maximum spatial structure of the observed height anomaly field during the month. The indices are then standardized for each pattern and calendar month independently. No index value exists when the teleconnection pattern does not appear as one of the ten leading rotated EOF's valid for that month.

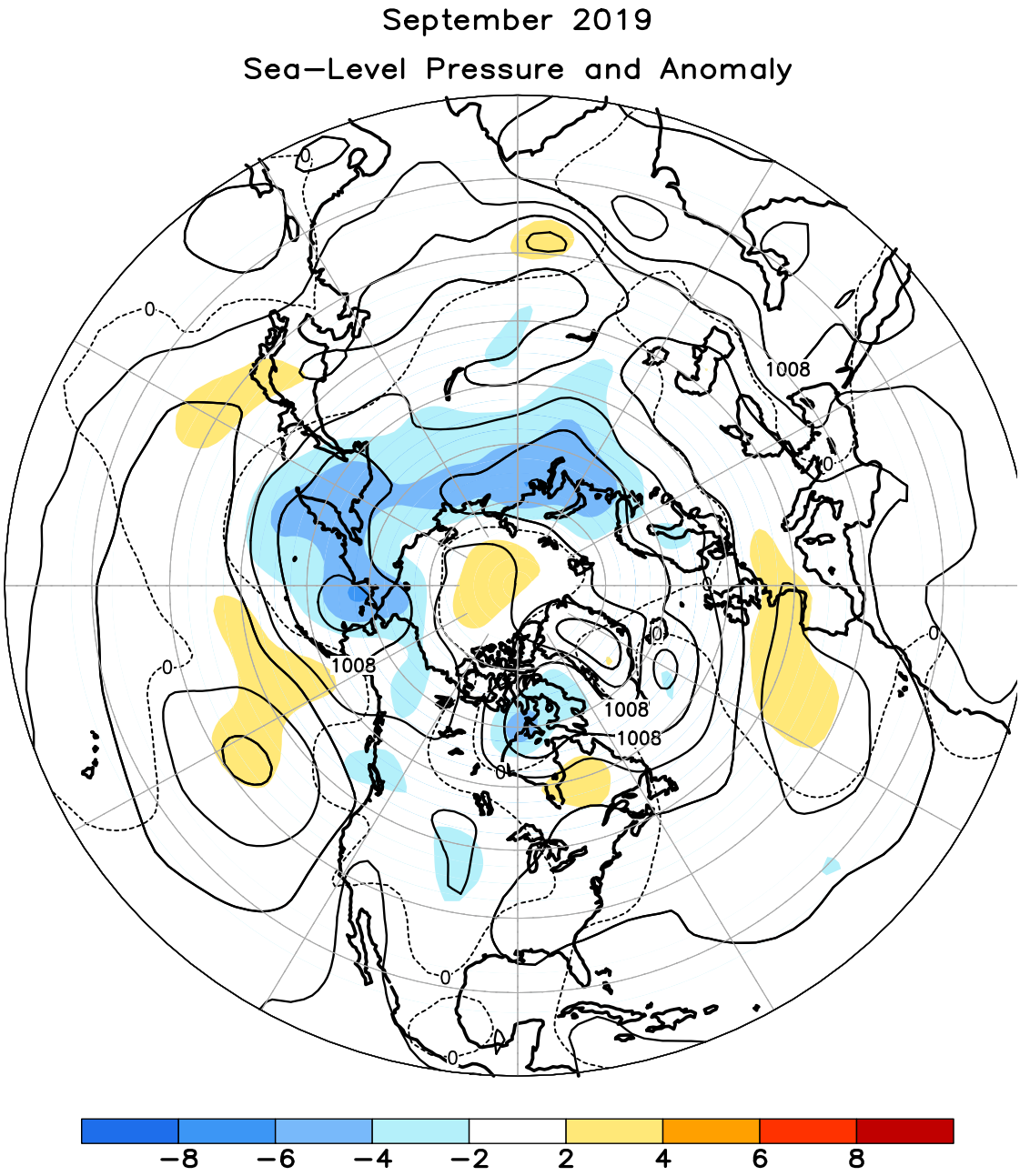


FIGURE E8. Northern Hemisphere mean and anomalous sea level pressure (CDAS/Reanalysis) for SEP 2019. Mean values are denoted by solid contours drawn at an interval of 4 hPa. Anomaly contour interval is 2 hPa with values less (greater) than -2 hPa (2 hPa) indicated by dark (light) shading. Anomalies are calculated as departures from the 1981-2010 base period monthly means.

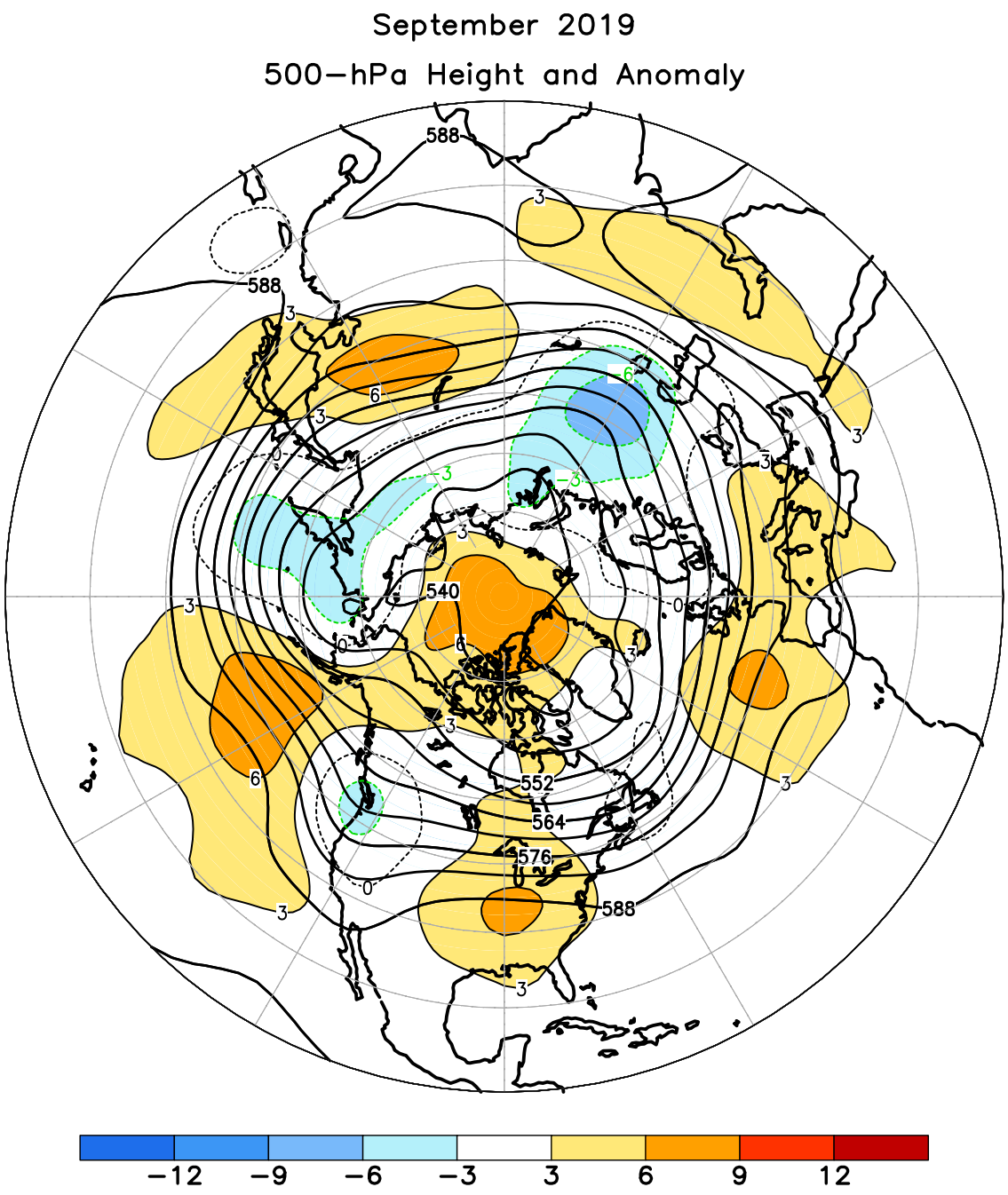


FIGURE E9. Northern Hemisphere mean and anomalous 500-hPa geopotential height (CDAS/Reanalysis) for SEP 2019. Mean heights are denoted by solid contours drawn at an interval of 6 dam. Anomaly contour interval is 3 dam with values less (greater) than -3 dam (3 dam) indicated by dark (light) shading. Anomalies are calculated as departures from the 1981-2010 base period monthly means.

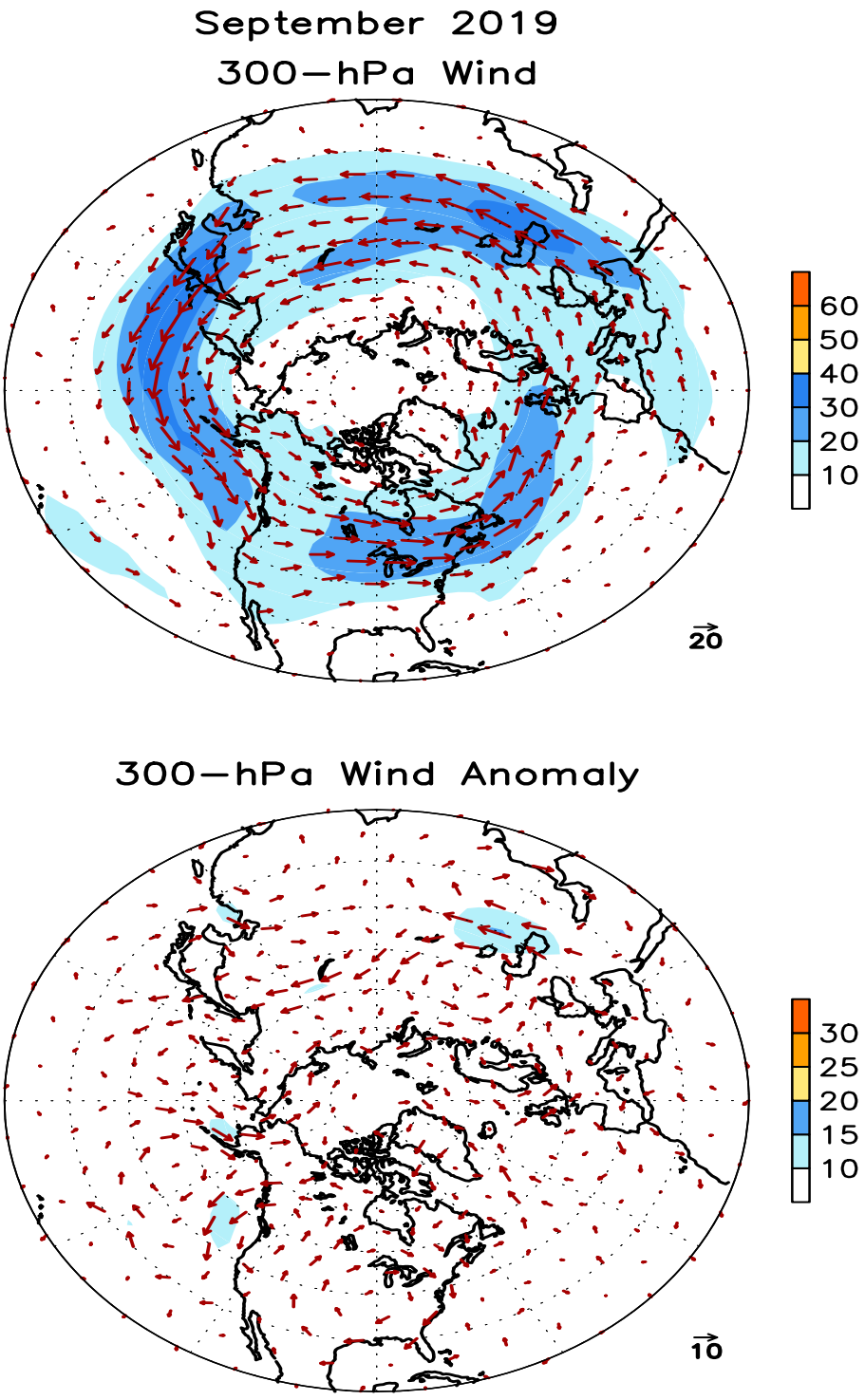


FIGURE E10. Northern Hemisphere mean (left) and anomalous (right) 300-hPa vector wind (CDAS/Reanalysis) for SEP 2019. Mean (anomaly) isotach contour interval is 10 (5) $ms^{-1}$. Values greater than 30 $ms^{-1}$ (left) and 10 $ms^{-1}$ (rights) are shaded. Anomalies are departures from the 1981-2010 base period monthly means.

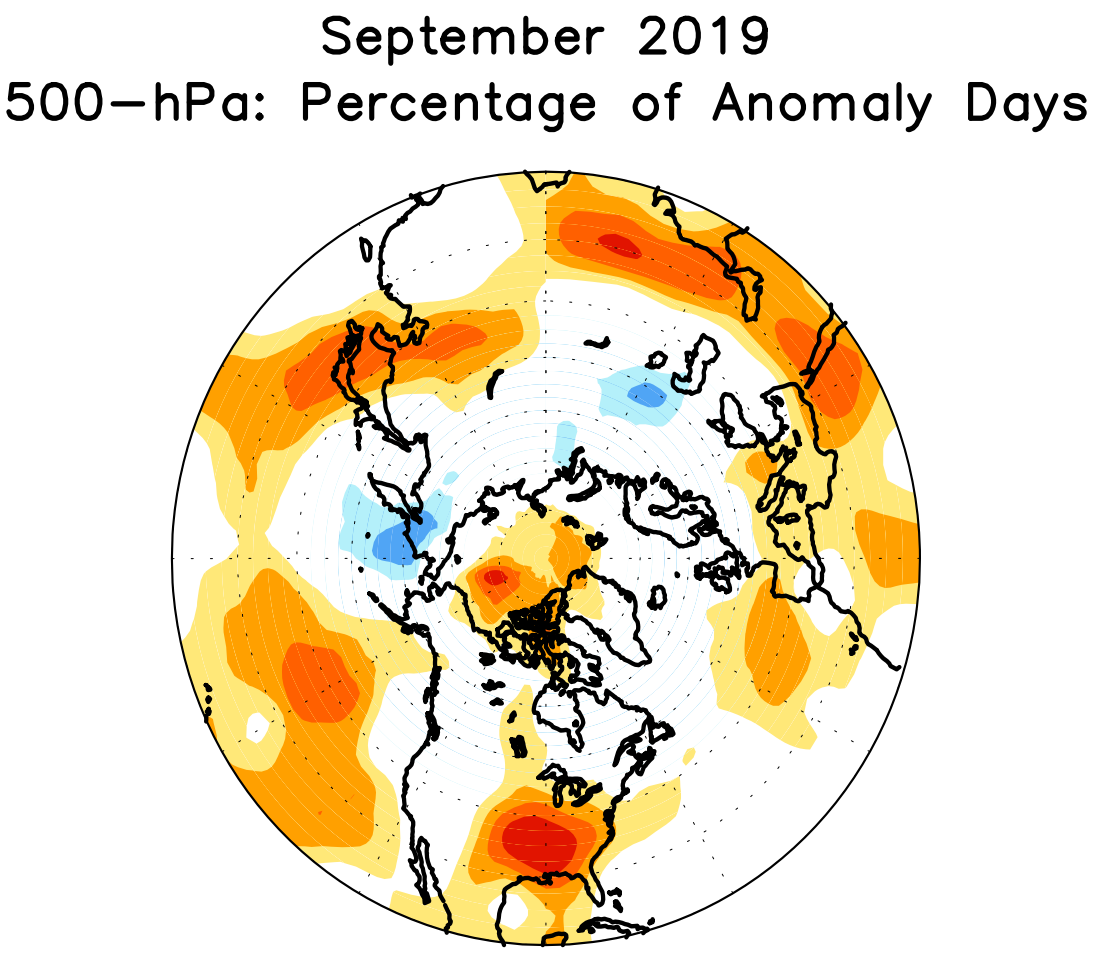


FIGURE E11. Northern Hemisphere percentage of days during SEP 2019 in which 500-hPa height anomalies greater than 15 m (red) and less than -15 m (blue) were observed. Values greater than 70% are shaded and contour in-

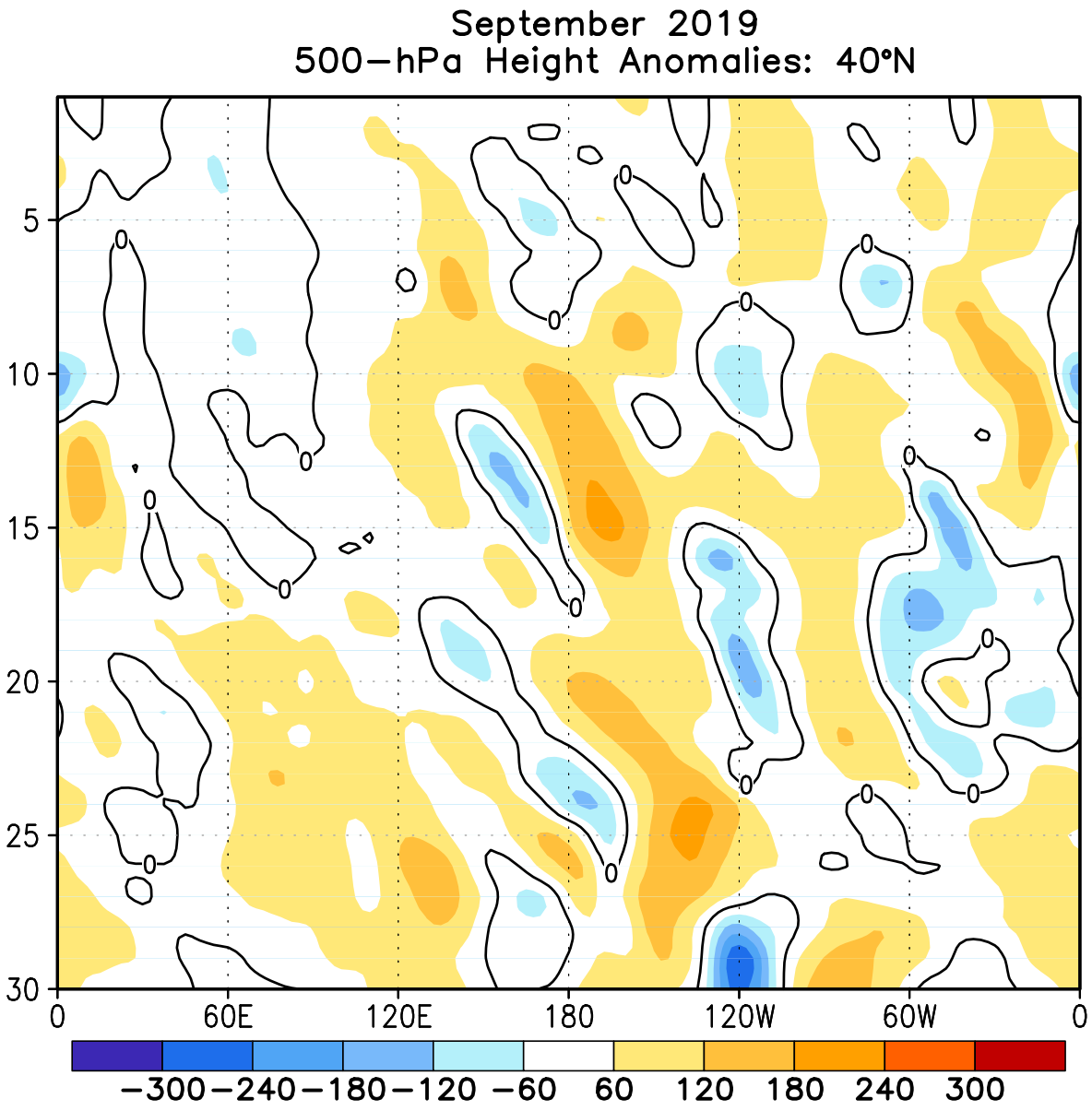


FIGURE E12. Northern Hemisphere: Daily 500-hPa height anomalies for SEP 2019 averaged over the 5° latitude band centered on 40°N. Positive values are indicated by solid contours and dark shading. Negative values are indicated by dashed coutours and light shading. Contour interval is 60 m. Anomalies are departures from the 1981-2010 base period daily means.

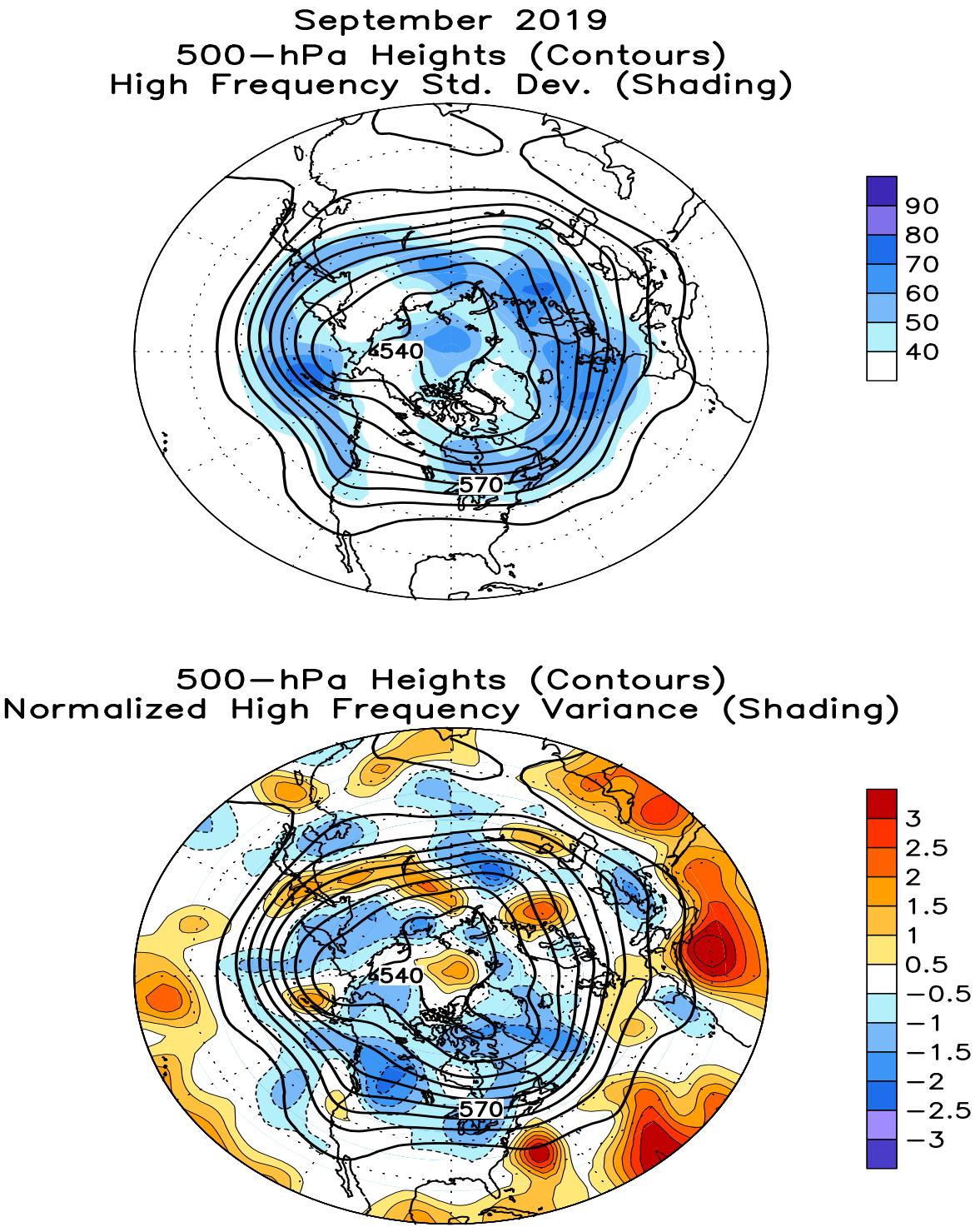


FIGURE E13. Northern Hemisphere 500-hPa heights (thick contours, interval is 6 dam) overlaid with (Top) Standard deviation of 10-day high-pass (HP) filtered height anomalies and (Bottom) Normalized anomalous variance of 10-day HP filtered height anomalies. A Lanczos filter is used to calculate the HP filtered anomalies. Anomalies are departures from the 1981-2010 daily means.

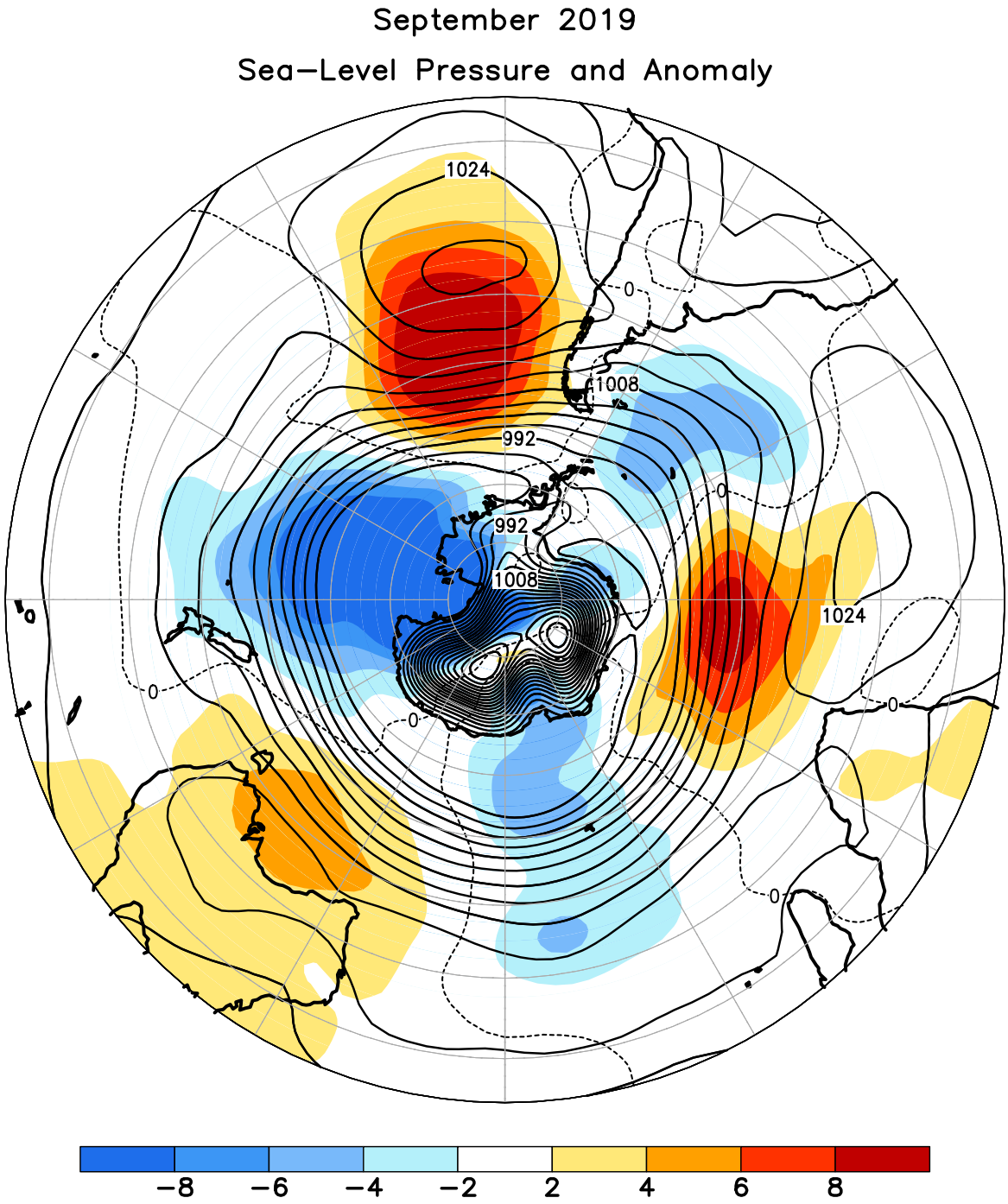


FIGURE E14. Southern Hemisphere mean and anomalous sea level pressure(CDAS/Reanalysis) for SEP 2019. Mean values are denoted by solid contours drawn at an interval of 4 hPa. Anomaly contour interval is 2 hPa with values less (greater) than -2 hPa (2 hPa) indicated by dark (light) shading. Anomalies are calculated as departures from the 1981-2010 base period monthly means.

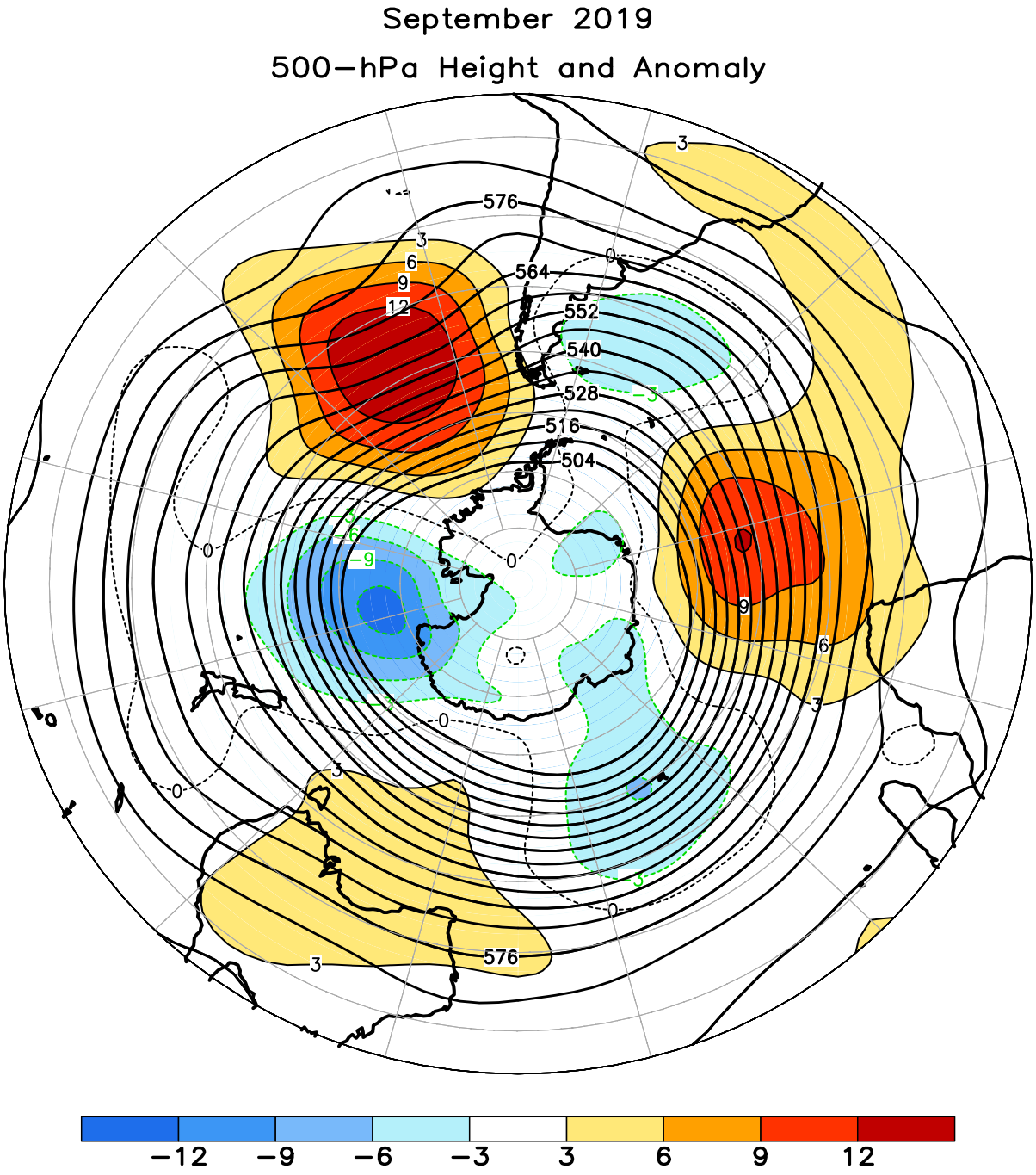


FIGURE E15. Southern Hemisphere mean and anomalous 500-hPa geopotential height (CDAS/Reanalysis) for SEP 2019. Mean heights are denoted by solid contours drawn at an interval of 6 dam. Anomaly contour interval is 3 dam with values less (greater) than -3 dam (3 dam) indicated by dark (light) shading. Anomalies are calculated as departures from the 1981-2010 base period monthly means.

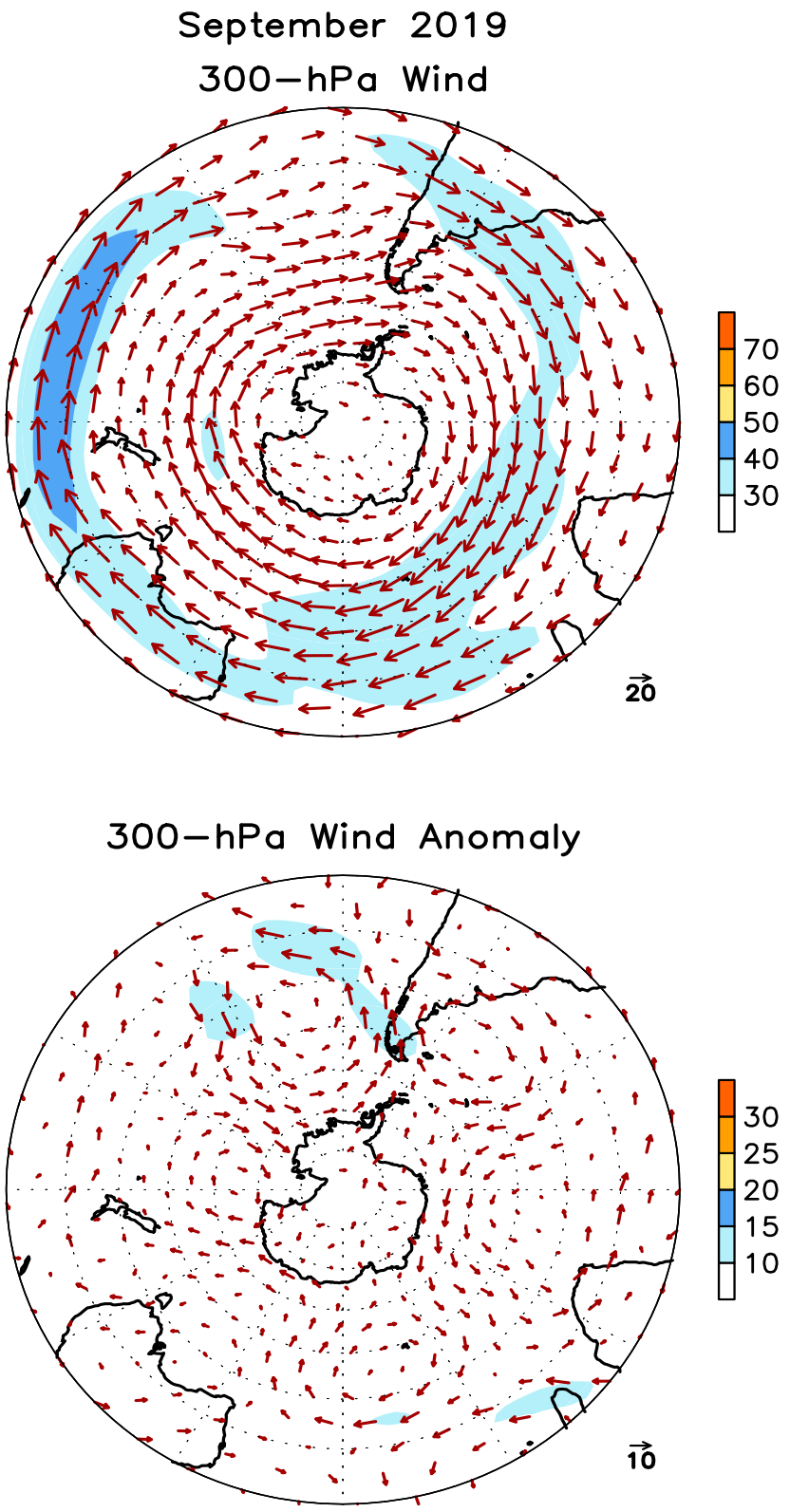


FIGURE E16. Southern Hemisphere mean (left) and anomalous (right) 300-hPa vector wind (CDAS/Reanalysis) for SEP 2019. Mean (anomaly) isotach contour interval is 10 (5) $ms^{-1}$. Values greater than 30 $ms^{-1}$ (left) and 10 $ms^{-1}$ (rights) are shaded. Anomalies are departures from the 1981-2010 base period monthly means.

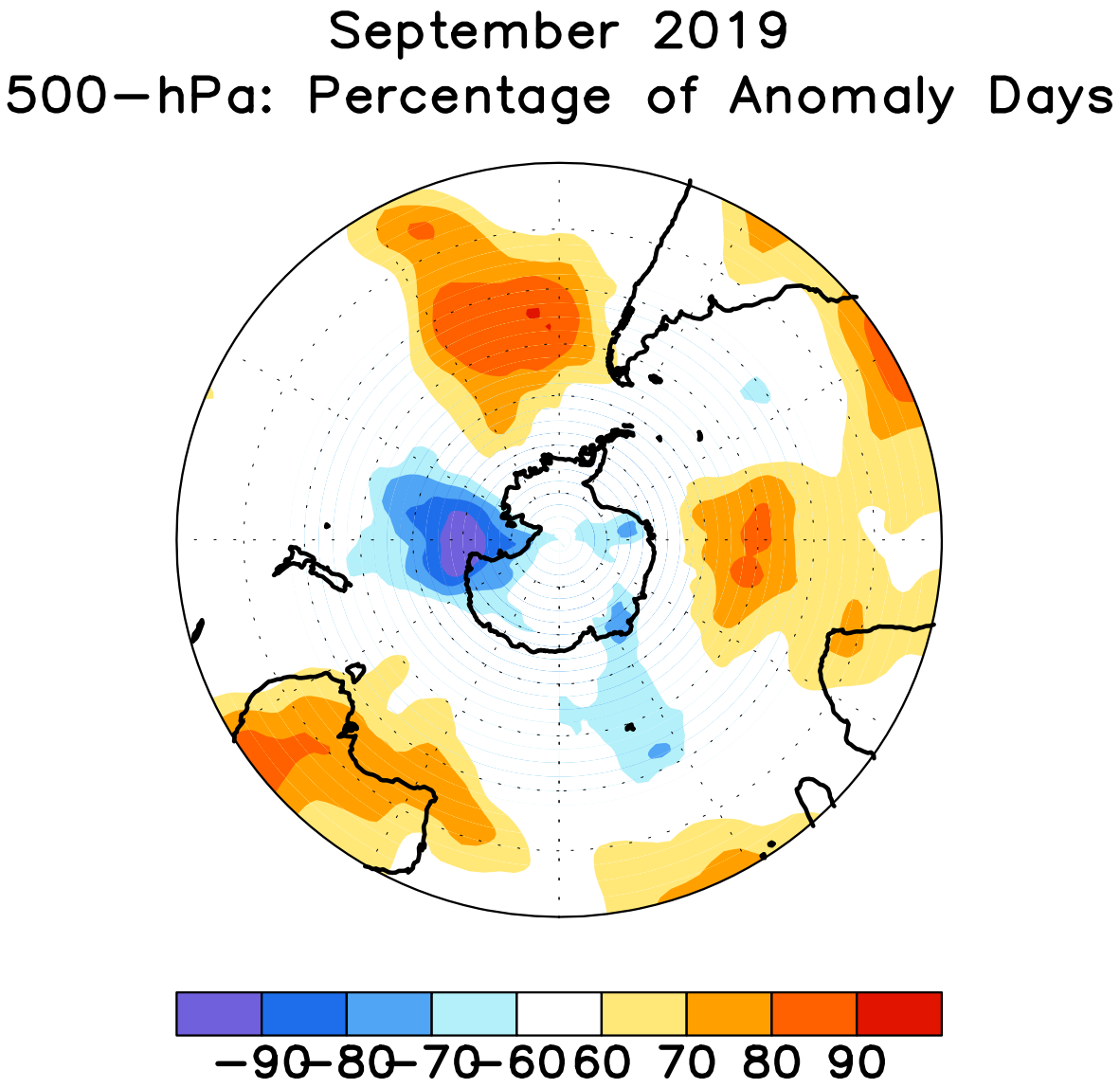


FIGURE E17. Southern Hemisphere percentage of days during SEP 2019 in which 500-hPa height anomalies greater than 15 m (red) and less than -15 m (blue) were observed. Values greater than 70% are shaded and contour in-

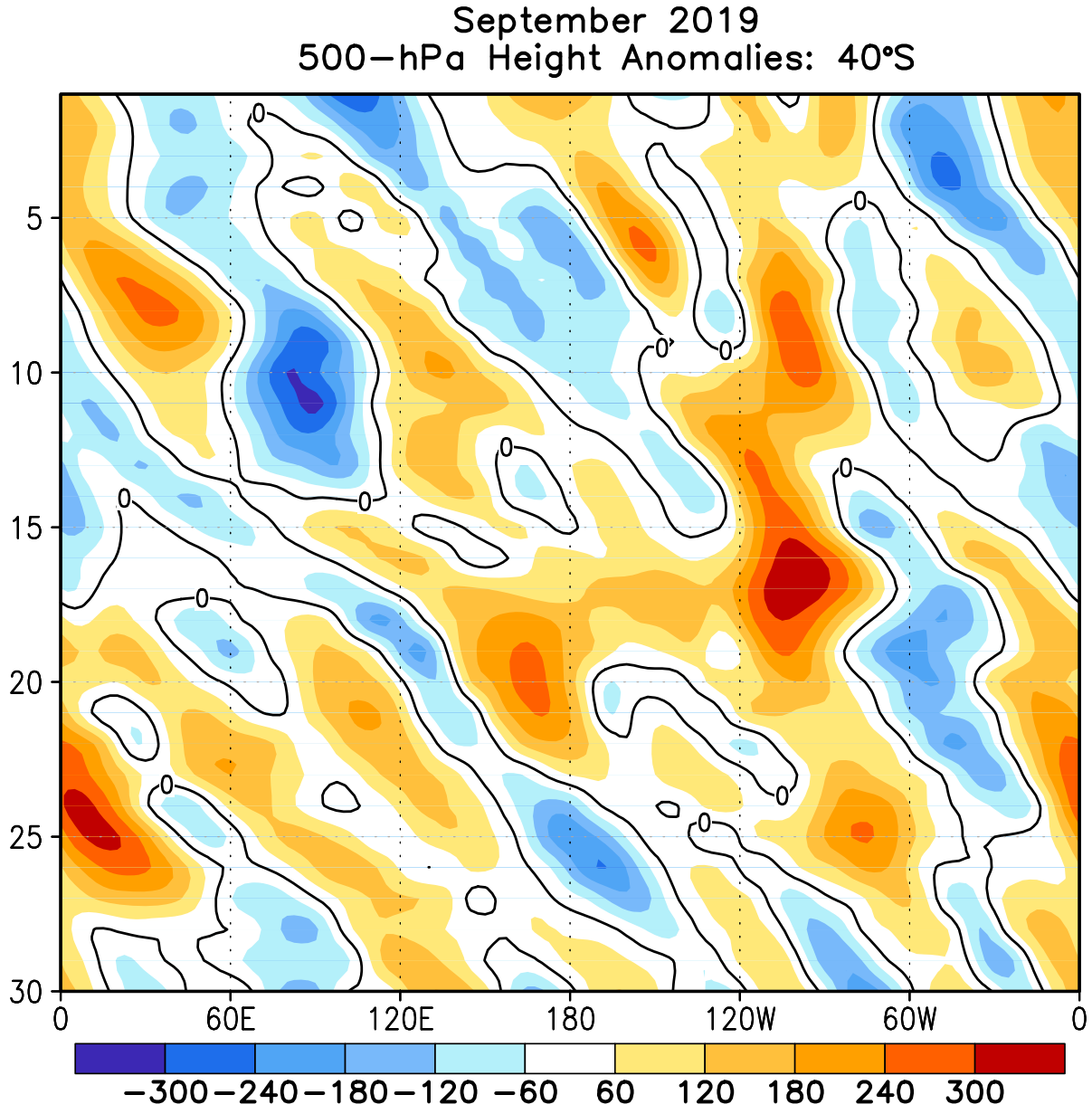


FIGURE E18. Southern Hemisphere: Daily 500-hPa height anomalies for SEP 2019 averaged over the 5° latitude band centered on 40°S. Positive values are indicated by solid contours and dark shading. Negative values are indicated by dashed coutours and light shading. Contour interval is 60 m. Anomalies are departures from the 1981-2010 base period daily means.

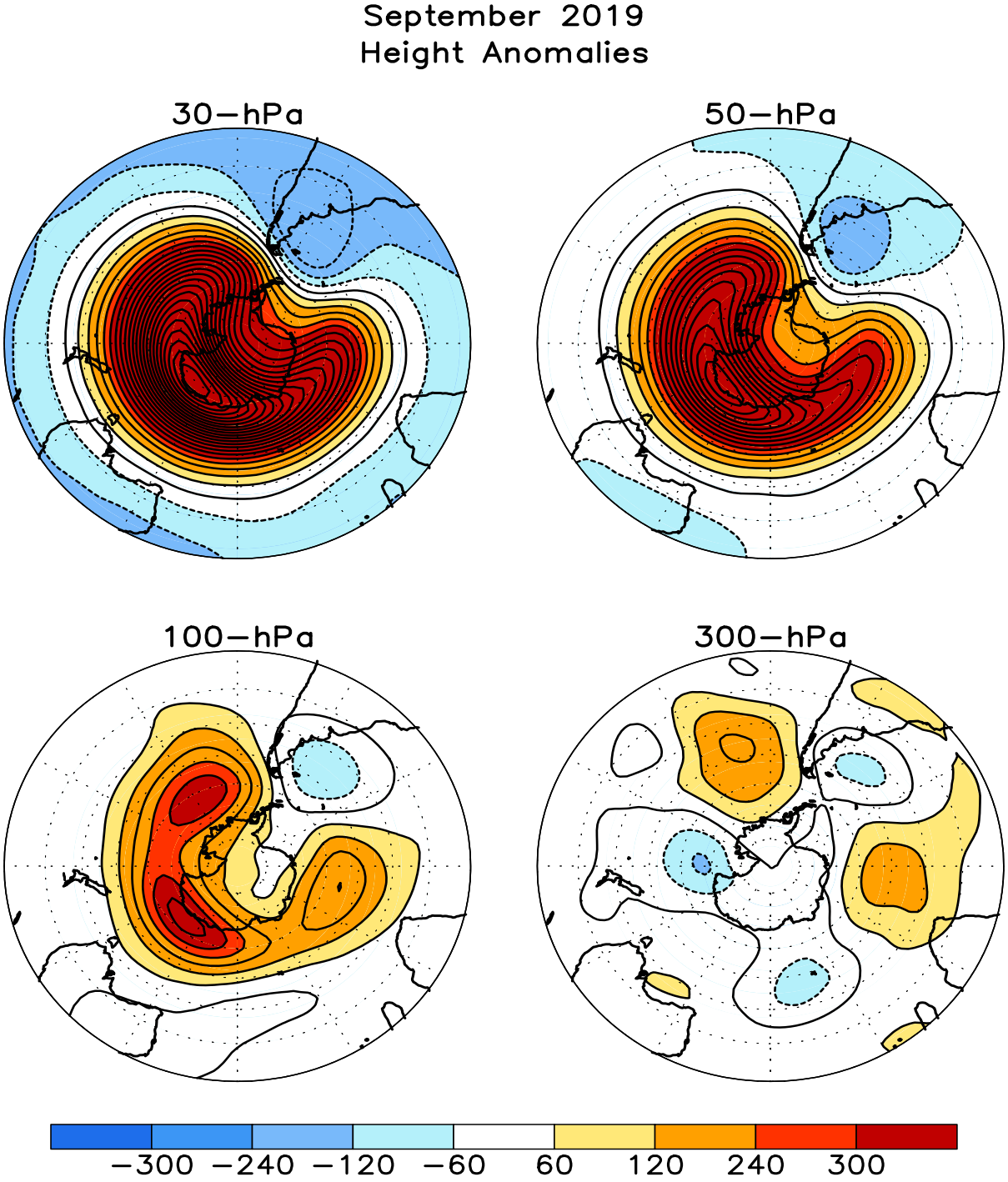


FIGURE S1. Stratospheric height anomalies (m) at selected levels for SEP 2019. Positive values are indicated by solid contours and dark shading. Negative values are indicated by dashed contours and light shading. Contour interval is 60 m. Anomalies are calculated from the 1981-2010 base period means. Winter Hemisphere is shown.

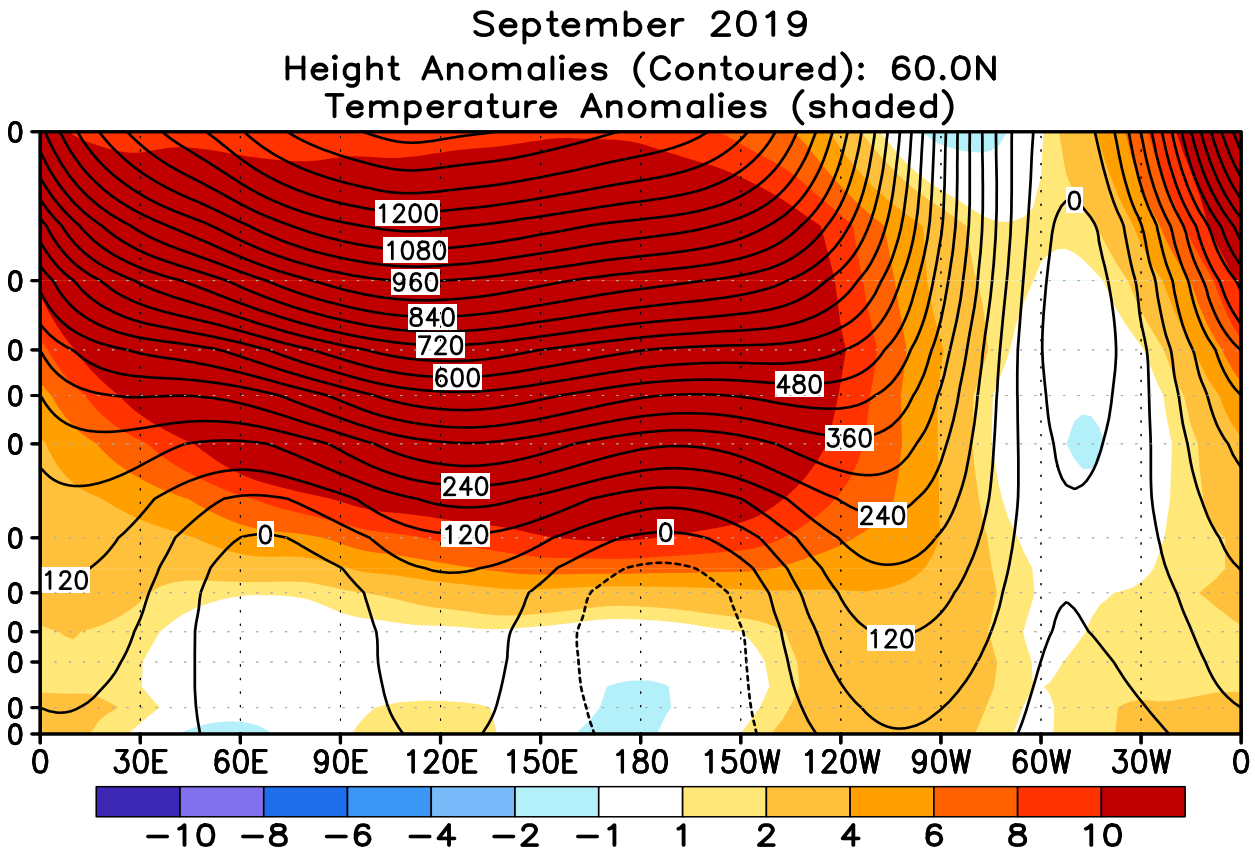


FIGURE S2. Height-longitude sections during SEP 2019 for height anomalies (contour) and temperature anomalies (shaded). In both panels, positive values are indicated by solid contours and dark shading, while negative anomalies are indicated by dashed contours and light shading. Contour interval for height anomalies is 60 m and for temperature anomalies is 2°C. Anomalies are calculated from the 1981-2010 base period monthly means. Winter Hemisphere is shown.

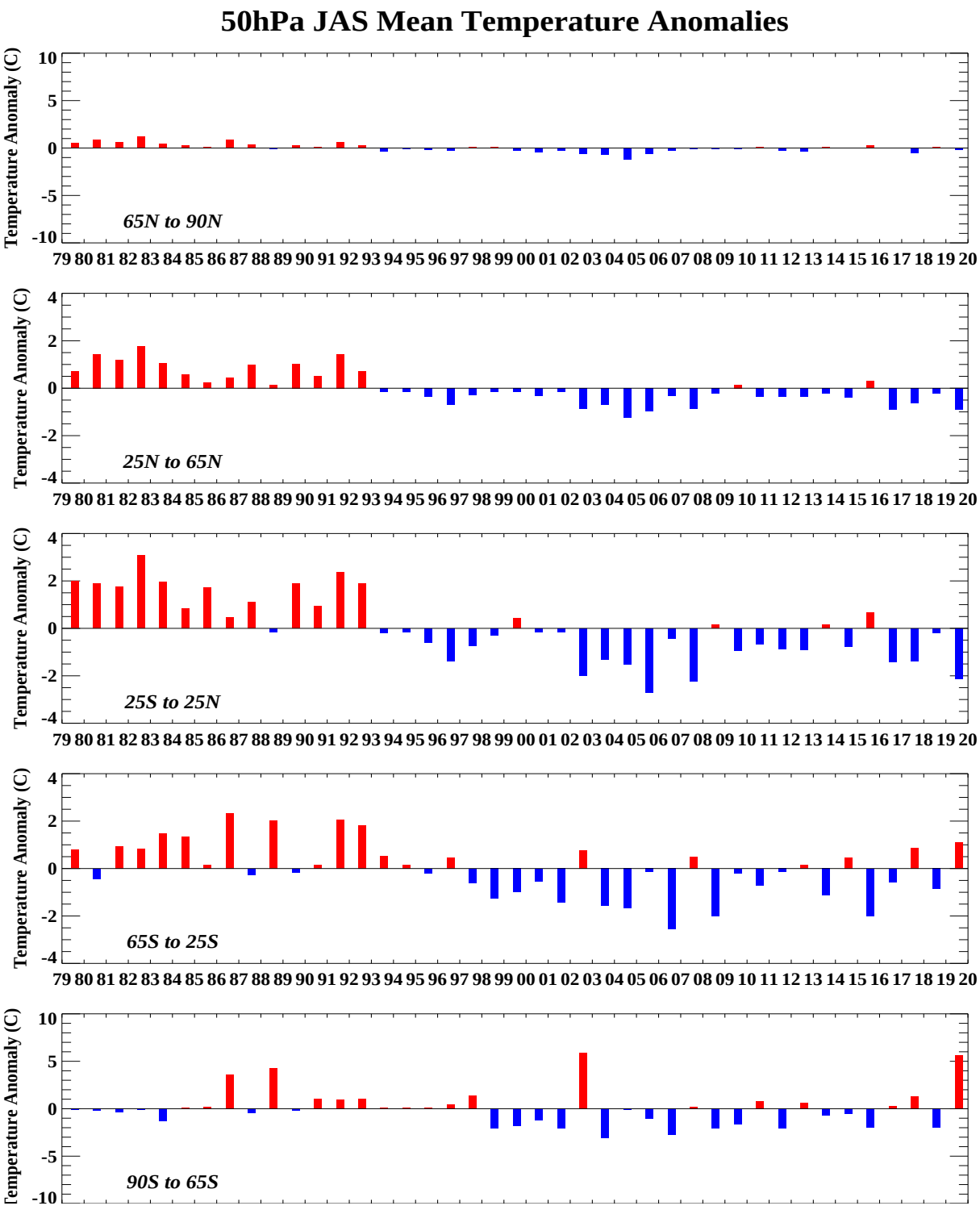


FIGURE S3. Seasonal mean temperature anomalies at 50-hPa for the latitude bands 65°–90°N, 25°–65°N, 25°N–25°S, 25°–65°S, 65°–90°S. The seasonal mean is comprised of the most recent three months. Zonal anomalies are taken from the mean of the entire data set.

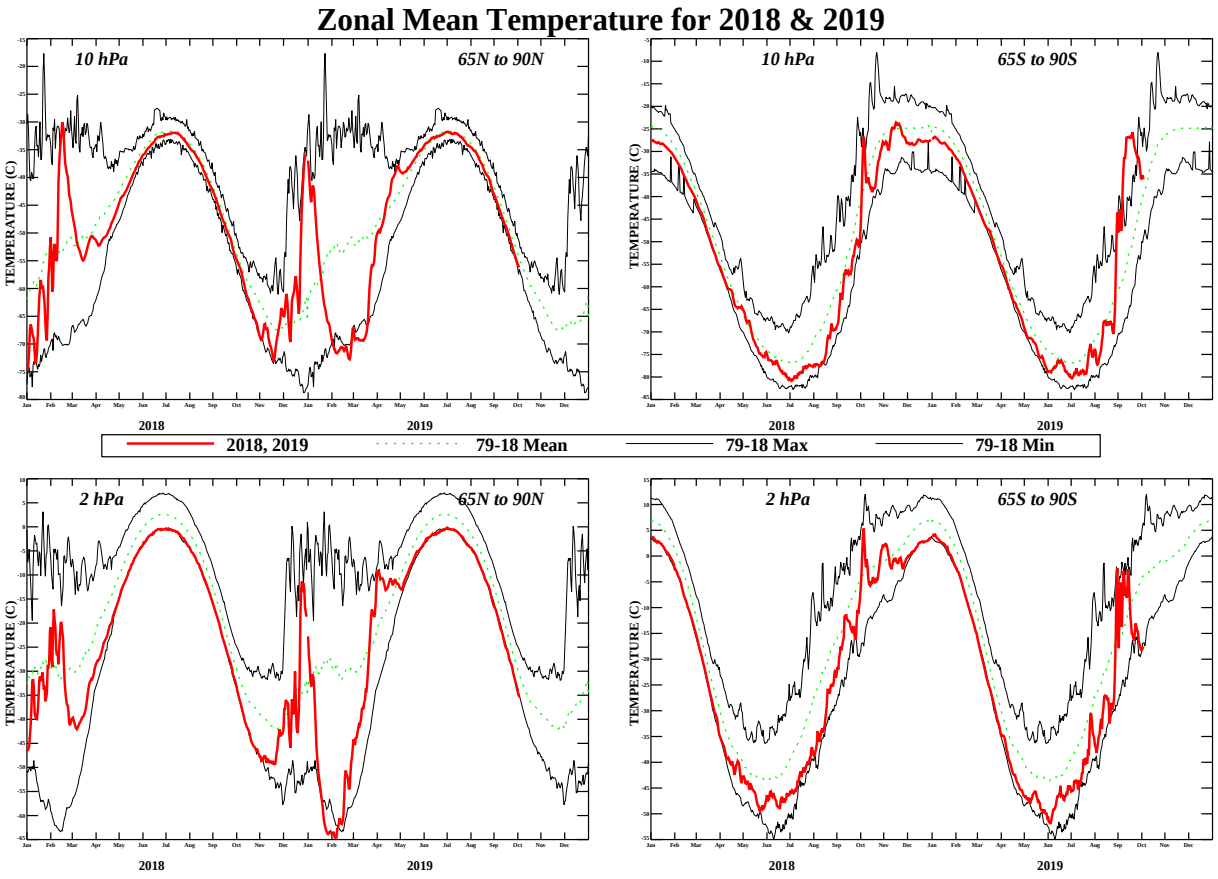


FIGURE S4. Daily mean temperatures at 10-hPa and 2-hPa (thick line) in the region 65°–90°N and 65°–90°S for the past two years. Dashed line depicts the 1981-2010 base period daily mean. Thin solid lines depict the daily extreme maximum and minimum temperatures.

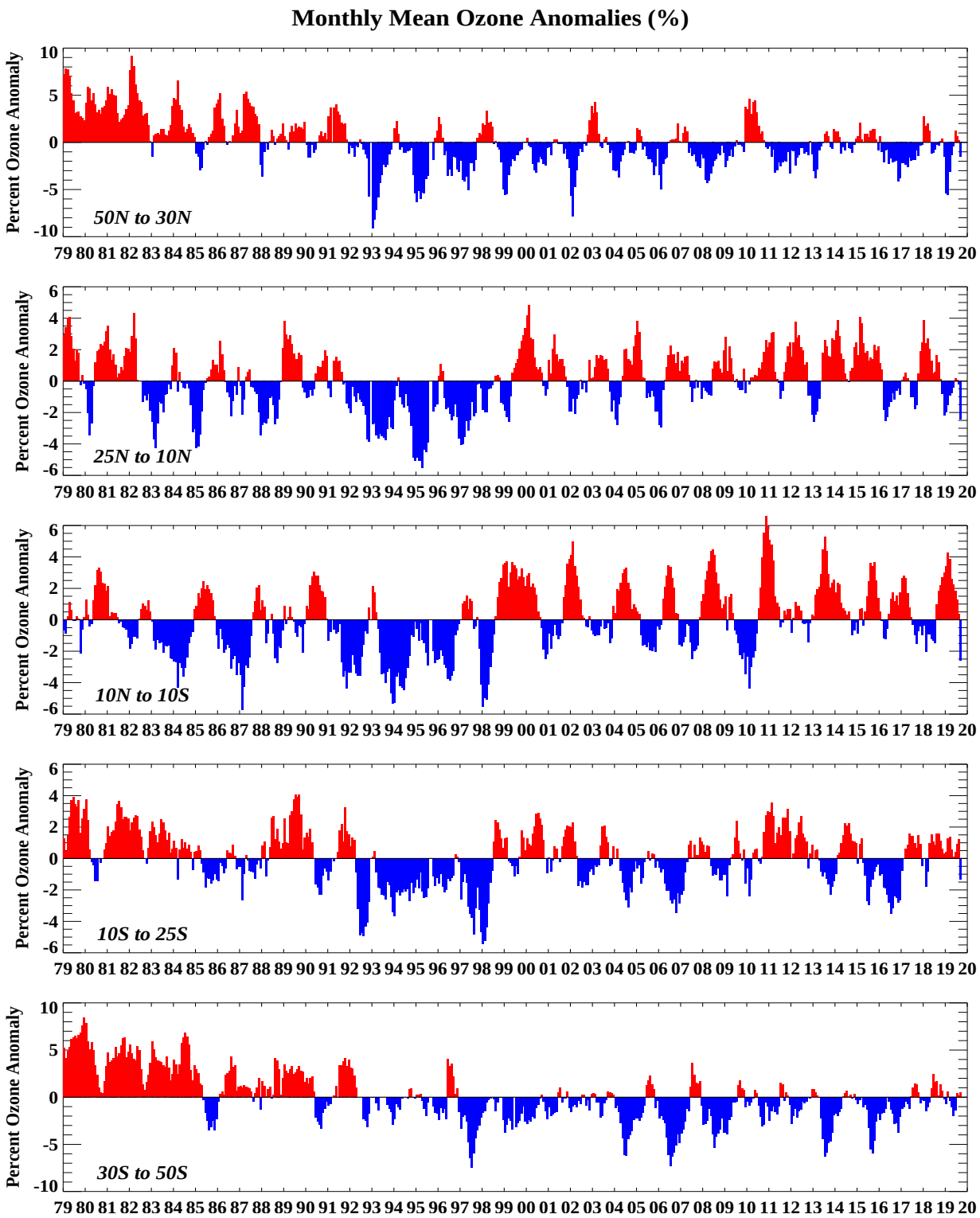


FIGURE S5. Monthly ozone anomalies (percent) from the long term monthly means for five zones: 50N-30N (NH mid-latitudes), 25N-10N (NH tropical surf zone), 10N-10S (Equatorial-QBO zone), 10S-25S (SH tropical surf zone), and 30S-50S (SH mid-latitudes). The long term monthly means are determined from the entire data set

**SEPTEMBER PERCENT DIFF (2019 - AVG[79-86])**

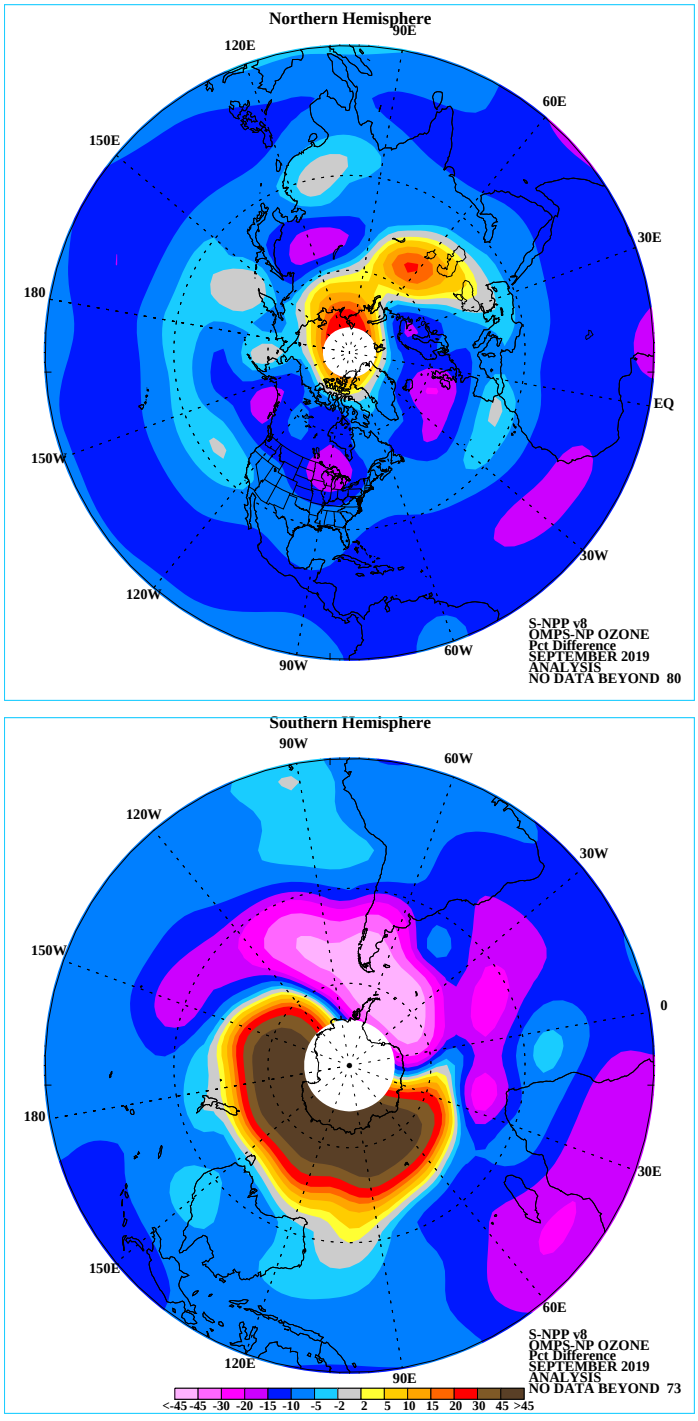


FIGURE S6. Northern (top) and Southern (bottom) Hemisphere total ozone anomaly (percent difference from monthly mean for the period 1979-1986). The region near the winter pole has no SBUV/2 data.

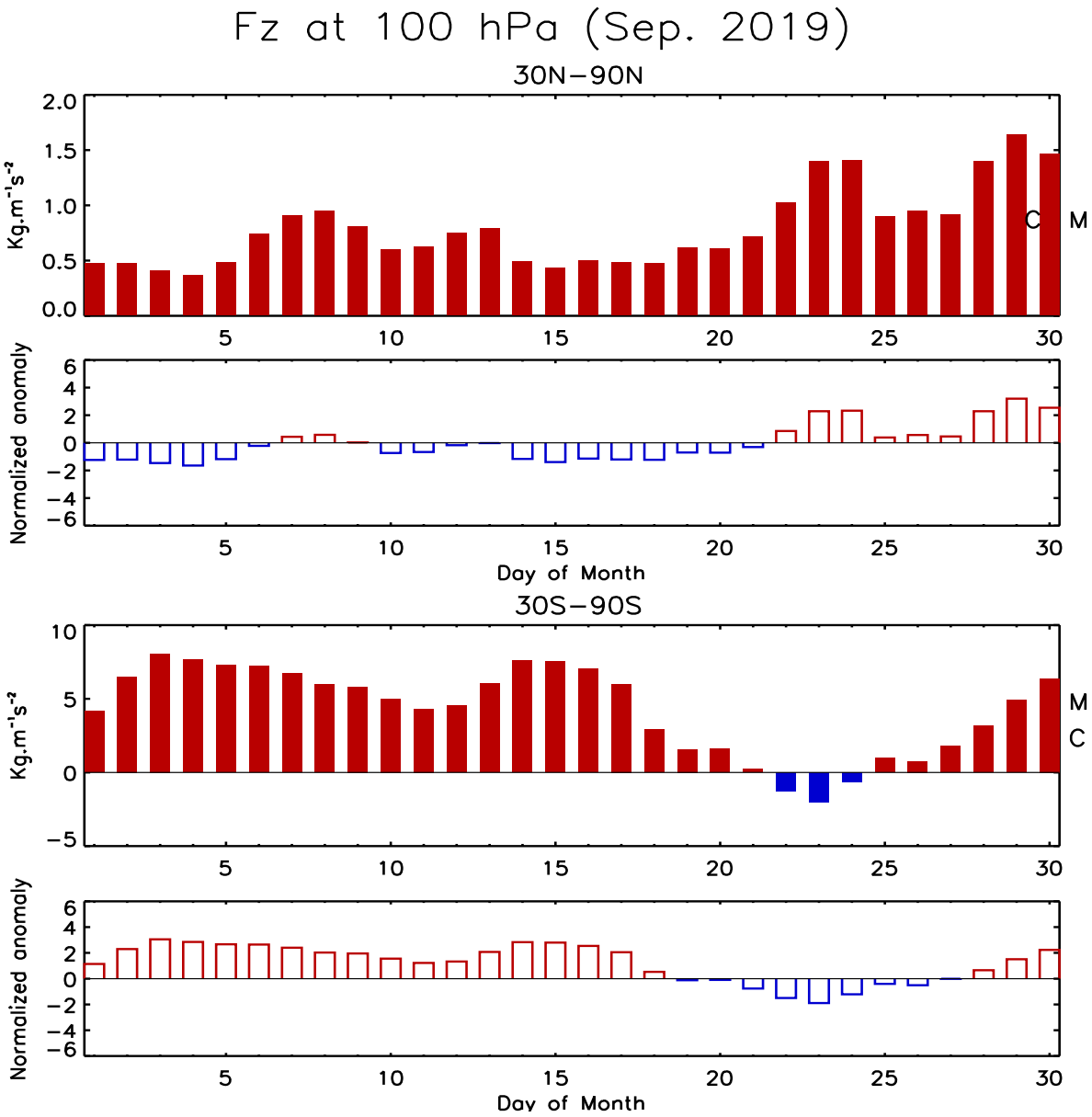


FIGURE S7. Daily vertical component of EP flux (which is proportional to the poleward transport of heat or upward transport of potential energy by planetary wave) at 100 hPa averaged over (top) 30°N–90°N and (bottom) 30°S–90°S for SEP 2019. The EP flux unit (kg $m^{-1}$ $s^{-2}$) has been scaled by multiplying a factor of the Brunt Vaisala frequency divided by the Coriolis parameter and the radius of the earth. The letter 'M' indicates the current monthly mean value and the letter 'C' indicates the climatological mean value. Additionally, the normalized departures from the monthly climatological EP flux values are shown.

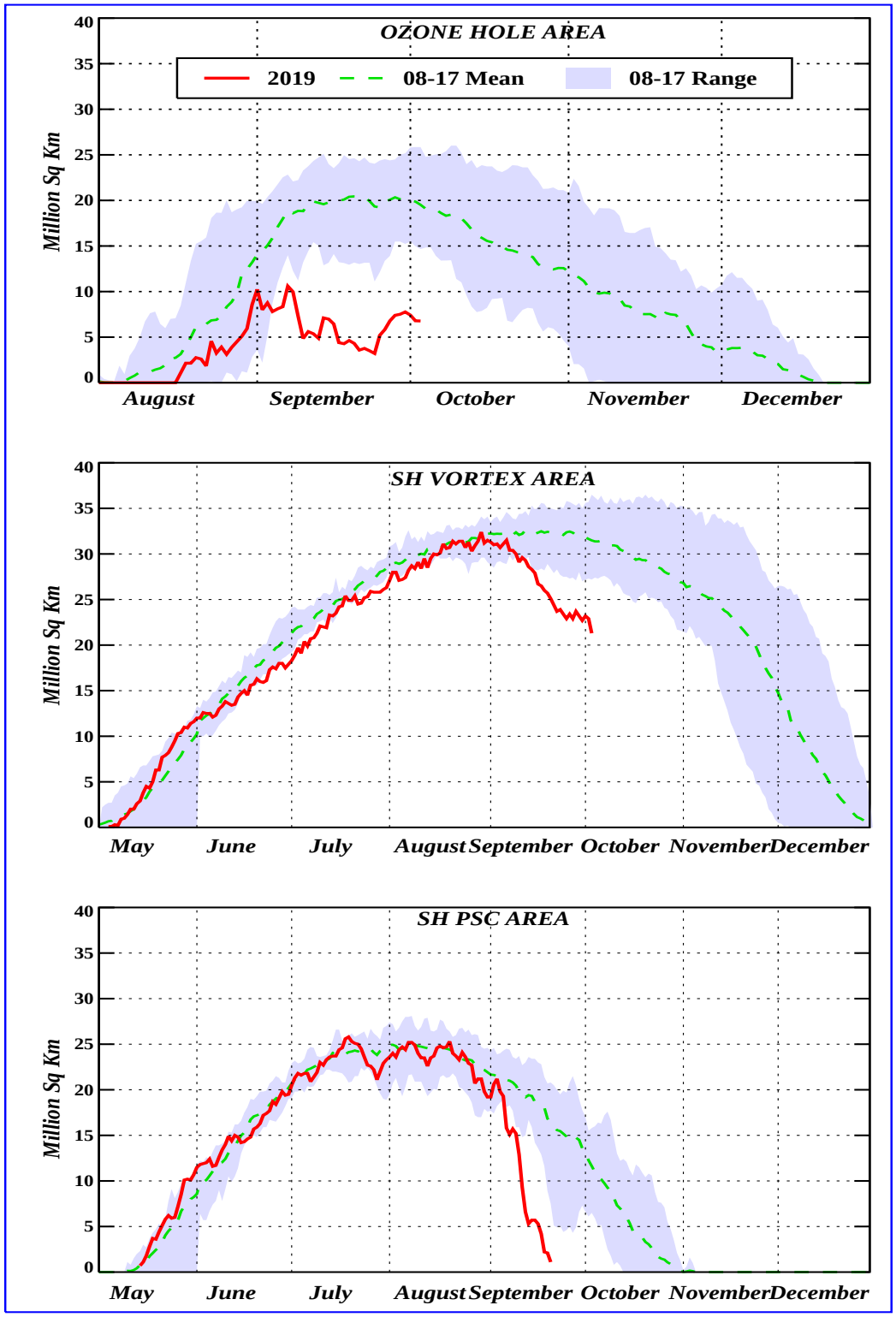


FIGURE S8. Daily time series showing the size of the SH polar vortex (representing the area enclosed by the 32 PVU contour on the 450K isentropic surface), and the areal coverage of temperatures < -78C on the 450K isentropic surface.

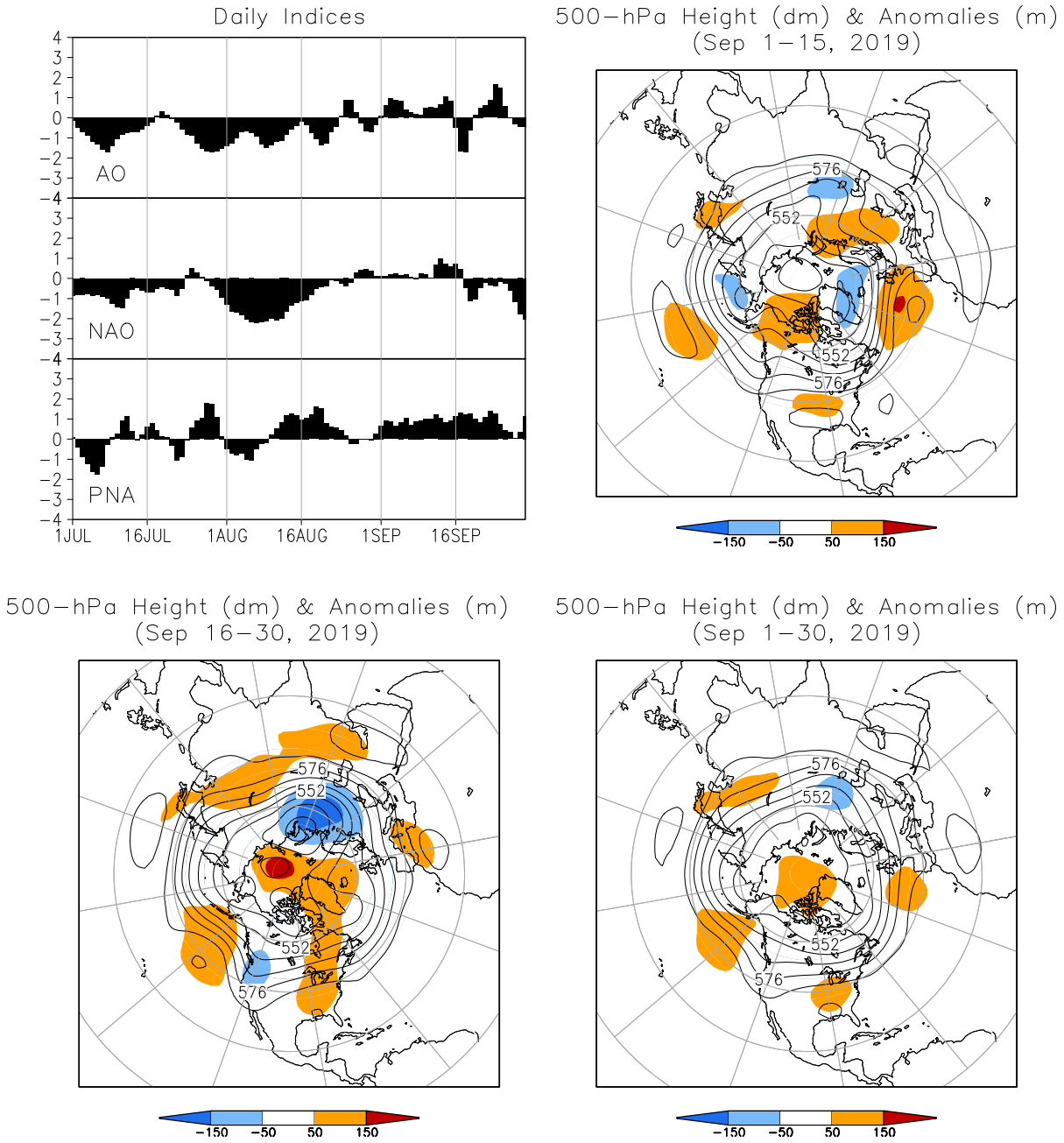


FIGURE A2.1. (a) Daily amplitudes of the Arctic Oscillation (AO) the North Atlantic Oscillation (NAO), and the Pacific-North American (PNA) pattern. The pattern amplitudes for the AO, (NAO, PNA) are calculated by projecting the daily 1000-hPa (500-hPa) height anomaly field onto the leading EOF obtained from standardized time- series of daily 1000-hPa (500-hPa) height for all months of the year. The base period is 1981–2010.

(b-d) Northern Hemisphere mean and anomalous 500-hPa geopotential height (CDAS/Reanalysis) for selected periods during SEP 2019 are shown in the remaining 3 panels. Mean heights are denoted by solid contours drawn at an interval of 8 dam. Dark (light) shading corresponds to anomalies greater than 50 m (less than -50 m). Anomalies are calculated as departures from the 1981-2010 base period daily means.

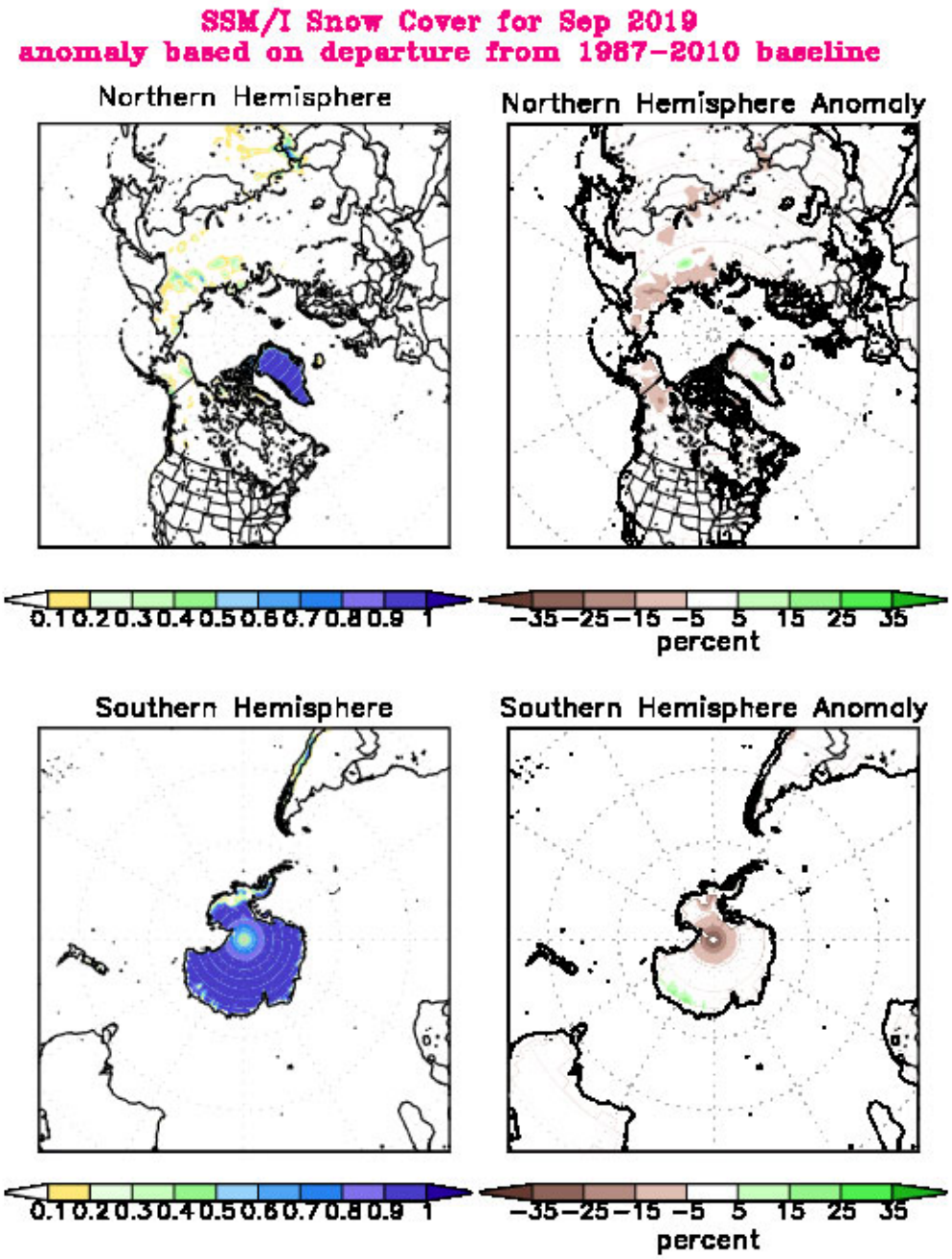


FIGURE A2.2. SSM/I derived snow cover frequency (%) (left) and snow cover anomaly (%) (right) for the month of SEP 2019 based on 1987 - 2010 base period for the Northern Hemisphere (top) and Southern Hemisphere (bottom). It is generated using the algorithm described by Ferraro et. al, 1996, Bull. Amer. Meteor. Soc., vol 77, 891-905.